Order Number 9224832

Turbulent magnetized plasmas from ionizing shock waves

Liang, Zuohua, Ph.D.

City University of New York, 1992

U·M·I

300 N. Zeeb Rd.
Ann Arbor, MI 48106

TURBULENT MAGNETIZED PLASMAS FROM IONIZING SHOCK WAVES

by

ZUOHUA LIANG

A dissertation submitted to the Graduate Faculty in Physics in partial fulfillment of the requirements for the degree of Doctor of Philosophy, The City University of New York.

1992

This manuscript has been read and accepted for the Graduate Faculty in Physics in satisfaction of the dissertation requirement for the degree of Doctor of Philosophy.

March 13, 1992
Date

Joseph A. Johnson
Chair of Examining Committee

March 20, 1992
Date

Joseph P. Veraguth
Executive Officer

Myriam P. Sarachik

Narlis Tzoar

Robert A. Ulseth

Supervisory Committee

The City University of New York

Abstract

TURBULENT MAGNETIZED PLASMAS FROM IONIZING SHOCK WAVES

by

Zuohua Liang

Advisor: Professor Joseph A. Johnson III

Turbulent argon plasmas produced behind hypersonic shock waves ($10 < M < 60$) are studied in the presence of weak magnetic fields at various strengths between 0 and 600 gauss, parallel and antiparallel to the shock tube's axis. The experiment is performed in a cylindrical arc discharge shock tube of 5 cm diameter and 210 cm overall length. Laser induced fluorescence and an electric probe are used as diagnostics of the ion density. Turbulent fluctuations behind the shock front are observed which persist for a time in the order of 10 μs. Using standard turbulent and chaotic analytical procedures, the influence of the magnetic field on the characterizing parameters is determined under circumstances of changing Mach number and pressure. These parameters include spectral index, correlation time scales, turbulent intensity and chaotic dimensionality. The parameters of turbulence obtained from the two diagnostics are quite consistent. Fluctuation power spectra follow a $P \sim f^{-n}$ behavior with $1.3<n<2.8$; this agrees with theoretical predictions as well as the results of other investigators. An increasing magnetic field

increases the characterizing correlation time, the turbulent intensity, and the chaotic dimension but decreases the small correlation time. Therefore the magnetic field decreases the order (increases the dimensionality) in the turbulent plasma, independent of the direction of the field parallel or antiparallel to the direction of the shock wave. A turbulent velocity-field-coupling model is proposed. A dispersion relation shows that, in the presence of an external magnetic field, varieties of new modes in a turbulent plasma are generated. The model predicts an increasing complexity of the turbulent system with increasing strength of the field and is in very good qualitative agreement with our experiment results.

ACKNOWLEDGEMENTS

I would like to express my gratitude to my adviser Professor Joseph A. Johnson III for his guidance, encouragement and support throughout my graduate education and research here.

I express my grateful acknowledgement to my graduate fellow as well as my husband, Jianjun, for his great help in my work.

Special thanks to Dr. Lynette E. Johnson for all kinds of help.

I thank the electronics-shop and the machine-shop as a whole for their professional design and construction. All of them have contributed to our high performance experimental systems.

I would like to express my appreciation to my parents, my parents in law and my sister in law, Yueping, for their encouragement and support.

TABLE OF CONTENTS

LIST OF FIGURES

Chapter I Introduction

Turbulent fluid motion is understood to be a condition of flow in which various physical quantities show an irregular instantaneous unpredictable variation with time and space coordinates.[1] Ionization instabilities arise in nonequilibrium systems when local particle density, temperature, and velocity couple with one another through ionization-recombination reaction and diffusion processes. A plasma is a gas of charged particles. In plasma turbulence, waves of one or more modes are excited; the excited modes and their harmonics produce spectral signatures over a wide range of frequencies.

The study of turbulent behavior is one of the most important problems in plasma physics. Shock waves have been a topic of considerable interest in plasma physics as a means of producing and then heating and compressing a plasma to thermonuclear temperatures.[2,3] Interest in a connection between turbulence and nonlinear dynamics has grown explosively in recent years.[4,5,6] Although some progress has been made in this regard on the subject of fluctuations in ionized gas, it now seems clear that new measurement are required on high temperature turbulent collisional plasmas.

Turbulence and instabilities have been observed in ionizing shock waves in monatomic gases.[7-12] A model for studying plasma and fluid turbulence has been presented;[13] an ionization reaction diffusion turbulence model was proposed for a nonequilibrium open system, in which post-shock chaotic

patterning can be induced by the ionization and diffusion effects and driven by the highly ordered pre-shock gas flow.[7] A considerable amount of theoretical and experimental work has been carried out on shock waves in plasma physics.[14] Wide ranging reviews of shock waves in plasma physics have been given.[14,15] Many experiments have been preformed with collisional shock waves propagating into a highly ionized plasma (using pinch devices), where the term "collisional" is used when the shock front transition length scale is larger than the mean free path of the pre-shock medium. A review of work in status of plasma turbulence has been published by Similon and Sudan.[16]

Nonetheless current theoretical models are woefully inadequate, even for the simplest issues and turbulent plasma dynamics. Ionizing shock waves in magnetic fields have been under extensive experimental and theoretical investigations since the fifties. A normal shock refers to a magnetic field ahead of the shock perpendicular to the plane of the shock and a transverse shock refers to the field parallel to the shock plane. A set of two-fluid Navier-Stokes equations with classical physical transport coefficients was used to compute the evolution and structure of collisional plasma shock waves and it was found that a strong transversely biased magnetic field would significantly alter the size and shape of the shock profiles.[17] The electron temperature and density profiles in deuterium plasmas produced by strong collisional shock waves (including transverse shock waves) and in plasmas created by reflecting a strong shock from a dielectric wall were studied.[18] The theoretical expectation that the electron

temperature would be much less than the ion temperature was confirmed. However, there are no predictions for turbulent plasma dynamics in the presence of weak magnetic field.

Recent studies have shown that there is some connection between dynamical systems theory and turbulence. A simple dynamical model of three ordinary differential equations for two dimensional Benard convection exhibited a bounded, non-periodic, apparently chaotic behavior.[19] Ruelle and Takens[20] proposed a model in which turbulence would be a deterministic, the chaotic regime reached after a small number of bifurcations. This ideas was totally opposite to Landau's theory in which turbulence involved the continuous amplification of indefinitely many modes. The basic question is as follows: To what extent can turbulent motion be described by a low dimensional attractor similar to those found in low order dimensional nonlinear systems? A correspondence has been shown in closed flow systems; i.e., systems constrained by boundaries. However, the connection is much more difficult for open, fully developed turbulent flows, since a large number of modes can easily be excited as the bifurcation parameter varies. It is therefore necessary to determine whether the dynamics of a complex turbulent flow can be described, at least qualitatively, by a finite, possibly small, number of modes.

A cascade model for chaotic flows was proposed[21] which enables us to explore fluid turbulence from the dynamical system viewpoint. The underlying concept of the cascade model is to distinguish two different regimes of space-time scale: one is a

dynamic local regime, where local causal space dynamics is useful, and the other is a stochastic global regime where a statistical approach must be used. The model has been further developed to determine the Hausdorff dimension D of some strange attractors and to relate the turbulence statistics to local vortex dynamics by applying it to dissipative systems and to fully-developed fluid turbulence.[22] It remains however to apply this novel analytical procedures to high temperature turbulent plasmas.

We notice that the continuity equation for the collisional ionizing shock has a nonlinear and dispersive structure similar to the Poisson's equation for the electrical field in the collisionless plasma shock wave in which solitary wave and turbulence have been predicted and observed.[23,24,25] Particle-like clumps can be developed as a consequence of the balance between the nonlinear ionization and the dispersive diffusion effects.[7] When the diffusion rates for different components are different, one and two dimensional instabilities can be induced.[26,27,28] It is known that the particle concentration behind an ionizing shock front can change not only through the usual compression, convection, and diffusion mechanisms, but also through ionization reactions as well; furthermore, a magnetic field parallel to the flow at the shock front can couple directly into at least two of the three components of fluctuating velocities in the reacting regions. Thus the magnetized ionizing shock wave has at least two more degrees of freedom than the unmagnetized neutral gas dynamic shock wave. Like many other similar open nonequilibrium

systems, the self-organizing patterning behind the ionizing shock is expected to be driven by the ordered incoming pre-shock gas flow. A determination of the role which deterministic nonlinear dynamics plays in these open nonequilibrium systems should provide a useful tool for the evolution of theoretical models for turbulence.

Physical understanding of turbulent nonequilibrium fluids is still far from complete, mainly because of difficulties associated with properly determining the role of nonlinear behaviors. Furthermore, many of the plasmas in nature and in important laboratory systems occur in the presence of magnetic fields. No efforts have been made to characterize the coupling of turbulent fluid-like plasmas with external magnetic fields.

The major purpose of this work is therefore to understand more completely the turbulent properties of the ionizing shock waves and investigate the effects of external magnetic fields on the turbulent plasmas behind the shock front. This thesis is divided into six chapters. Following the introduction, a brief review of the theories of ionizing shock waves and turbulent plasmas, and of the influence of a magnetic field on plasmas is given in chapter II. In chapter III, the overall scheme of the experiment is outlined. The design of the shock tube, the discharge system and the electric probe and optical system, the operation of the shock tube and the diagnostics are discussed in detail. Chapter IV describes the methods of analysis. Chapter V presents the data and gives the experimental results and discussion. The last chapter interprets the results of the

experiment measurements and data analyses for the turbulent plasmas. A new model is proposed and compared with the results of our experiment. Conclusions are given and suggestions for some possible further investigations are given in the last section.

Chapter II Background

The classical theory of shock waves in plasma physics is well developed. The results of this theory are presented in the first section of this chapter. Ionizing shock waves and shock propagation parallel to the magnetic field are described. A review of the previous theoretical and experimental works on turbulence related to our work is given. Turbulence in plasmas is discussed in the second section. It includes the discussions of the theory of "weak turbulence", quasilinear theory, etc. The turbulent mechanism is considered in the third section. Finally, we discuss some possible effects of a magnetic field on turbulent fluid-like plasmas.

2.1 Shock Waves in Plasma Physics

A shock wave arises when a large amount of energy is suddenly released into a continuous medium. The shock wave heats, compresses, and accelerates the medium through which it propagates. Using fluid equations, including the effects of non-linearity and dissipation, the steepness of the wavefront is limited and it ultimately reaches a stable shape. This is the steady profile produced by the balance of non-linear and dissipative effects which corresponds to a shock wave.[29] Shock waves occur in gases, liquids, solids, and analogs have been found in various electromagnetic phenomena.

A shock wave is an adiabatic but not an isentropic process; the temperature produced by shock wave compression can exceed that in an isentropic compression by a very large factor.[30] The changes in pressure, density, temperature and velocity of the gas across the shock front occur at a fast (in the order of 1 μs) but finite rate. The gas flow velocity changes across the front due to the gas collision processes, and it is the degradation of this directed kinetic energy of gas motion into random kinetic or thermal energy of the molecules which raises the state of the shocked gas above that in an ordinary isentropic compression. This process is irreversible; an increase in entropy occurs across a shock front. Since the entropy of a gas is a function only of its thermodynamic state, a detailed knowledge of the nature of these irreversible collision processes is not required in order to calculate the final state of the shocked gas; this may be evaluated from the resulting

change in gas flow velocity across the front and the initial conditions alone. The shock speed is greater than the characteristic sound speed at which the molecules communicate a weak compression. For example, the sound speed for argon gas at temperature 20°C is 331 m/s. The shock speed is from 3,000 m/s to 20,000 m/s in our shock tube.

2.1.1 Phenomena in Ionizing Shock Waves

The shock wave is called an ionizing shock wave if the pre-shock gas is nonionized and the post-shock gas is ionized. Strong shock waves will ionize the gas. We distinguish three different situations in terms of their pre-shock (subscript 1) and post-shock (subscript 2) electrical conductivity σ:

$\sigma_1 = \sigma_2 = 0$	gas dynamic shock
$\sigma_1, \sigma_2 > 0$	plasma shock
$\sigma_1 = 0, \sigma_2 > 0$	ionizing shock

The ionizing shock propagates into an initial cold (about 293 K) low pressure gas. The ionizing shock may be considered as consisting of two stages. The first is a fast relaxation zone, with thickness of a few mean free paths, in which there is a sharp density jump and excitation of translational degrees of freedom of the gas. Viscosity and thermal conductivity are the dissipative processes at this stage. The second is the "slow" relaxation zone with a much thicker stage. Its thickness is proportional to $\varepsilon\lambda$,

where λ is the electron-atom ionization mean free path and $\varepsilon=(m_e/m_a)^{1/2}$. $\varepsilon\lambda$ is in the order of 0.4 mm under our experimental conditions. In this zone the excited translational motion relaxes to other degrees of freedom. The processes which occur are: Molecular rotation, oscillation, and dissociation; excitation of electronic levels; and ionization.

The compression and heating behind the shock front are due to the conservation of mass, momentum, and energy flux. The mechanism can be easily understood in the frame of reference moving with the shock front. Because of the high density compression behind the shock front, the pre-shock gas must slow down in order to conserve the mass flux. The extra flow energy is converted to excite new degrees of freedom. The theory of collisional shock waves predicts preferential heating of ions as opposed to electrons in an ionizing shock wave. In other words, the plasma electron temperature is much less that the ion temperature. This has been confirmed by experiment.[18] Following the initial shock heating, equilibration of ion and electron temperatures should occur due to energy exchange between ions and electrons in Coulomb collisions.

In monatomic gases, ionization may be produced by atom-atom collisions, by electron-atom collisions, by electron-ion collisions and by photo-ionization. While the electron-ion collisions are individually most likely to be inelastic because of the long range of the Coulomb force, the number of such collisions will be extremely small until the ionization is already high, so that such collisions make a negligible contribution to the initial

ionization process. Photo-ionization of argon requires light in the far ultra-violet below 80.0 nm, and it may make a contribution only at temperatures above 20,000 K.

The amount of ionization to be expected for a hot gas in thermodynamic equilibrium can readily be calculated from the Saha equation which relates the concentration of ions and electrons to the temperature, ionization potential, gas pressure and partition functions.[30] For argon, the ionization potential is 15.75 eV so that the ionization is almost negligible below about 8000 K.

The structure of an ionizing shock wave is determined basically by two features: The requirement of quasineutrality and the great mass difference between ions and electrons. In the coordinate system fixed to a stationary shock front, most of the directed motion of the incident gas is converted to thermal motion by viscous dissipation in the shock structure. A shock front of speed U in the lab frame is much greater than the thermal speed of the initial gas and provides the ions with a kinetic energy $E_i \propto m_i U^2$ and the electrons with $E_e \propto m_e U^2$. Since the ion mass is much greater than the electron mass (for argon, $m_i/m_e \approx 7 \times 10^4$), one has $E_i/E_e \propto m_i/m_e >> 1$. The temperature has the same mass and velocity dependence as energy; it yields $T_i >> T_e$ immediately after heating by the shock front. Electrons may be further heated in the shock by adiabatic compression, resistive heating, acceleration in the ions' electric field, or by elastic collisions with ions. In a collisionless plasma shock, collective field heating

mechanisms generally heat electrons more strongly. However, some collisionless heating mechanisms may heat ions as well.[18]

Finally we notice that a shock transition often acts as a source of disturbances that may propagate ahead of the shock front and thereby spread its effect over much wider length scales.[23] They are usually referred to as shock precursors. In the case of ionizing shock wave, there is a weakly ionized precursor running ahead of the shock front, which makes the pre-shock gas with $\sigma_1>0$. Possible mechanisms for the formation of the precursor have been proposed: Electron diffusion from the shock front,[31] photo-ionization by the absorption of UV light from the post-shock gas,[32] electric field break down waves, or a combination of mechanisms.[33]

The movements of the shock front, the contact surface and several flow regimes are schematically indicated by an x-t diagram in Figure 2.1. The shock front D separates a pre-shock equilibrium gas and a post-shock transition plasma region. Plasmas behind the shock front are generated because the temperature in that region is sufficiently high to cause ionization of the neutral gas. The temperature in the post shock region is of the order of 10^5 to 10^6 K. The contact surface is the interface between the post-shock plasma and the arc discharge heated expanding plasma (driver gas); it moves rapidly along the tube behind the shock front. Our interest is in the post-shock transition plasma shown by the shaded area, which is where the turbulence takes place; i.e., the turbulent plasma region. The diagram also shows that the relation between x and t for the

shock wave is not linear: The speed of the shock front decreases as it travels downstream.

2.1.2 Shock Propagation Parallel to the Magnetic Field

When shock waves propagate in the direction of the initial magnetic field, in general, the magnetic field after the shock has passed may have both a normal and a tangential component. Considering a plane shock in a frame of reference moving with the shock velocity, the undisturbed fluid flows into the front of the shock with a relative velocity U_1, and the shocked fluid flows out from the back of the shock with a relative velocity U_2. When v is the velocity of the gas relative to the shock tube, and U_s the velocity of the shock front relative to the tube, we may then write

$$U_1 = U_s - v_1$$
$$U_2 = U_s - v_2.$$

A coordinate system in the rest frame of the shock wave is chosen so that x is perpendicular to the shock surface and y, z are in the plane of the shock. For an ideal gas without chemistry, we may write the shock jump equations[30,34-36]

$$\rho_1 U_1 = \rho_2 U_2$$
$$\rho_1 U_1^2 + P_1 = \rho_2 U_2^2 + P_2 + \frac{B_{z2}^2}{8\pi}$$

$$\rho_1 U_1\left[\frac{\gamma P_1}{(\gamma-1)\,\rho_1}+\frac{1}{2}U_1^{\,2}\right]=\rho_2 U_2\left[\frac{\gamma P_2}{(\gamma-1)\rho_2}+\frac{1}{2}(U_2^{\,2}+W_2^{\,2})\right]+\frac{E_y B_{z2}}{4\pi}$$

$$\rho_1 U_1 W_2-\frac{B_x B_{z2}}{4\pi}=0$$

where the subscripts 1 and 2 denote the undisturbed fluid region and shock fluid region respectively, and γ is the ratio of the specific heats, U the flow speed relative to the shock front and W is the velocity parallel to the front in the z direction, the density and pressure are denoted by ρ and P, E is the electric field and B is the magnetic field. These shock jump equations give the post shock state in terms of the initial state.

Considering a weak initial magnetic field, we have $B_{z2}=0$, and $W_2=0$.[34] Thus, the shock jump equations become

$$\begin{aligned}
&\rho_1 U_1=\rho_2 U_2\\
&\rho_1 U_1^{\,2}+P_1=\rho_2 U_2^{\,2}+P_2\\
&\frac{\gamma P_1}{(\gamma-1)\rho_1}+\frac{1}{2}U_1^{\,2}=\frac{\gamma P_2}{(\gamma-1)\rho_2}+\frac{1}{2}U_2^{\,2}
\end{aligned}\qquad (2.1)$$

The magnetic field plays no part in this case. The field itself is not changed and it does not appear in the above equations governing the changes in ρ, U, and P.

The Mach number M is the ratio of the shock speed in the laboratory frame in a gas to the local speed of sound in the gas; i.e. $M=U_s/a$. Noting that the gas ahead of the shock is stationary, $U_s=U_1$. Solving the equations above and applying strong shock condition $M>>1$ gives

$$\begin{aligned}
\frac{\rho_2}{\rho_1} &= \frac{U_1}{U_2} \approx \frac{\gamma+1}{\gamma-1} \\
\frac{T_2}{T_1} &\approx \frac{2\gamma(\gamma-1)}{(\gamma+1)^2} M^2 \\
\frac{P_2}{P_1} &\approx \frac{2\gamma}{(\gamma+1)} M^2
\end{aligned} \tag{2.2}$$

The density ratio is 4 for $\gamma=5/3$ of argon. The expression for temperature ratio shows that strong shocks may convert the initially nonconducting neutral gas into a plasma by creating a temperature, T_2, behind the shock sufficiently high to cause ionization. The resulting plasma can interact with electromagnetic fields.

When the initial magnetic field is very strong, a case called "switch-on shock" occurs, in which a transverse magnetic field is "switched on" behind the shock.

2.2 Turbulence in Plasmas

A plasma is a gas of charged particles. Plasma turbulence is a phenomenon driven by a variety of agents; e.g., currents, gradients in density, temperature, current density, etc. It is the state of a plasma in which waves of one or of several modes are excited in a wide range of frequencies and of wave numbers. The particle concentration behind an ionizing shock front can change not only through the usual compression, convection, and diffusion mechanisms but also through ionization reactions as well.

When the amplitudes of the dispersive eigenmodes are small, the state of the plasma may be treated as a linear superposition of these modes but with amplitudes having a slow time variation governed by weak nonlinear interaction.[29] This is the theory of "weak turbulence", in which the nonlinearities are small and yield small corrections to linear behavior. Strong turbulence means that the nonlinearities are as strong as the linear terms. The usual conditions for the validity of weak turbulence are (a) small mode amplitudes in the sense mentioned above and (b) the wave growth over the correlation time of the members of the spectrum is small.

Another issue is the effect of small-scale, high-frequency fluctuations on large-scale, low-frequency modes. It can be handled by a relatively elementary technique called quasilinear theory. In this theory, the nonlinear terms are so small that they can be neglected in the equations for high frequency fluctuations and the wave propagation can be treated by linear theory. The

nonlinear part of quasilinear theory concerns the long term effect of many waves on the background distribution function. In the presence of the turbulent electric fields, the particles are accelerated. Because the fields are turbulent, the acceleration is not constant but is random, being alternately positive and negative. Thus, a typical particle will perform a random walk in velocity space. This implies a diffusion of particles in velocity space. Diffusion tends to spread out the particles in velocity space. Quasilinear theory involves the linear wave-particle interaction.

The magnetohydrodynamic (MHD) description is valid when the collision frequencies of the electrons and ions are much greater than their cyclotron frequencies, and when there is strong coupling through collisions between the electrons and ions so that they act as one fluid defined by a viscosity and an electrical conductivity. MHD is often used to describe the equilibrium state of a plasma.

Some progress in the treatment of turbulence in a low-pressure, magnetized plasma has been made by stressing the homology between fluid turbulence and low-frequency plasma turbulence and invoking the Kolmogorov cascade of a system invariant, such as the energy density.[37-41] Plasmas generally have more than one system invariant (e.g. energy, entropy, helicity, etc.). Different modes with different spectral characteristics may dominate different regions of **k**-space. Additionally, the turbulence is strongly anisotropic in a magnetized plasma. The fluctuations have slow phase variations

along the magnetic field but change rapidly across the field ($k_{//} << k_{\perp}$ for the wave vector **k**).

2.3 Ionization Reaction Diffusion Turbulence

A reaction-diffusion system can be treated as a system composed of many local nonlinear limit cycle oscillators coupled with each other spatially through diffusion and convection.[26] A turbulent spatio-temporal pattern appears even in a two component one dimensional system with multiple diffusion processes. It can be roughly divided into phase turbulence and amplitude turbulence. In the former case, the disturbance is small. The turbulent pattern is due to the different diffusion rates of multiple diffusion processes. In the latter case, the spatial inhomogeneity is strong enough to produce the turbulence.[27] Instability and turbulence can also be developed along the wave fronts in a two dimensional reaction diffusion system.[28] A simple bistable system composed of an activator x and inhibitor y is applied in Kuramoto's model. Suppose a straight wave front separates the medium into two regions with the steady state condition $P_1 = (x_1, y_1)$ and $P_2 = (x_2, y_2)$, where $x_1 > x_2$ and $y_1 > y_2$. A small pushing of the straight wave front from region 1 toward region 2 will be unstable if the diffusion coefficients have relation $D_x < D_y$. Since y diffuses faster than x, there will be more x left in the perturbed region and it will keep the disturbance growing. The instability and turbulence of the wave front might be considered to be one of the phenomena resulting from the competition between the cross-inhibitary and the cross-excitory nature of the system.

Our system is one kind of reaction-diffusion system in which particle density, temperature and velocity couple with one another through ionization-recombination reaction and diffusion processes. Due to the difference between particle and thermal diffusion rates, turbulence is possible. The ion acoustic wave is another mechanism through which the flow can be made turbulent. An ionization wave characterization of shock wave turbulence which is a mixture of acoustic and reaction-diffusion mechanisms can be suggested.

The system behind the ionizing shock front is a nonequilibrium open system due to the presence of a constant energy and mass flow from the boundary (shock front). The dynamic equations of different variables of the system can generally be written as:

$$\partial \mathbf{X}/\partial t + \mathbf{v} \cdot \nabla \mathbf{X} = D \cdot \nabla^2 \mathbf{X} + \mathbf{F}(\mathbf{X},\lambda) \qquad (2.3)$$

where $\mathbf{X}$ represents a set of space-time dependent variables describing the state of the system, $\mathbf{v}$ is the flow velocity, D is a diffusion matrix, $\mathbf{F}$ is the nonlinear term corresponding to ionization, recombination and other nonlinear processes, and λ is a set of external parameters controlling the process. The ionization-recombination reaction gives rise to nonlinear source and sink terms, and diffusion makes the system dispersive and gives spatial coupling.[7] A typical example of a general nonlinear dispersive system is a solitary wave.[29]

Diffusion induced chemical turbulence has been demonstrated experimentally.[42,43] Turbulence and ionization waves in a discharge tube have been studied.[44-47] In this case, the system is a nonequilibrium open system with ionization reaction, thermal diffusion and particle ambipolar diffusion. The instability or turbulence is driven by the external electric field or the electron beam. For an ionizing shock wave, it is possible to excite ionization instability and turbulence since there are high energy atomic (neutral) streams; viz., the incoming pre-shock gas flow and charged particle streams from the precursor flow.

2.4 Influence of a Magnetic Field on Plasmas

In plasma physics, the complete Boltzmann equation is derived from classical kinetic theory. It describes the evolution of the distribution function in seven-dimensional space. It is expressed as

$$\partial_t f(\mathbf{x},\mathbf{v},t) + \mathbf{v}\cdot\nabla_{\mathbf{x}} f + \frac{q}{m}\left(\mathbf{E} + \frac{\mathbf{v}}{c}\times\mathbf{B}\right)\cdot\nabla_{\mathbf{v}} f = F_{coll.} \tag{2.4}$$

where f denotes the distribution function. The Vlasov equation is a collisionless Boltzmann equation, in which the collisional term is neglected. It is written as[29]

$$\partial_t f(\mathbf{x},\mathbf{v},t) + \mathbf{v}\cdot\nabla_{\mathbf{x}} f + \frac{q}{m}\left(\mathbf{E} + \frac{\mathbf{v}}{c}\times\mathbf{B}\right)\cdot\nabla_{\mathbf{v}} f = 0 \tag{2.5}$$

These two equations can be used to determine the role of a magnetic field in fluid-like plasmas.

There are many phenomena in plasma physics that can be studied by thinking of the plasma as two interpenetrating fluids, an ion fluid and an electron fluid. In this approach, it is not necessary to consider the fact that each species consists of particles with different velocities so that the plasma can be treated as fluid flows. We use the normalization

$$n_s(\mathbf{x}, t) = \int d\mathbf{v}\, f_s(\mathbf{x}, \mathbf{v}, t) \tag{2.6}$$

and note that the fluid velocity $\mathbf{V}_s$ is

$$\mathbf{V}_s = \frac{1}{n_s} \int d\mathbf{v}\, \mathbf{v}\, f_s(\mathbf{x}, \mathbf{v}, t) \tag{2.7}$$

where f_s is considered as a probability density. Integrating (2.5) over all velocity space, we obtain the continuity equation

$$\partial_t n_s(\mathbf{x},t) + \nabla\cdot (n_s \mathbf{V}_s) = 0 \tag{2.8}$$

Multiplying (2.5) by $\mathbf{v}$ and integrating over all velocity space, using above equations and noting that

$$\nabla_{\mathbf{x}} \cdot \int d\mathbf{v}\, \mathbf{v}\, \mathbf{v}\, f_s = \nabla_{\mathbf{x}} \cdot (n_s \ <\mathbf{v}\, \mathbf{v}>) = \nabla\cdot (n_s \mathbf{V}_s \mathbf{V}_s) + \nabla P_s / m_s \tag{2.9}$$

We find

$$\partial_t \mathbf{V}_s + (\mathbf{V}_s \cdot \nabla)\mathbf{V}_s = \frac{1}{m_s n_s} \nabla P_s + \frac{q_s}{m_s} \mathbf{E} + \frac{q_s}{m_s c} (\mathbf{V}_s \times \mathbf{B}) \tag{2.10}$$

where P_s is pressure, which can be expressed as

$$\nabla P_s = \nabla (n_s T_s) = n_s \nabla T_s + T_s \nabla n_s = \gamma_s T_s \nabla n_s$$

and where γ_s is the ratio of specific heats and T_s is the temperature. The total charge density ρ is defined by

$$\rho(\mathbf{x},t) = \sum_s q_s n_s(\mathbf{x},t) \tag{2.11}$$

while the total current density **J** is defined by

$$\mathbf{J}(\mathbf{x},t) = \sum_s q_s n_s(\mathbf{x},t)\, \mathbf{V}_s(\mathbf{x},t) \tag{2.12}$$

When these combine with Maxwell's equations

$$\nabla\cdot\mathbf{E}\,(\mathbf{x},t) = 4\pi\rho \tag{2.13}$$

$$\nabla\cdot\mathbf{B}\,(\mathbf{x},t) = 0 \tag{2.14}$$

$$\nabla\mathrm{x}\mathbf{E}\,(\mathbf{x},t) = -\frac{1}{c}\,\partial_t\mathbf{B} \tag{2.15}$$

$$\nabla\mathrm{x}\mathbf{B}\,(\mathbf{x},t) = \frac{4\pi}{c}\,\mathbf{J} + \partial_t\mathbf{E} \tag{2.16}$$

we can study various kinds of waves in plasma.

Consider a case in which we assume quasineutrality; i.e., $n_{e1} \approx n_{i1}$ with $n_s = n_0 + n_{s1}$. Then we need the force and continuity equations to describe the plasma motion. From the linearized equations (2.8) and (2.10), we find

$$m_e n_0 \partial_t \mathbf{V}_e + \gamma_e T_e \nabla n_{e1} + e\, n_0\, \mathbf{E} + \frac{e n_0}{c}(\mathbf{V}_e \mathrm{x}\, \mathbf{B}) = 0 \tag{2.17}$$

$$\partial_t\, n_e(\mathbf{x},t) + n_0 \nabla\cdot\, \mathbf{V}_e = 0 \tag{2.18}$$

$$m_i n_0 \partial_t \mathbf{V}_i + \gamma_i T_i\, \nabla n_{i1} - e\, n_0\, \mathbf{E} + \frac{e n_0}{c}\,(\mathbf{V}_e \mathrm{x}\, \mathbf{B}) = 0 \tag{2.19}$$

$$\partial_t\, n_i(\mathbf{x},t) + n_0 \nabla\cdot\, \mathbf{V}_i = 0 \tag{2.20}$$

where the subscripts e and i represent the electron and ion respectively. These equations can be solved, and a dispersion relation can be obtained.

Therefore, based on the force equation, and combining it with the continuity equation and Maxwell's equations, we can study the wave propagating in plasmas. When a magnetic field is present, a variety of new modes will be generated in the plasma system.[29] The modes occurring in the presence of the magnetic field B_0 are: (a) Upper hybrid waves. They are high frequency waves traveling across the magnetic field and known as perpendicular longitudinal electrostatic waves. The electrons are performing a sort of gyromotion in the wave. The frequency $\omega^2=\omega_e^2+\Omega_e^2$ is higher than the wave where the magnetic field is absent, where $\omega_e^2=\frac{4\pi n_0 e^2}{m_e}$ and $\Omega_e=\frac{-eB_0}{m_e c}$. (b) Electrostatic ion waves. They are low frequency electrostatic waves whose physics is dominated by ions. Let us consider these waves in various limits. Define an angle θ as the angle between wave number $\mathbf{k}$ and magnetic field $\mathbf{B_0}$, we can find the following: (i) when $\theta=0$ and $k_x=0$, we have three solutions: $\omega^2=k^2c_s^2$, which is ion-acoustic wave; $\omega^2=\Omega_i^2$, which is ion-cyclotron wave; $\omega^2=\Omega_e^2$, which is electron-cyclotron wave; where $c_s^2=(\gamma_e T_e+\gamma_i T_i)/m_i$, $\Omega_i=\frac{eB_0}{m_i c}$ and $\Omega_e=\frac{-eB_0}{m_e c}$; (ii) when $\theta<\pi/2$, $1>>k_z/k_x>>(m_e/m_i)^{1/2}$, we have $\omega^2=k^2c_s^2+\Omega_i^2$; (iii) when $\theta=\pi/2$, $k_z=0$, two solutions are obtained: $\omega^2=k^2c_s^2+|\,\Omega_i\Omega_e\,|$; $\omega^2=0$. (c) Electromagnetic waves. They include waves traveling perpendicular to magnetic field and waves traveling parallel to the field. In the first case, there exist ordinary wave (O-mode) and extraordinary wave (X-mode), depending on the angle between electric field and magnetic field.

The dispersion relation for the ordinary mode is $\omega^2=\omega_e^2+k^2c^2$. This wave propagates as if there were no magnetic field. For the extraordinary mode, the dispersion relation is expressed as $\frac{k^2c^2}{\omega^2}$ $=1-\frac{\omega_e^2}{\omega^2}\frac{\omega^2-\omega_e^2}{\omega^2-\omega_{UH}^2}$. In the second case, there are right circularly polarized R-wave and left circularly polarized L-wave, i.e., $\omega_{L,R}=\pm\frac{\Omega_e}{2}+\sqrt{\omega_e^2+\Omega_e^2/4}$ with plus sign corresponding to L-wave and minus sign R-wave. (d) Alfven waves. These are low frequency parallel electromagnetic waves traveling along magnetic field, which combine ion motion with electromagnetic effects. The dispersion relation is $\omega^2=\frac{k^2V_A^2}{1+(V_A^2/c^2)}$, where Alfven speed $V_A^2=(B_0^2/4\pi\rho_m)^{1/2}$, $\rho_m=n_0m_i$. (e) Magnetosonic waves. They are low frequency perpendicular electromagnetic waves, traveling across magnetic field. The expression of dispersion relation is $\omega^2=\frac{k^2V_A^2}{1+(V_A^2/c^2)}$. (f) Drift waves. They are linear fluid waves in magnetized, inhomogeneous plasma. Spatial inhomogeneities can give rise to their own wave motions. The dispersion relation for electrostatic drift waves is $\omega=k_yv_{De}$, $v_{De}=\frac{v_e^2}{|\Omega_e|L_n}$ is electron diamagnetic drift speed, where $L_n\equiv-(\frac{1}{n_0}\frac{dn_0}{dx})^{-1}$.

The different modes described above can be excited simultaneously by a magnetic field. Therefore, in a magnetized plasma, there is a greater variety of natural modes of oscillation. This makes the system more complicated. A parametric excitation of electrostatic waves in magnetized plasmas has been

investigated.[48] The Vlasov-Poisson system of equations were used to derive a dispersion relation for electrostatic waves in a magnetized plasma in the presence of a uniform high-frequency electric field. Tzoar[49] has studied the excitation of long wavelength waves propagating perpendicular to the magnetic field and has derived a dispersion relation. The excitation of ion acoustic waves and purely growing ion modes in a warm plasma, when the driving frequency is near the resonant frequency of electron modes, was also studied.[50]

Nonlinear phenomena in a plasma system arise from wave-particle interactions and wave-wave interactions. Diffusion in a fully ionized gas is a nonlinear problem because the diffusion coefficient varies with density. Wave-particle interactions take place when the speed of particles is very close to the phase speed of the wave, such as is the case for the phenomenon of plasma echoes.[51] A nonlinear interaction between long and short waves can occur strongly if the phase velocity of the long wave coincides with the group velocity of the short wave. This kind of resonant interaction has been examined for long ion acoustic and short electron plasma waves [52] and other systems.[53,54] It is found that the chaotic state can appear even if only a single unstable mode exists.[55]

The magnetic field parallel to the turbulent flow at an ionizing shock front can couple directly into the two components of fluctuating velocities transverse to the axis of the flow. Thus the magnetized region can have at least two more degrees of freedom than the region where the magnetic field is absent. An

increase in the number of degrees of freedom would ordinarily be expected to increase the degree of instability in the system.

The effects of turbulent motion on magnetic fields were investigated by Steenbeck et al.[56] It was shown that in turbulent velocity fields the average crossproduct of velocity fluctuation and magnetic field fluctuation has a non-vanishing component parallel to the average magnetic field. The system they considered was an electrically conducting fluid in a turbulent motion. The calculations were base on the following assumptions: the magnetic field is weak, and the Lorentz force in the Navier-Stokes equation is correspondingly negligible. Under these assumptions it is possible to develop an electromagnetic theory for the mean values of fluctuating fields. The equations used are Maxwell's equations, which are linear relations between fields and remain valid for the mean fields; i.e.:

$$\nabla \times \bar{\mathbf{E}} = -\frac{\partial \bar{\mathbf{B}}}{\partial t}, \quad \nabla \times \bar{\mathbf{H}} = \bar{\mathbf{i}}, \quad \nabla \cdot \bar{\mathbf{B}} = 0.$$

Ohm's law is expressed as:

$$\bar{\mathbf{B}} = \mu \bar{\mathbf{H}}, \quad \bar{\mathbf{i}} = \sigma(\bar{\mathbf{E}} + \bar{\mathbf{v}} \times \bar{\mathbf{B}}).$$

where $\mathbf{i}$ is the electric current density, $\mathbf{v}$ is the velocity fluctuation of the fluid, μ is its permeability, and σ is its electrical conductivity. Setting $\mathbf{H} = \bar{\mathbf{H}} + \mathbf{H}'$, $\mathbf{H}'$ is fluctuation part and is calculated as a perturbation created by $\mathbf{v}'$ from

$$\frac{\partial \mathbf{H}'}{\partial t} - \frac{1}{\mu\sigma}\nabla^2\mathbf{H}' = \nabla \times (\mathbf{v}' \times \bar{\mathbf{H}}) \tag{2.21}$$

It follows from (2.21) that

$$H_i'(\mathbf{x},t) = (\delta_{il}\,\delta_{jm} - \delta_{im}\,\delta_{jl})\,\mathbf{x} \int_0^t dt' \int d\mathbf{x}' \frac{\partial}{\partial x_j}[v_l(\mathbf{x}',t')\,\bar{H}_m(\mathbf{x}',t')]\,\Gamma(\mathbf{x}-\mathbf{x}',t-t')) \tag{2.22}$$

where

$$\Gamma(\mathbf{x},t) = \left(\frac{\mu\sigma}{4\pi t}\right)^{3/2} e^{-\mu\sigma x^2/4t},$$

$d\mathbf{x}'$ denotes the element of volume, and δ_{il} is the unit tensor. The mean value of $\mathbf{v}' \times \mathbf{H}'$ is given as

$$\overline{\mathbf{v}' \times \mathbf{H}'} = \gamma\mu\sigma\overline{v'^2}\,L^2\{-\frac{1}{3}\nabla(\log\sqrt{\overline{v'^2}})\times\bar{\mathbf{H}} - \frac{4T}{15}[4\,\bar{\mathbf{H}}\,\boldsymbol{\omega}\cdot\nabla(\log\rho\sqrt{\overline{v'^2}}) - (\bar{\mathbf{H}}\cdot\boldsymbol{\omega})\nabla(\log\rho\sqrt{\overline{v'^2}}) - \boldsymbol{\omega}\,\bar{\mathbf{H}}\cdot\nabla(\log\rho\sqrt{\overline{v'^2}})]\} \tag{2.23}$$

where γ is a dimensionless factor of the order of magnitude unity. This result shows that the mean value of the product $\mathbf{v}'\times\mathbf{H}'$ possesses a nonzero component in the direction of $\bar{\mathbf{H}}$. The consequences of this effect for rotating, electrically conducting plasma were considered.[57]

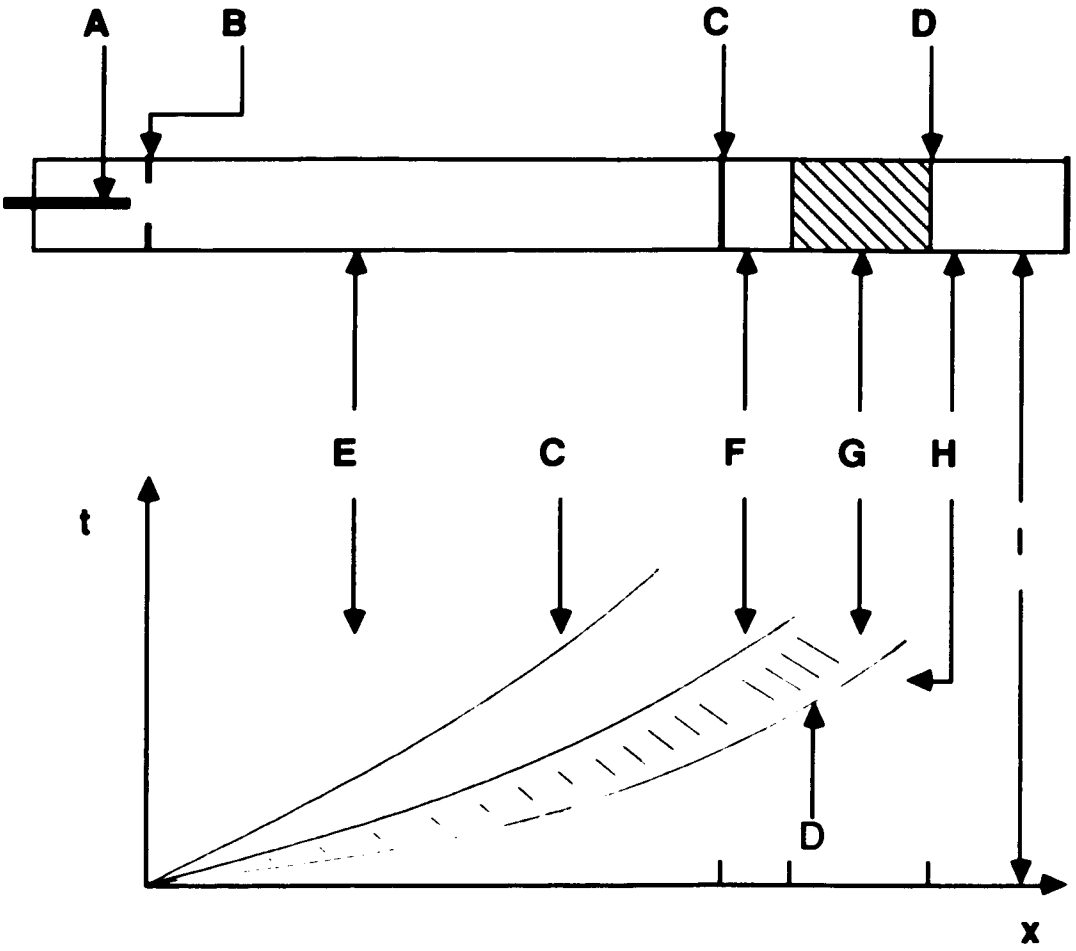

Figure 2.1 An x-t Diagram

A and B: Discharge electrodes.

C: Contact surface.

D: Shock front.

E: Hot expanding discharge heated plasma.

F: Post-shock equilibrium plasma.

G: Post-shock transition plasma.

H: Weakly ionized precursor.

I: Pre-shock equilibrium gas.

Chapter III Experiment

This chapter describes the experimental apparatus used to obtain turbulent plasma density profiles in the arc driven shock tube. A brief description of the operation of the shock tube is followed by an overall description of the tube. Subsequently, the mechanical, optical, and electronic design of the apparatus is described. Finally, the items of equipment for collecting and analyzing data are discussed.

The shock waves are produced in a cylindrical arc discharge shock tube of 5 cm diameter and 210 cm overall length filled with argon. The discharge is generated symmetrically through a ring electrode by triggering a capacitor charged to 15~20 kV. The principal diagnostic port has three windows arranged at 90° intervals for fluorescence induced resonance radiation, a port for the ion probe being arranged such that all these measurements are made at the same axial location. Magnetic coils are placed so that the diagnostic port is in the center of the set of coils and a magnetic field is generated which is parallel (or antiparallel) to the direction of the shock wave. The shock speed can be varied between 3.3 x10^3 m/s and 2.0 x10^4 m/s for different initial filling pressures and discharge voltages. This corresponds to a range of ionization between 1% and 100%, and typically plasmas of N_i~10^{16}/cm^3 and T_i~5 eV.

Data processing and analysis are accomplished using an Apple Mac IIx with real time data acquisition from a set of Nicolet 440 ADC's. The transient recorders provide time histories

for Ar^+ florescence and two measurements of the ion probes at two different positions at a 10 MHz sampling frequency. Phase space trajectories, chaotic dimensions, power spectra, correlation functions and time scales can thereby be obtained.

3.1 Arc Driven Shock Tube

A shock tube is essentially any device in which a shock wave is produced. The conventional shock tube uses a diaphragm separating a gas at high pressure from one at lower pressure. A plane shock wave is generated by sudden bursting of the diaphragm. Numerous strong shock devices have been developed. One of them is the arc driven shock tube used in our experiment. A compression wave is formed in the gas after a large amount of the electric energy from the capacitor is suddenly released, this wave rapidly steepening to form a shock front. Vibrational relaxation times in gases at ordinary temperature are usually measured by studying supersonic dispersion; at high temperatures the shock tube has proved a valuable supplementary tool. The gases behind strong shock waves are highly ionized by the high temperature, and results are therefore of interest in relation to work in plasma physics. In addition, turbulent flow in plasmas may be created by shock tubes for studies of high temperature plasma fluctuations.

3.1.1 Shock Tube Set-Up

The experiments reported here are performed in a cylindrical arc discharge shock tube. The major part of it is made of stainless steel, which shows superior corrosion resistance, very low vapor pressure and thermal conductivity, and it is almost nonmagnetic. It consists of a driver section, a driven section and a

test section. The overall layout is shown in Figure 3.1. The total length of the tube is approximately 2 meters, and the inner diameter is 5 cm.

The driver section of our tube is constructed of a 10 cm long brass tube outfitted with two electrodes. To keep the discharge symmetric, a stainless steel ring of 4 cm inner diameter and 2 mm thickness is used as the cathode which is grounded through the tube wall. An 8 cm long and 6 mm diameter threaded steel anode is put through the center of a 2.5 cm thick plastic plate which closes the end of the driver section and insulates the anode from the tube wall. A schematic drawing of the driver section is shown in Figure 3.2.

A stainless steel tube of 150 cm length is the driven section connected to the driver section via an O-ring seal. There are three ports separated by 15 cm at the end of the tube for electric probes and two ports with the same separations for pressure transducers. Another port is for the gauge monitoring the pressure in the tube .

The main test section is a tube of 14 cm length. It possesses 3 optical windows of 2 cm diameter which allow fluorescence induced resonance radiation measurements. These quartz windows can stand the high power of the incident laser beam, and have a 1/4 wave flatness. It also contains a port for an ion probe. This port is radially located in the middle of the section and about 160 cm from the discharge. The section is enclosed externally by a set of magnet coils producing the magnetic field. The current through the coils is provided by a dc power supply of 0-30 A.

There is a switch between the dc power supply and coils so that the coils will not be over heated by turning off the switch after each run. Figure 3.3 gives a schematic view of the test section.

Another 33 cm long section is added to the test section, which makes certain that the reflected shock wave passes through the test point after data collection is finished and therefore does not affect the measurement.

3.1.2 Charge and Discharge System

Details of the discharge system are showed in Figure 3.4. It consists of the following components:

(1) Electrodes in shock tube driver section.

(2) High voltage power supply

The output of it is between 0-30 kV. It is used to charge the capacitor from -15 kV to -20 kV.

(3) Trigger System

a. Oscilloscope

Its trigger output sends out a pulse to trigger the generator.

b. Trigger generator

It is made by Maxwell, with four outputs which supply a positive or negative 40 kV pulse.

c. Air gap switch

It receives signals from the generator to turn on the discharge.

(4) 14.5 μF and 40 nH capacitor

It serves as an energy bank for the discharge.

(5) 30 kΩ charging resistors

They are used for limiting the charging current.

(6) Isolating chokes

They are used to isolate the big transient discharge current.

(7) Switches

The operating voltage of this relay is 25 kV. It is used to connect or isolate the power supply and the capacitor.

(8) Mechanical safety grounding switch

It is used to dump the capacitor charge.

The arc discharge shock tube is fired by discharging voltage at a 14.5 microfarad capacitor. The capacitor is charged to high voltage through a charging resistor. Normal operating voltage is -15 to -20 kV, corresponding to stored energies of 1.6 kJ to 2.9 kJ. A trigger signal coming from an oscilloscope triggers the pulse generator. The high voltage generator sends out four channels of 40 kV pulses to create four streamers between the electrodes of the switch. Once the air in the switch gap is broken down, a uniform arc is formed, which brings the voltage on one side of the capacitor very close to ground and forces the other side to positive high voltage. As a result, a strong shock wave is produced.

3.1.3 Shock Tube Calibration and Operation

The plasma studied in this experiment is produced in the arc driven shock tube. Different sections of the tube are connected by

means of O-ring gasket made by Viton. Those ports in the test and driven section are also based on O-ring seals. The system is evacuated to lower than 10^{-6} Torr before each filling gas. The leak rate at isolation is less than $9x10^{-6}$ Torr/min.

The overall configuration is chosen so as to minimize the influence of reflected expansion waves on measurements of the shock front in the test section. Typically, the first expansion waves arrive at the test section at least 350 μs after the discharge, while all measurements are finished in less than 200 μs.

Firings of this tube using electrodes have shown an adequate Mach number range even when the diaphragm is not used. The discharge voltage is varied between 15 kV and 20 kV, and initial filling pressure is varied from P_1=20 mTorr to 250 mTorr. By changing the discharge voltage and filling pressure independently, the shock wave's Mach number at the test section can be varied from M=10 to M=60. The Mach number increases as the discharge voltage does. Higher filling pressure results in lower Mach number. Therefore, we have options to fixing Mach number by choosing different sets of discharge voltage and pressure. Figures 3.5 and 3.6 show the relation between Mach number and the pressure. The result of Mach number versus discharge voltage is given in Figure 3.7.

As the shock propagates downstream, its speed slows down very rapidly at the beginning and appears to approach a steady speed.[58] The measurements are done 160 cm from the discharge where the shock wave has reached a nearly steady speed and the noise induced by discharge vanishes.

The intensity of the external magnetic field can be varied between 0 and 600 gauss by changing the current through the coils from 0 to 10 amperes. The field is produced either parallel or antiparallel to the direction of shock propagation. The switch installed between the dc power supply and the coils is only turned on just before each firing to avoid overheating the coils.

There is signal noise caused by the electromagnetic field immediately after firing. The signal collecting system, especially the electronic equipment, is sensitive to the noise. To reduce the signal noise level, the analog to digital converter is grounded through the power supply and shielded in a grounded aluminum box. It is found that the length of the coaxial cable influences the signal noise level.

All of the experiments reported upon in this thesis used argon as a fill gas. In general, the firing condition options correspond to a range of ionization between 1% and 100%, and typically plasmas of $N_i \approx 10^{16} cm^{-3}$ and $T_i \approx 5$ eV.

3.2 Diagnostics

The techniques for measuring the properties of plasmas, generally referred to as plasma diagnostics, have played a critical role in advancing our knowledge of plasma physics. The task of determining with strictly noninvasive techniques the many significant plasma parameters that are varying in complex spatial and temporal patterns remains a formidable challenge. Diagnostic methods can be and, in many cases, are based on phenomena which are only remotely related to intrinsic plasma characteristics; thus in each instance, there should be a well understood connection between such properties and the condition of the plasma.

The development of plasma diagnostics has a somewhat interdisciplinary character, borrowing methods from many branches of physics including optics, spectroscopy, high-energy physics, microwave technology, and fluid mechanics. We will discuss in detail the two diagnostic methods used in our experiment. They are laser induced fluorescence and the electric probe.

3.2.1 Laser Induced Fluorescence (LIF)

Laser induced fluorescence is a sensitive diagnostic method with wide applicability in plasma and fluid physics. The LIF method was used to investigate the structure and dynamics of round turbulent jets.[59] A quantitative two- and three-

dimensional LIF images of the scalar field in fully turbulent flows were obtained.[60,61] Different ways of using resonant laser excitation of ions in plasmas have been conceptually explored. The technique is very useful in argon plasmas and can be used to observe ion density fluctuation.[62] The technique has the advantage that no material probe is inserted into the plasma so that there is a greatly reduced possibility of contamination.

The probability for excitation per particle is the basic parameter underlying the processes, which is $P=\int N(\upsilon)\sigma(\upsilon)d\upsilon$. Here the absorption cross section $\sigma(\upsilon)$ at resonance tends to the limit $\lambda^2/8\pi$. For wavelength λ in the visible region, the magnitude of it is about 10^{-11} cm^{-2}, which is much larger than the Thompson or Raman cross sections.

LIF occurs as a result of the emission of photons when an excited ion or molecule decays back to its ground state. A moderate power laser, operating at a frequency that coincides with the frequency of an emission line, can selectively excite a large number of the appropriate particles into the upper state of the transition along the path of the laser beam. This will cause an intensification of the spontaneous emission, which can be explained as scattering of the laser beam, from the volume exposed to the laser radiation. If this enhanced emission can be distinguished from the background radiation emanating from the rest of the plasma, it will provide useful localized information about the state of the plasma. An important feature of this technique is that if the upper level of the laser excited transition

gas has alternative radiative decay modes, a frequency different from that of the laser can be monitored.

Consider the case in which, along a 488.0 nm laser beam, argon ions in the initial state $4s^2P_{3/2}$ are excited into a upper state $4p^2D_{5/2}$. Ions in the upper state can decay either to the $4s^2$ state with emission of a 488.0 nm photo or to the $4s^4P_{3/2}$ state with emission of a photon at 422.8 nm. The fluorescence intensity, or the number of photons emitted, is proportional to the number of excited ions, which in turn is proportional to the number of ground state ions as well as the illuminating light intensity. Therefore, following excitation by the laser beam, the fluorescent emission of either 488.0 or 422.8 nm radiation provides a diagnostic of the condition of a target ion.

In our experiments, a 7 Watt 488.0 nm laser beam from an Ar^+ laser made by Coherent is sent through the shock tube at an optical window and is focused to a 0.5 mm diameter by means of a convex lens at the test point. The fluorescence signal is picked up at the other window which is perpendicular to the one through which the laser beam travels. A filter which transmits at 422.8 nm is placed in front of a fiber-optic light pipe so that only fluorescent emission of the 422.8 nm radiation is obtained. An aperture with 50 μm diameter pinhole is placed between two lenses to reduce the stray light and improve the spatial resolution. The optical signal is collected by a photomultiplier tube (PMT). It is an extremely sensitive light detectors, providing a current output proportional to the light intensity. The tube is quoted by the manufacturer as having good time response of 12 nsec and

very low background noise. The light collecting system is in an aluminum box which is painted black on the inside. The sketch of the laser light source arrangement and light collection optics is given in Figure 3.8.

3.2.2 Electric Probe

The electric probe has been extensively used for plasma diagnostics and has been one of the major tools in the study of plasma waves, instabilities and turbulence. The technique was developed by Langmuir in 1924 and is therefore sometimes called the method of Langmuir probes.

Simply stated, an electrostatic probe is merely a small metallic electrode, usually a wire, inserted into a plasma. They are very simple devices. Basically, compared to many other diagnostic tools the probe is distinguished by the possibility of direct local measurement of plasma parameters; most of techniques give information averaged over a large volume of plasma. The conducting probe immersed in a plasma will emit or collect current, depending on the voltage impressed. The probe is attached to a dc power supply capable of biasing it at various voltages positive and negative relative to the plasma, and the current collected by the probe then provides information about conditions in the plasma. Ion density, electron density, and electron temperature can be measured by varying the bias voltage on the probe.[63,64] Density fluctuations can be monitored when the probe is biased at its saturation voltage.[64]

In the case of no magnetic field, when the bias voltage is made very negative, almost all the electrons are repelled and only ions are collected. The random ion current passing through an area in the plasma is related to the ion density and the velocity.[65] It was shown[66] that ion saturation current is

$$I_i \propto \alpha\, p_1 M$$

where $\alpha = \frac{n_i}{n_i+n_e}$ = the ionization degree,

p_1 = filling pressure,

M = Mach number.

We can see that the current is linearly proportional to the ion density flux and the flow velocity. In the lab frame, the fluctuation of the flow velocity is very small compared with the density fluctuation. Hence we can assume that the current fluctuation observed is linearly proportional to the density fluctuation.

In the presence of a magnetic field, the ion saturation current is not much affected until the field strength is fairly large. The insensitivity exists because the ion gyroradius is much bigger than that of electrons.[65]

The presence of the probe produces a perturbation in the plasma. However, it will not influence the proportional property of the current with ion density. Along with the perturbations caused by the probe in the plasma, there are also certain plasma perturbations upon the probe. Probe deterioration is the most

serious of these. A probe immersed in plasma suffers continual particle bombardment, which evaporates away metal from the probe, and plates it on surrounding surfaces, including the insulating probe support. This may either decrease or increase the current-collecting area, depending on whether the metal gets away or is plated onto the insulating support adjacent to the probe tip.

Several different kinds of probes have been tested in a previous experiment.[66] Our choice has the advantages of low cost, good mechanical strength, small local disturbance, high frequency response, good spatial resolution and high reliability. It is a straight probe with a 0.75 mm diameter stainless steel wire, which is welded to a BNC connector and enclosed by a 1.5 mm OD 99% ceramic insulating tube. Probes are inserted radially into the tube via O-rings. A schematic view of the electric probe is shown in Figure 3.9.

A BNC cable connects the electric probe to a circuit which provides a bias voltage. Figure 3.10 gives a schematic description of the probe circuit. The whole circuit is shielded by an aluminum box. The probe bias voltage can be adjusted by using a variable resistor. A switch is used for changing the polarities of the voltage on the probe. An ion current signal is sent to a data acquisition system by a BNC cable.

To observe ion density fluctuations in the present experiment, the electric probe is biased at the region of saturation ion current. The region is a fairly flat portion of the probe characteristic, and is obtained point by point in a pulsed discharge,

the probe bias being changed from pulse to pulse. In other words, the discharge voltage and filling pressure are fixed while changing the bias voltage. The ion current saturates when the absolute value of bias voltage is greater than 5 V; the probe arcs to the wall of the tube when it is greater than 20 V. Usually, the probe is biased at -7 V to collect saturated ion current. Typically, the probe current is less than 2 mA and lasts less than 0.1 ms in our measurements.

The plasma sheath around the probe only extends a few Debye lengths (~10^{-5} cm); hence we expect that the potential perturbation is negligible. Since the probe size is much greater than the particle mean free path (~10^{-2} to 10^{-3} cm) in this region, the probe might create some density disturbances. It has been shown that the density perturbation is localized and not carried downstream by the flow behind the shock front.[7]

The probe operation is affected seriously by the impurity on its tip. The shock tube discharges leave impurities on the collecting area of the probe (including the insulating tube), especially on the side facing the direction of the primary shock wave propagation. It is therefore necessary to clean the probe tip from time to time.

The two ion probes used are separated from each other by 13 cm; one is located upstream from the magnetic coils while the other is located in the test section and coincident with the source of resonance radiation. The shock speed can be obtained by ion signals collected at these two stations.

3.3 Data Acquisition

Ion probe and fluorescence signals are digitized and recorded simultaneously in an analog to digital converter (Nicolet model 440) using frequency of 10 Megasamples per second. This four channel model is configured with 12-bit digitizers and has a range from 30 mV to 120 V. Its recording length can be varied and the maximum length is 64,000 samples per channel. We use one of the channels for the electric probe located upstream from the magnetic coils, one for the electric probe located in the test section, and two with different amplifications for the fluorescence signal. The post-trigger delay of the ADC is 10^9 x (selected time per point). The external trigger signal to the ADC comes from the output of an oscilloscope which also triggers the discharge. The delay time is set in the Nicolet since it takes some time (in the order of 10 microseconds) for a shock wave to reach the test point. When the shock wave comes, there is a big increase in ion density. The 12-bit resolution is very important if we are to observe those density fluctuations behind the shock front. The signals received are stored on the diskettes.

Data processing and analyses are accomplished in a Macintosh IIx. First, the Nicolet DOS files must be translated into Macintosh files. This takes place in two steps: The first translation produces a binary file; the second combines the binary bytes into numbers that can be manipulated. Data analyses are done by using Macspin, and various other codes of our own design developed under Macintosh Programmers' Workshop software.

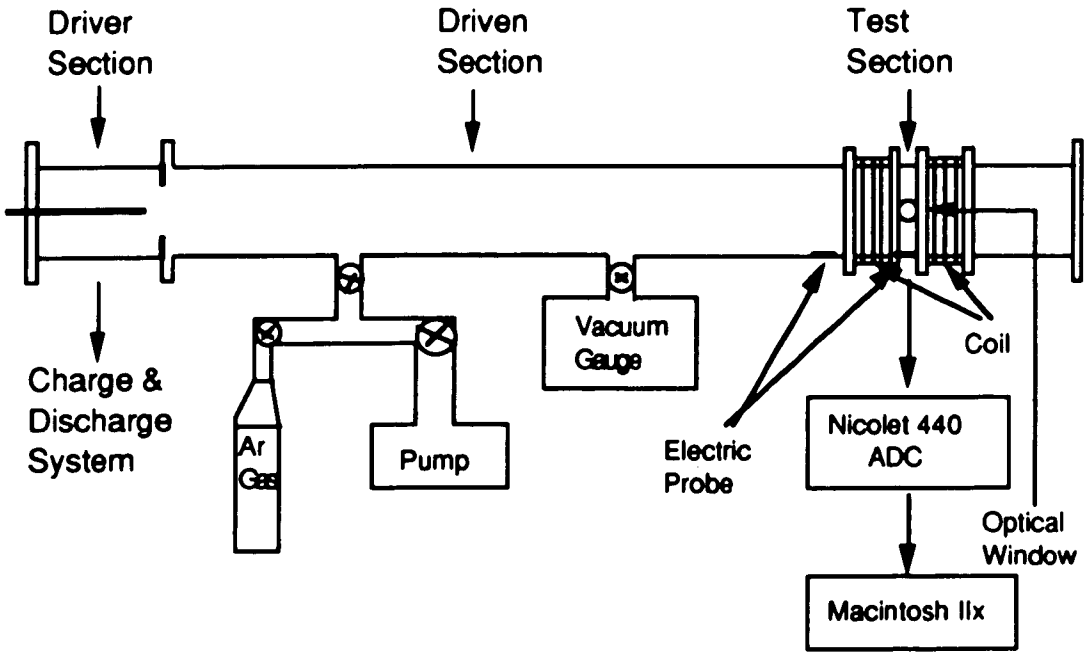

Figure 3.1 Arc Driven Shock Tube

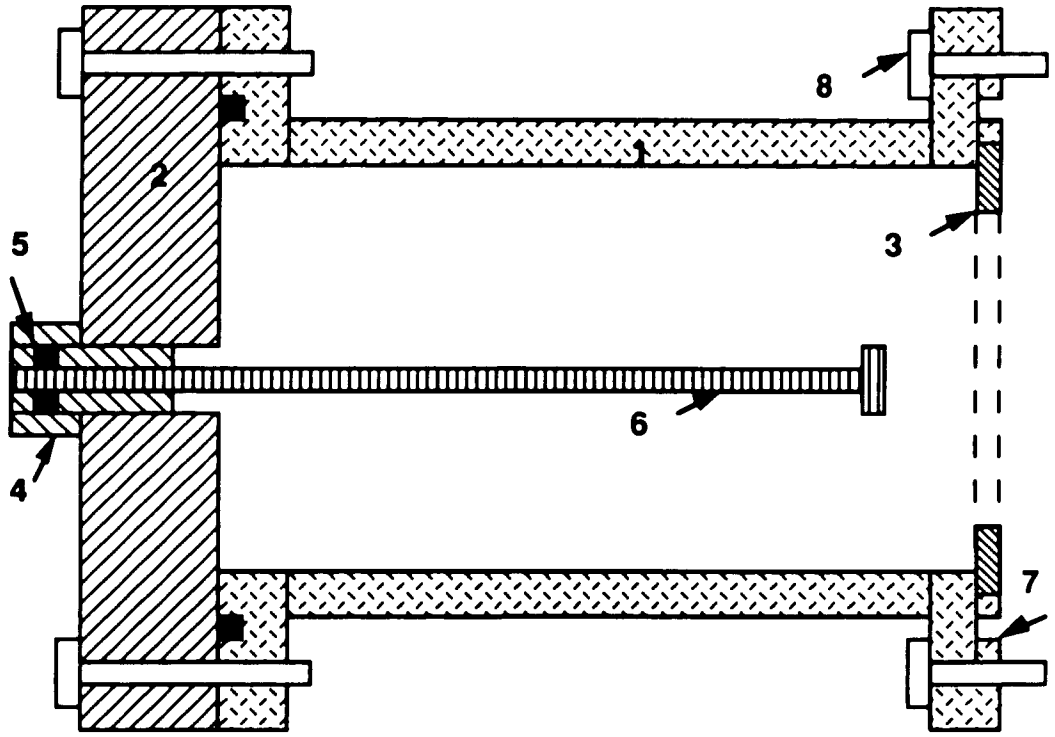

Figure 3.2 Driver Section

1. Brass tube. 2. Plastic end plate. 3. Steel ring electrode (cathode). 4. Swage lock. 5. Viton O-ring. 6. Allen cap screw (anode). 7. O-ring groove. 8. 1/4" screw.

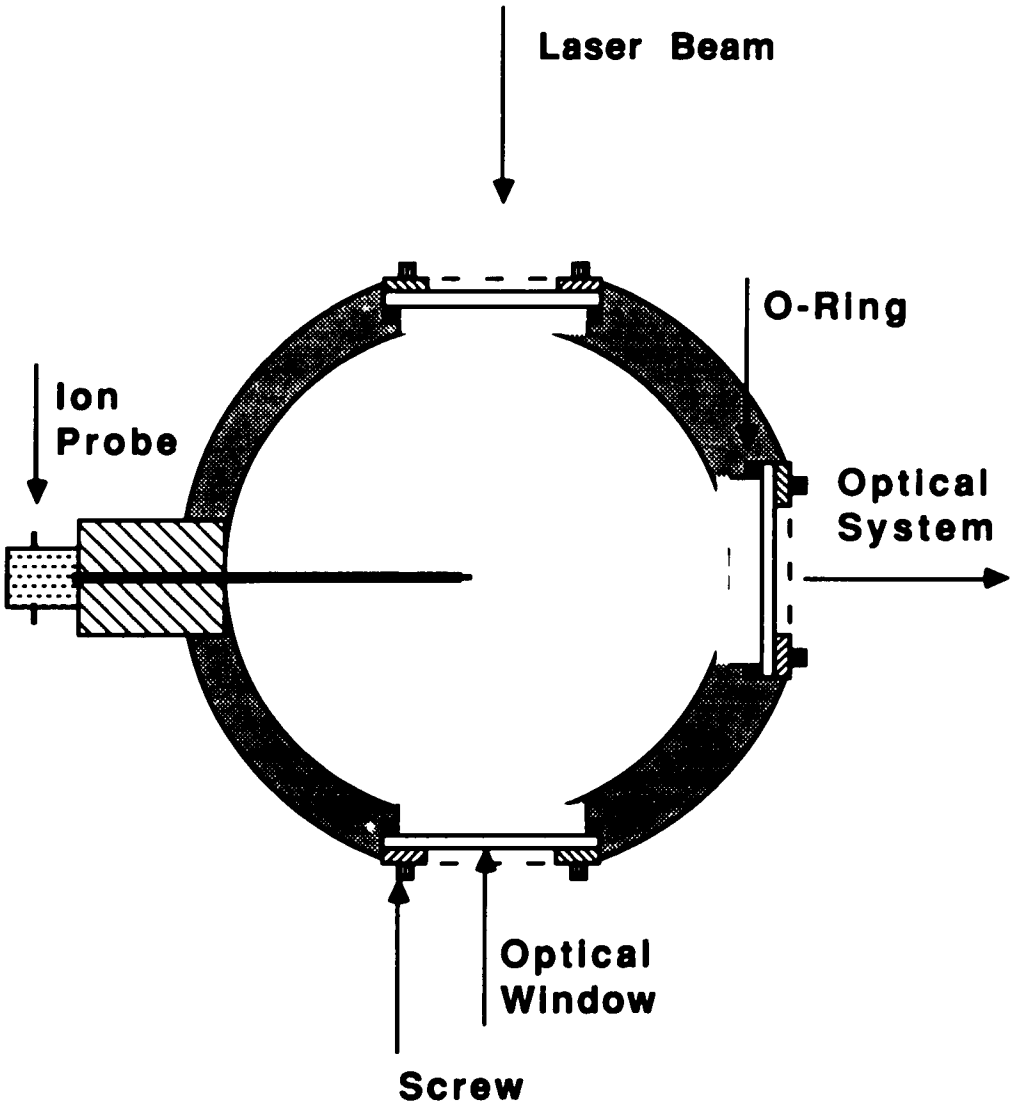

Figure 3.3 Test Section

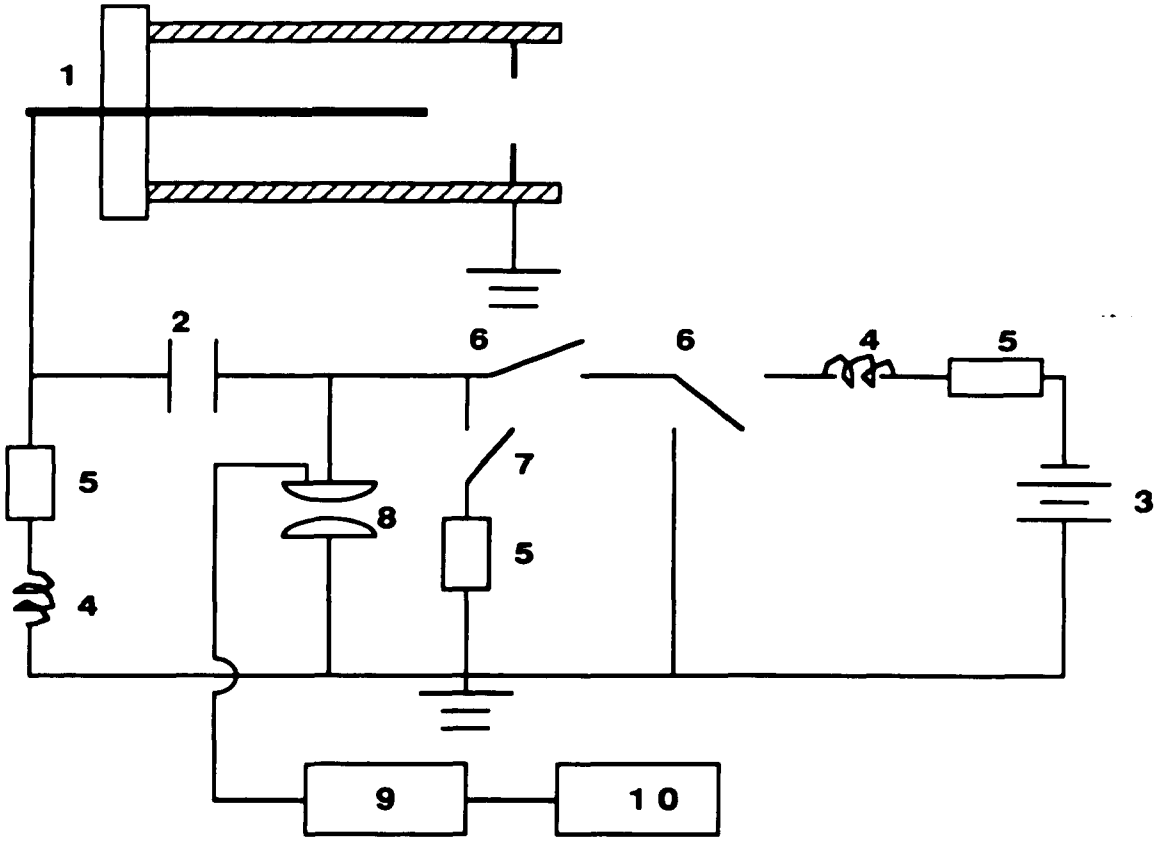

Figure 3.4 Charge and Discharge System.
1. Driver section 2. 14.5 μF capacitor. 3. High voltage power supply. 4. Isolating chokes. 5. 30 kΩ charging resisters. 6. Switches. 7. Mechanical safety switch. 8. Air gap switch. 9. High voltage pulse generator. 10. Oscilloscope.

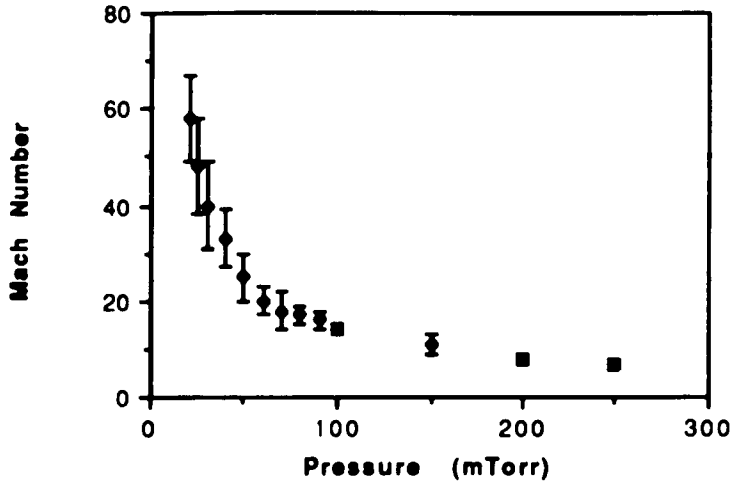

(a)

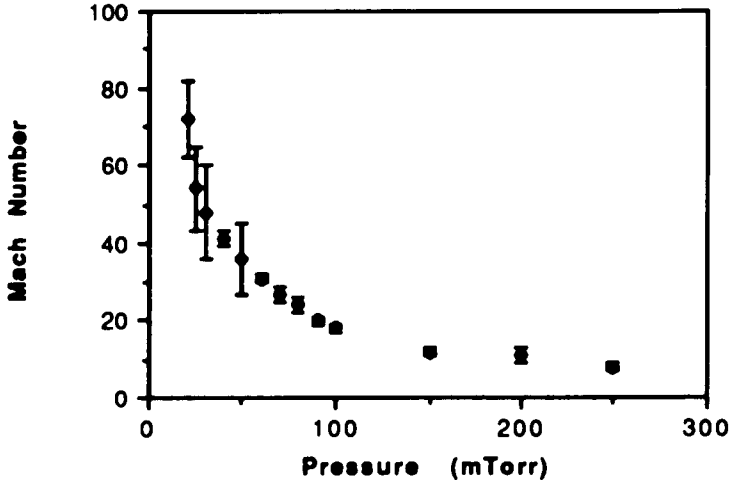

(b)

Figure 3.5 Mach Number versus Pressure

(a) Discharge voltage = 17 kV

(b) Discharge voltage = 18 kV

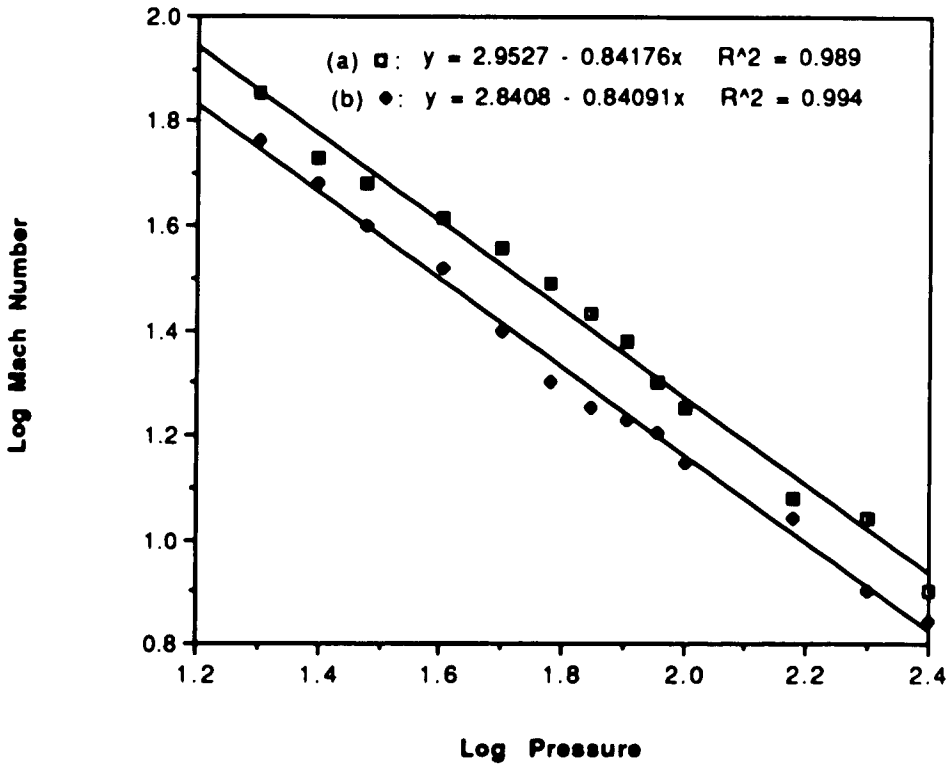

Figure 3.6 Mach Number versus Pressure (logarithmic plot)

(a) Discharge voltage = 17 kV

(b) Discharge voltage = 18 kV

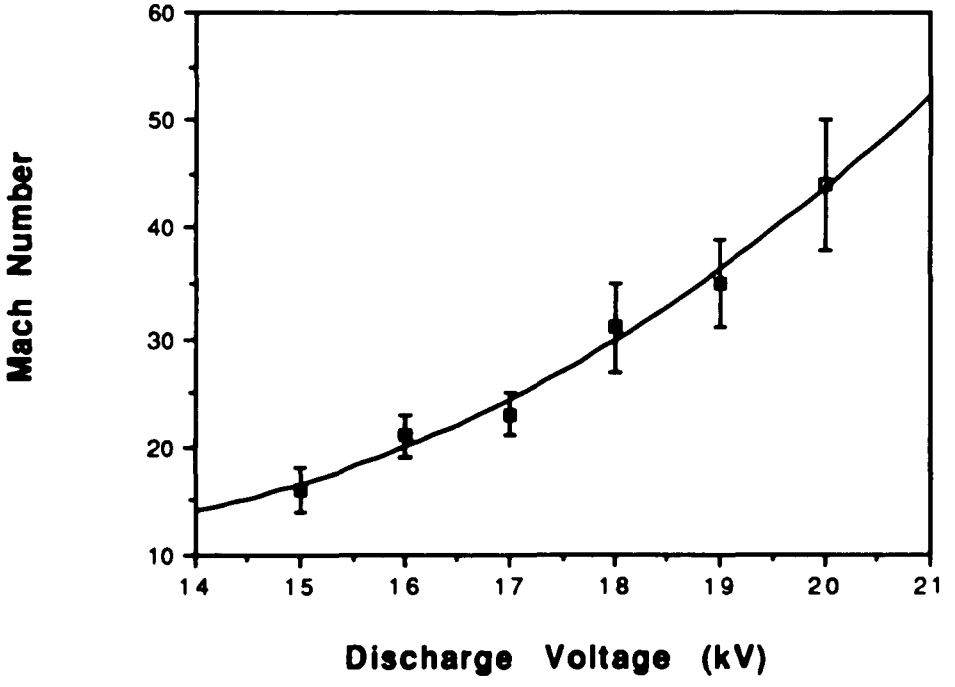

Figure 3.7 Mach Number versus Discharge Voltage
Pressure = 60 mTorr

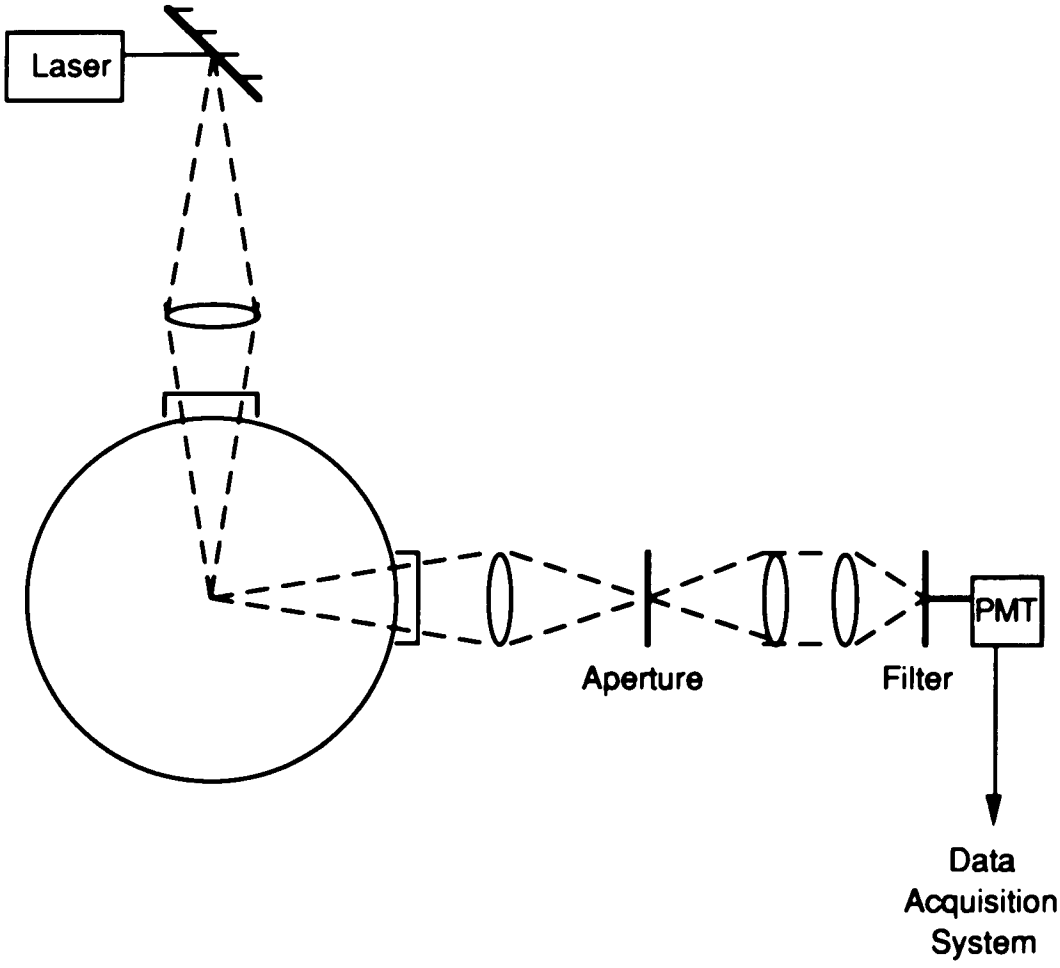

Figure 3.8 Fluorescence Signal Collecting System

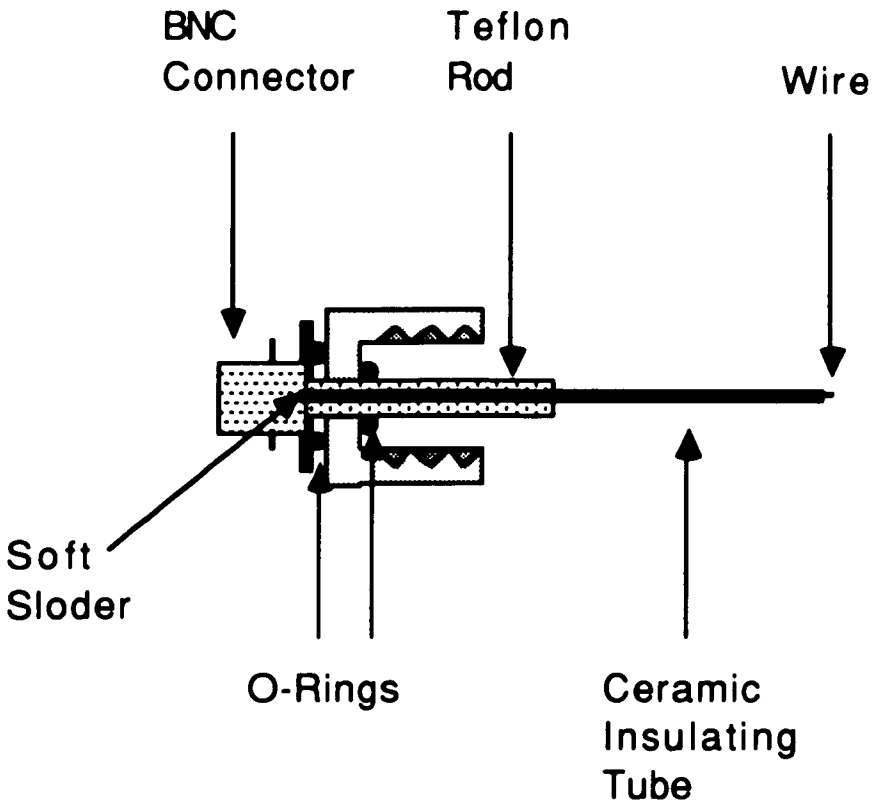

Figure 3.9 Electric Probe

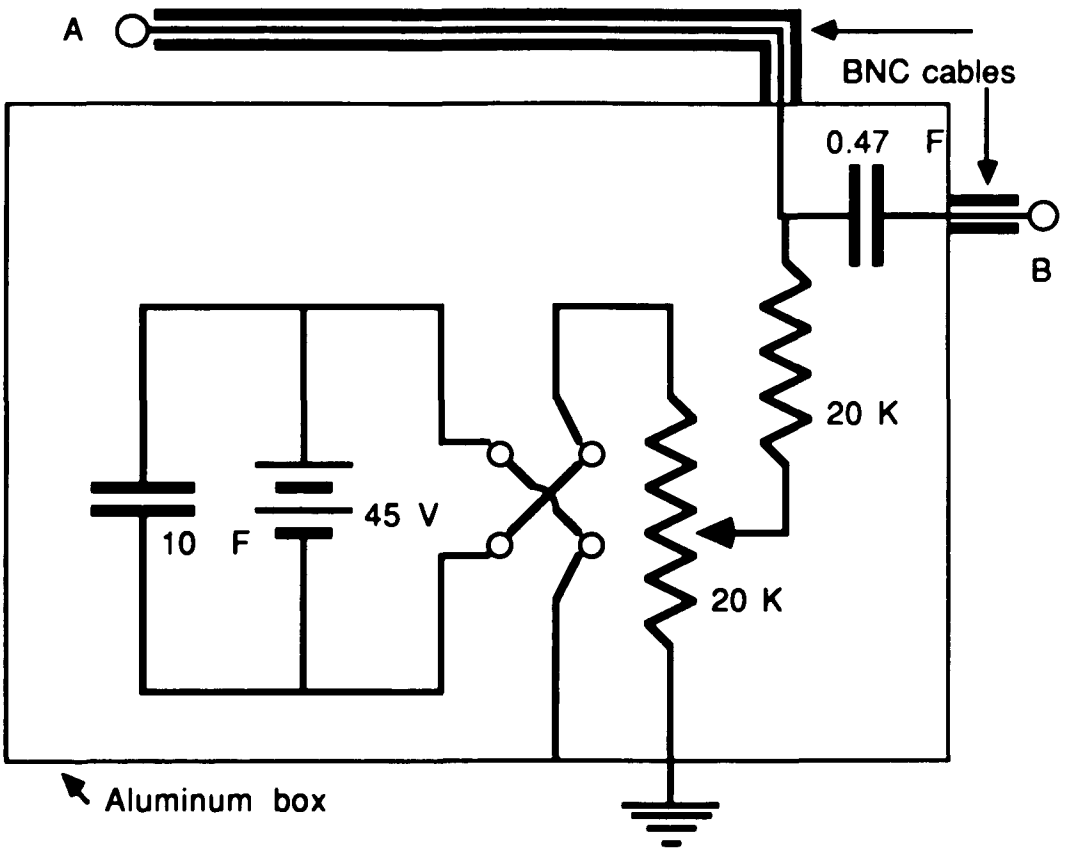

Figure 3.10 Probe Circuit

A: To electric probe.

B: To 50 Ω resistive load and data acquisition system.

Chapter IV Analytical Techniques

A variety of analytic and computational tools may be used in the study of turbulent systems. A dimension determination using nonlinear approaches may describe the statistics of fluid turbulence. The power spectrum is computed using Fourier analysis in order to display the frequency composition of the time variation of the dynamical variables and to derive the power law behavior. Correlation techniques can be used to obtain information regarding the statistical characteristics of the turbulence. The analytical tools we employ are Fourier transform, correlation method and fractal dimensional analysis.

4.1 Fourier Transform and Correlation Methods

The Fourier transform is one of the ways to identify and to characterize a dynamical regime. The usefulness of the Fourier spectrum is that it reveals the periodic properties of the evolution of fluctuations in the system. A Fourier transform can be applied to continuous functions, as well as to discrete sequences, with integrals replacing summations. Since we are implementing spectral analysis techniques with a digital computer, it is necessary to Fourier transform the sampled time data lengths into the frequency domain via the discrete Fourier transform. We define the Fourier transform of a discrete time series x_j to be the operation creating a corresponding discrete series x_k such that:

$$x_k(f_k) = \frac{1}{\sqrt{N}} \sum_{j=1}^{N} x_j \exp(-i \frac{2\pi jk}{N})$$

$$k = 1, \ldots, N$$

$$i = \sqrt{-1} \text{ pure imaginary}$$

$$f_k = k\,\Delta f = k \frac{1}{t_{max}}, \qquad t_{max} = N\,\Delta t.$$

For convenience we have taken Δt as the unit of time.

The graph representing $|x_k|^2$ as a function of the frequency f is called the power spectrum. The area under each peak in the spectrum is proportional to the strength of that mode. Several theories and experiments concerned with the spectrum

of plasma turbulence indicate that in the turbulent state, the power spectrum falls off as f^{-n}; a large spread in the values of n, $1 \leq n \leq 7$, has also been noted,[67-69] where n can be obtained from the slope of the plot of log $|x_k|^2$ versus logf. For example, Noon *et al.*[70] have observed n=1.0; Hooper[67] has reported n=3.65; Smith and Powers[68] have obtained n=5.00. Fourier spectra are an indicator of the existence turbulent motion. Therefore, it is possible to determine experimentally the spectral index n from the power spectra, and determine if the plasma in our discharge is turbulent.

In principal, there is no difficulty in using the formula to calculate $|x_k|^2$ explicitly. But in practice, the extent of the task becomes substantial as soon as N takes on appreciable values. However, when N is a power of two, an algorithm, called a Fast Fourier Transform (FFT), permits calculation of the spectrum with a tremendous saving in computer execution time relative to the direct Fourier transform. Therefore, FFT has been applied to compute the Fourier transform.

Correlation methods have been used in communications analyses, control theory, the testing of electronic equipment, the study of fluid turbulence, and in plasma physics. There are numerous discussions of the procedures in the literature.[71,72] Such techniques have proven to be very powerful as averaging techniques, for measuring phase velocities, etc., in plasmas, and for the qualitative study of statistical effects.[67] Correlation methods can be used to obtain information regarding the statistical characteristics of the turbulence.

One use of correlation techniques is to determine whether and to what extent different signals are related. The autocorrelation function measures the correlation between subsequent signals. It remains constant or oscillates for regular motion and decays rapidly (mostly with an exponential tail) if the signals become uncorrelated in the chaotic regime.[73] The correlation $R(\tau)$ between the values of x at two different times is called the autocorrelation. It is defined as

$$R(\tau)=\langle x(t)x(t+\tau)\rangle/\langle x(t)^2\rangle$$

where $\langle x(t)x(t+\tau)\rangle = \lim_{T\to\infty}\frac{1}{T}\int_0^T dt\, x(t)x(t+\tau)$ in a continuous case, and $\langle x(t)x(t+\tau)\rangle = \frac{1}{n}\sum_{j=1}^{n} x_{j+\tau}x_j$ for discrete signals. The Wiener-Khinchin theorem states that the autocorrelation function is merely the Fourier transform of the power spectrum of the quantity of interest:

$$\langle x(t)x(t+\tau)\rangle = \frac{1}{n}\sum_{k=1}^{n} |x_k|^2 \cos\left(\frac{2\pi\tau k}{n}\right)$$

where the Fourier transform has been defined above.

From the autocorrelation profile, two characterizing time parameters are determined. A characterizing correlation time τ_c is calculated from $\tau_c=\int_0^{t_z} R(\tau)d\tau$, where t_z is the value of τ for which $R(\tau)$ first becomes zero.

A small correlation time τ_s is generally considered a measure of the dimensions of the smallest structure or the lifetime of the most rapidly decaying structure. It is defined by the curvature of the autocorrelation coefficient at the origin:

$$d^2R/d\tau^2 \mid_{\tau=0} \equiv -2/\tau_s^2$$

Expanding R in a Taylor series about the origin, we can write, for small τ,

$$R(\tau) \approx 1-\tau^2/\tau_s^2$$

4.2 Fractal Dimension

Dissipative dynamical systems which exhibit chaotic behavior often have an attractor in phase space which is strange.[19,20,74] Fractal dimensions give a useful indicator for characterizing chaotic flows and strange attractors of the systems. Strange attractors are typically characterized by a fractal dimensionality D which is smaller than the number of degrees of freedom. Dimension is perhaps the most basic property of an attractor. So far, this fractal dimension has been the most commonly used measure of the "strangeness" of attractors.

The dimension of an attractor is the first level of knowledge necessary to characterize its properties. The dimension of an object gives information about its degree of complexity. Takens' theorem[75] states that the important properties of an attractor can be reconstructed from a single component. An ultimate objective of the analyses would be to derive an estimate of the minimum number of phase space dimensions required to resolve the system's aperiodic evolution in terms of a "strange" attractor[76] and, with this, an experimental classification of the "chaotic" component of the turbulent flow. It is very difficult to distinguish a purely chaotic motion from a quasiperiodic one or from a motion perturbed by external noise by simply looking at the finite sequence of data. The dimension determination is a quantitative procedure so as to recognize, characterize and classify the chaotic motion on the attractors.

The dimension of the attractor D is lower than the dimension of the original phase space. D is zero for a fixed point, which attracts all nearby initial points towards itself and is in a stationary time independent equilibrium. D equals one for a limit cycle, which is a closed curve corresponding to a periodic motion of the system. One can predict its state at all later times if the state of the system is known at a given time. D is two for 2-torus, which is an attracting closed tube, around the unstable limit cycle. It is possible to calculate the state of the system starting from an initial condition. The motion becomes quasiperiodic if the two frequencies on the torus are incommensurable. However, the dimension of strange attractors often turns out to have noninteger value. Strange attractors are complicated geometric objects, typically with a fractal structure,[77] which appear in the state space of chaotic flows.

We can define an n dimensional space using as coordinates (with m=1, 2, 3, ... n): $x_m=x(t+(m-1)t')$; in our analysis t'=constant. Experience has shown that optimal results are obtained if t' is somewhat smaller than the typical turnover time. The value of time t' should not be chosen too large. Otherwise different coordinates in the space would no longer be deterministically related, resulting in a large value of D. On the other hand, a too small value of t' would mean that all coordinates in the space are roughly equal. We also partition the n-dimensional phase space into M cells of size l on side. The probability p_i of finding a point of the attractor in cell number i (i=1,2,...M(l)) is

$$p_i = \lim_{N\to\infty} \frac{N_i}{N}$$

where N_i is the number of points in the cell.

To characterize the inhomogeneous static structure of the attractor, one introduces an infinite set of dimensions, D_f, which are related to the fth powers of p_i via

$$D_f = \lim_{l\to 0} \frac{1}{f-1} \frac{\log\left(\sum_{i=1}^{M(l)} p_i^f\right)}{\log l} \qquad f=0,1,2,...$$

where M(l) is the number of phase space elements and p_i is the probability that an attractor point falls in the ith element.[6]

In fact, numerical determination of the dimensions D_f is rather cumbersome and impossible for attractors of higher dimensions. However, for f=2, a determination of D_2, the so-called correlation dimension, is relatively simple. It can be easily obtained from any time series.[7,8] In this case we have

$$D_2 = \lim_{l\to 0} \frac{\log\left(\sum_{i=1}^{M(l)} p_i^2\right)}{\log l}.$$

D_2 can be computed by the correlation integral C(l), which is defined by

$$C(l) = \lim_{N\to\infty} \frac{1}{N^2} \sum_{(i,j=1)}^{N} H(l-|x_i - x_j|)$$

where $\mathbf{x}_i$ and $\mathbf{x}_j$ are points on the attractor, H(y) is the Heaviside function (1 if $y \geq 0$ and 0 if $y<0$), and N is the number of points randomly chosen from the entire data set. The Heaviside function simply counts the number of points within a radius l of the point denoted by $\mathbf{x}_i$, and C(l) gives the average fraction of points within a cell. D_2 is related to C(l) via

$\sum_{i=1}^{M(l)} p_i^2$ = the probability that two points of the attractor lie within a cell l^n

$\approx$ the probability that two points at the attractor are separated by a distance smaller than l

$= \lim_{N\to\infty} \frac{1}{N^2}$ {number of pairs ij whose distance $|\mathbf{x}_i-\mathbf{x}_j|$ is less than l}

$= \lim_{N\to\infty} \frac{1}{N^2} \sum_{(i,j=1)}^{N} H(l-|\mathbf{x}_i-\mathbf{x}_j|)$

$= C(l)$

Therefore,

$$D_2 = \lim_{l\to 0} \frac{\log(C(l))}{\log l}$$

This is the correlation dimension. It can be obtained from the slope of a graph of logC(l) versus logl.

Some other different methods can also be used to determine the fractal dimension. In the box-counting method, one covers the whole plane with square elements of varying sizes and counts the number N(r) of elements containing the boundary. The

negative slope of log N(r) versus log r gives the dimension of the fractal boundary. It turns out that it is very difficult to compute D whenever D>2.[79] A co-dimension method involves computing the smallest distance from each pixel to the boundary and determining the number of pixels $N_c(r)$ lying within a distance r from the boundary. The slope of this straight region in log-log plots of $N_c(r)$ versus r is the co-dimension D of the boundary; its fractal dimension is 2 - D.[80]

Chapter V Results

In this chapter we present and discuss the results of this experiment. The measurements are performed under the following various firing conditions: The magnetic field strength changes from 0 to 600 gauss; Mach numbers range from 10 to 60; the operating pressure is between 15 mTorr and 200 mTorr; the discharge voltage is in the range of 15 kV and 20 kV. The fluid-like turbulent parameters are determined by using standard turbulent and chaotic analytical procedures on the data as discussed in Chapter IV. General trends of the parameters under the different running conditions are illustrated.

5.1 Ion Density Profiles from Laser Induced Fluorescence and Electric Probe Measurements

Ion density profiles are observed by fluorescence emissions and ion probe measurements. Both light and probe measurements are made at the same axial location, which is about 160 cm from the discharge. The time when the shock front arrives is coincident for both diagnostic methods. Both signals exhibit the same fluctuating property.

Figure 5.1 shows the ion density profiles behind the shock front from LIF measurements under three different magnetic fields. The three magnetic coil currents correspond to fields of +480 gauss, 0 gauss, and -480 gauss where positive and negative field strengths indicate a field parallel and antiparallel to the direction of shock wave propagation. Initial filling argon gas pressure p_1 is 60 mTorr. The voltage applied to the capacitor is V=18kV. The Mach number in this case is 32. The graphs show typical turbulent fluctuations after the shock front which persist for roughly 30 μsec. A 10 MHz sampling frequency is used for all runs.

Examples of data obtained from ion probe for different Mach numbers are shown in Figure 5.2. It shows the ion density fluctuating transition region following a sharp spike at the shock front; the region is about 10 to 15 cm long. The bias voltage on the probe is -7 V and magnetic field strength is +600 gauss provided by a coil current of 10 amps. The top signal is obtained under the conditions of filling pressure 90 mTorr and discharge voltage 17

kV. The middle one is run at p_1=60 mTorr; V=18 kV. The firing conditions for the bottom signal are p_1=60 mTorr; V=20 kV.

Two electric probes separated by 13.2 cm are used to obtain the speed of a shock wave. The probe in the upstream position of the test section will detect a large density change when the shock wave arrives. The one in the test section will receive the shock waves signal later. The time interval can be measured from the recording signals; hence the speed of the shock wave can be calculated along with the Mach number.

The relation between Mach number and initial filling pressure follows $M \propto p_1^{-0.84}$ (Figure 3.6). At a fixed discharge voltage of 18 kV, the Mach number increases from 14 to 56 as the pressure decreases from 100 mTorr to 20 mTorr. Hence, we conclude that the higher the initial filling pressure is, the lower the Mach number is. This is consistent with $M \propto \sqrt{1+\frac{\alpha}{p_1}}$ given theoretically.

5.2 Statistical Properties of the Turbulent Plasmas

We use standard turbulent and chaotic analytical procedures on the (relative) ion density fluctuations indicated by the fluorescence emissions and the ion probe from our arc discharge shock tube to obtain the characteristics of the system. Power spectra, correlation functions and time scales, turbulent intensities, and chaotic dimensions are displayed under various conditions. The parameters of turbulence on the two diagnostics are compared during simultaneous measurements.

5.2.1 Power Spectra and Power Law Behavior

Two sets of fluctuation power spectra are plotted in Figures 5.3 and 5.4 for density fluctuations from LIF and probe respectively. Log-log plots of P versus frequency are displayed in Figure 5.3 for three different magnetic fields. We use log(P) versus log(f) of the output of the fast Fourier transform algorithm because it has been shown that wave number is linearly proportional to frequency.[7,68,69] A region is determined for which there is a maximum likelihood of a power law dependence and the values of n are calculated from a standard least squares fit to that region in the power spectra. These spectra of runs under different firing conditions have many common features. They are quite consistent and show a general trend $P \sim f^{-n}$, with $1.3 \pm 0.2 \leq n \leq 2.8 \pm 0.3$. That means all the power spectra follow the behavior of typical turbulent spectrum. Furthermore,

these power spectra are characterized by many discrete modes. In Figure 5.3, comparing the cases (a) and (c) in which magnetic field is present with the case (b) in which the field is absent, we find that more modes are generated when magnetic fields are employed. In other words, the magnetic field adds more modes to the system and makes the system more complex.

The spectral index n increases with increasing initial filling pressure at a constant magnetic field strength. Figure 5.5 shows that $1.3\pm0.2 \le n \le 2.1\pm0.2$ for 40 mT $\le p_1 \le$ 75 mT at M=30, and that $1.4\pm0.2 \le n \le 2.5\pm0.3$ for 40 mT $\le p_1 \le$90 mT at M=20. In both cases, it is obtained that $n \propto 2.27 \times 10^{-2} p_1$. This trend is reasonable since an increasing pressure for a fluid-like plasma increases the kinematic viscosity and collisional frequency, and hence the fluctuations damp faster.

From the relation between Mach number and the spectral index as shown in Figure 5.6, we find that the spectral index decreases up to a limit as Mach number increases for both light and probe signals. The index varies from about 2.5 to 1.3 when Mach number changes from 20 to 60. The reason can be explained as follows: When the Mach number is higher, which is equivalent to the Reynolds number of plasma flow being higher, the viscosity effect of the flow is smaller; therefore, the energy dissipation rate is smaller. From a particle motion point of view, when the Mach number is higher, the temperature of plasma is higher; therefore, the collisional effect in plasmas is smaller. When the Mach number increases to about 40, the viscosity effect becomes so small that further increases in the Mach number do

not produce much change in viscosity. That is why the relationship becomes flat when the Mach number is higher than 40.

We show in Figure 5.7 the behavior of the spectral index n with changing magnetic field. The two sets of n are obtained at fixed Mach numbers of 20 and 30 respectively under the different strengths of the magnetic field. The index n is insensitive to the change of the magnetic field.

5.2.2 Autocorrelation Functions and Time Scales

The autocorrelation profiles are calculated from the Fourier transform of the power spectrum, as discussed in 4.1. Figure 5.8 shows that the autocorrelation function decays rapidly. The width of the first peak of the correlation function is in the order of one microsecond, which implies that the signals become uncorrelated for this time interval. This feature is consistent with typical turbulent behaviors discussed in Section 4.1. The decay is independent of the change of the Mach number and magnetic field.

Systematic correlation times behaviors are observed with changing magnetic fields in the 0-600 gauss range. The small correlation time is obtained by fitting $R(\tau)$ for $\tau \to 0$ to the parabola, as discussed in 4.1. This procedure is used in order to confirm to the standard analytical approaches for turbulence. However, even though the goodness-of-fit estimators are quite satisfactory, other error sources contribute substantially to the measurement.

The small correlation time (220±50 ns ≤ τ_s ≤ 1,400±200 ns) decreases with the increasing strength of magnetic field, independent of the direction of the magnetic field parallel or antiparallel to the direction of the shock wave. Thus increasing the magnetic field strengths causes a corresponding increase in chaotic motion of the system. This can be seen from Figure 5.9, in which the small correlation time calculated from LIF signals is plotted against magnetic field strength for different Mach numbers, and from Figure 5.11(a) where the time is calculated from the ion probe signals. The maximum values of τ_s occur in the absence of the magnetic field for all cases mentioned above. This means that the system is more turbulent when a magnetic field is applied. However, the characterizing correlation time (2.2±0.3 μs ≤ τ_c ≤ 9.5±1.0 μs) increases with the magnetic field strength regardless of the direction (parallel or antiparallel) of the field and Mach number. When there is no magnetic field, the magnitudes of τ_c are minimum. This shows in Figure 5.10 for light signals and Figure 5.11(b) for probe signals. In Figures 5.12 and 5.13, the comparisons between small correlation times and characterizing correlation times are displayed. The first figure is obtained from the fluorescence measurements and the second from the probe measurements. Each point in the plot represents one run at the same Mach number but different current through the coils. The values of small and characterizing correlation times are coupled when the changes arise from changes in the magnetic field strength; increasing τ_c means decreasing values for τ_s.

The data also show that the small correlation time decreases with the initial pressure in the tube when the Mach number and magnetic field are unchanged. These trends are shown in Figure 5.14, in which 820±150 ns $\leq \tau_s \leq$ 300±40 ns for 35 mTorr $\leq p_1 \leq$ 70 mTorr at Mach number 30, and 850±160 ns $\leq \tau_s \leq$ 520±60 ns for 40 mT $\leq p_1 \leq$ 90 mT at Mach number 20.

5.2.3 Turbulent Intensity

We calculate the root-mean-squared fluctuations about the average density, i.e., $\sqrt{\frac{(\rho_{ave.}-\rho_i)^2}{N(N-1)}}$. This is defined as a measure of turbulent intensity. It is an indicator of the strength of the fluctuations.

In Figure 5.15, we isolate the influence of Mach number from the influence of changing magnetic field. At fixed Mach number, the field is varied. In this case, turbulent intensity tends to increase with the field. The minimum value of the turbulent intensity occurs in the absence of magnetic field. That is, the strength of the fluctuation increases as the field increases.

Keeping the magnetic field constant, turbulent intensity is plotted against Mach number in Figure 5.16. When the Mach number changes from 23 to 31, turbulent intensity increases from 0.23±0.02 to 0.38±0.04. Therefore, the higher the Mach number is, the larger the density fluctuation is.

Figure 5.17 shows the tendency of turbulent intensity to increase as the initial pressure in the tube increases when the

Mach number and magnetic field are unchanged. The reason is that when pressure increases the collisional effect increases.

5.2.4 Effect of a Weak Magnetic Field on Chaotic Dimension

Phase space trajectories for chaotic dimension analysis are shown in Figures 5.18 and 5.19, in which three dimensional projections of a seven dimension phase space for the data at I=8 amperes and I=0 amperes are displayed at the top plots, and these same data are connected by lines in time-ordered sequence at the bottom ones. The axes {x, y, z} display data $\{x_1, x_2, x_3\}$ from a time series in ion density fluctuations x(t) as $x_m(t+(m-1)t')$, where t'=400 ns and m=7. The correlation exponents are insensitive to changes in the number of dimensions n as long as $n \geq 5$ as shown in Figure 5.20. Figure 5.21 gives a typical correlation integral for a seven dimensional phase space trajectory of 256 points. The region $-3.5 \leq \log(C(l)) \leq -1.8$ is used to determine D_2. The sample of the data is large enough so that there is very little difference in the estimate of the correlation exponent $\delta=\log(C(l))/\log(l)$ from the correlation integrals.

A quantitative measure of the dimensionality of the chaotic behavior has been obtained successfully from the correlation integral. The magnetic field increases the chaotic dimensionality in the turbulent plasma, both in the parallel and the antiparallel cases, and thereby increases the complexity of the flow. In Figure 5.22 and Figure 5.23, chaotic dimension versus magnetic field current is plotted. The difference between part (a) and part (b) in

Figure 5.22 is attributed to the narrower range in flow Mach numbers. In the first case, the Mach number is held to the range $21 \leq M \leq 33$; in the second case, it is held to the range $30 \leq M \leq 33$. When there is no magnetic field, $D_2 \leq 2.0$, while as the magnetic field increases to 600 guass, $D_2 \approx 3.0$. Part (a) and part (b) in Figure 5.23 are for different Mach numbers respectively. In the absence of magnetic field (I=0 ampere), the values of D_2 are minimum for all cases.

Other trends have been determined. In Figure 5.24, chaotic dimension shows a trend of D_2 decreasing with increasing Mach number. We have $2.10 \pm 0.20 \leq D_2 \leq 2.45 \pm 0.30$ for $21 \leq M \leq 34$. We show that the chaotic dimension is insensitive to the initial pressure filled before firing in Figure 5.25 at the fixed Mach numbers of 20 and 30 respectively.

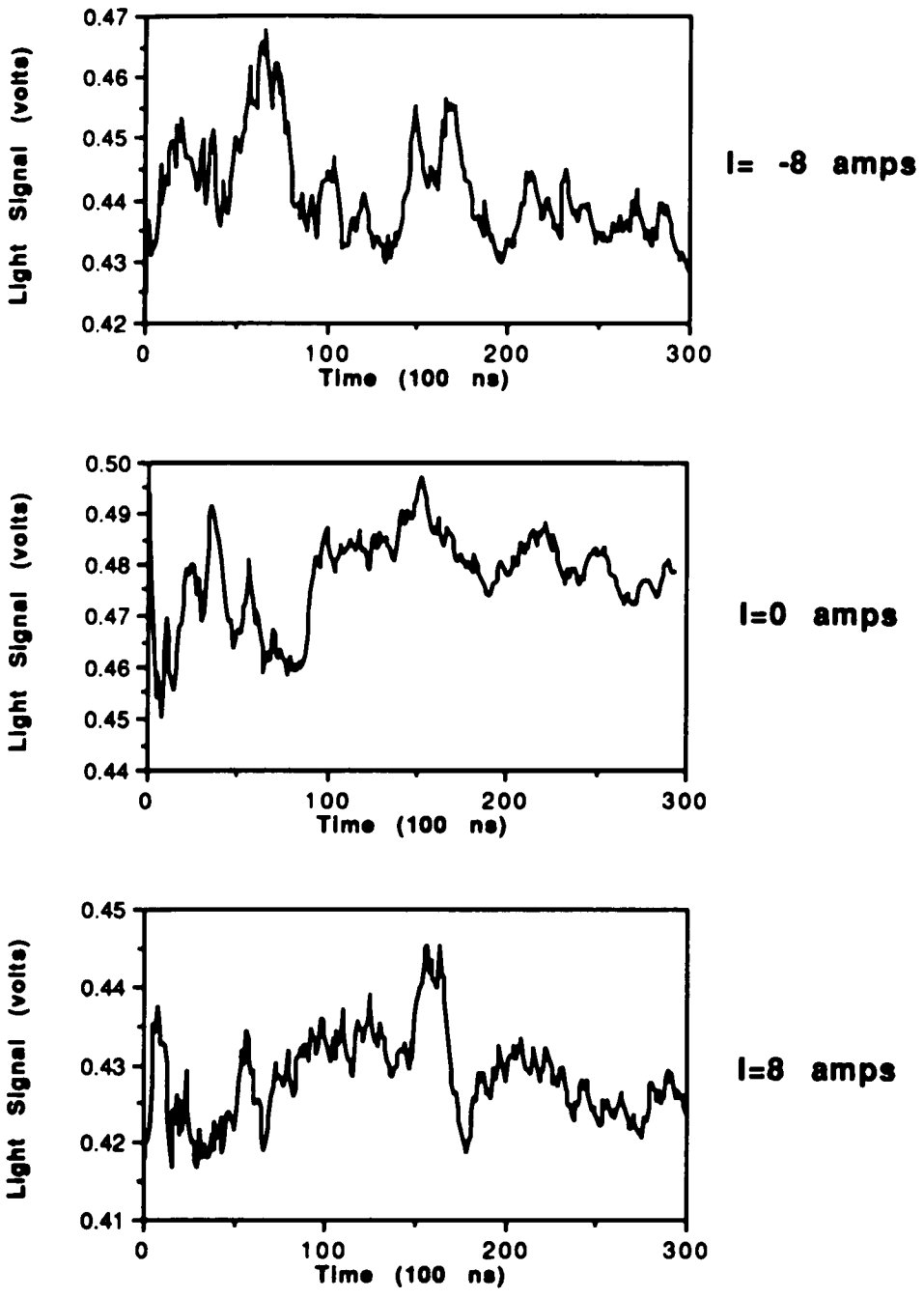

Figure 5.1 Fluorescence signals behind shock fronts.

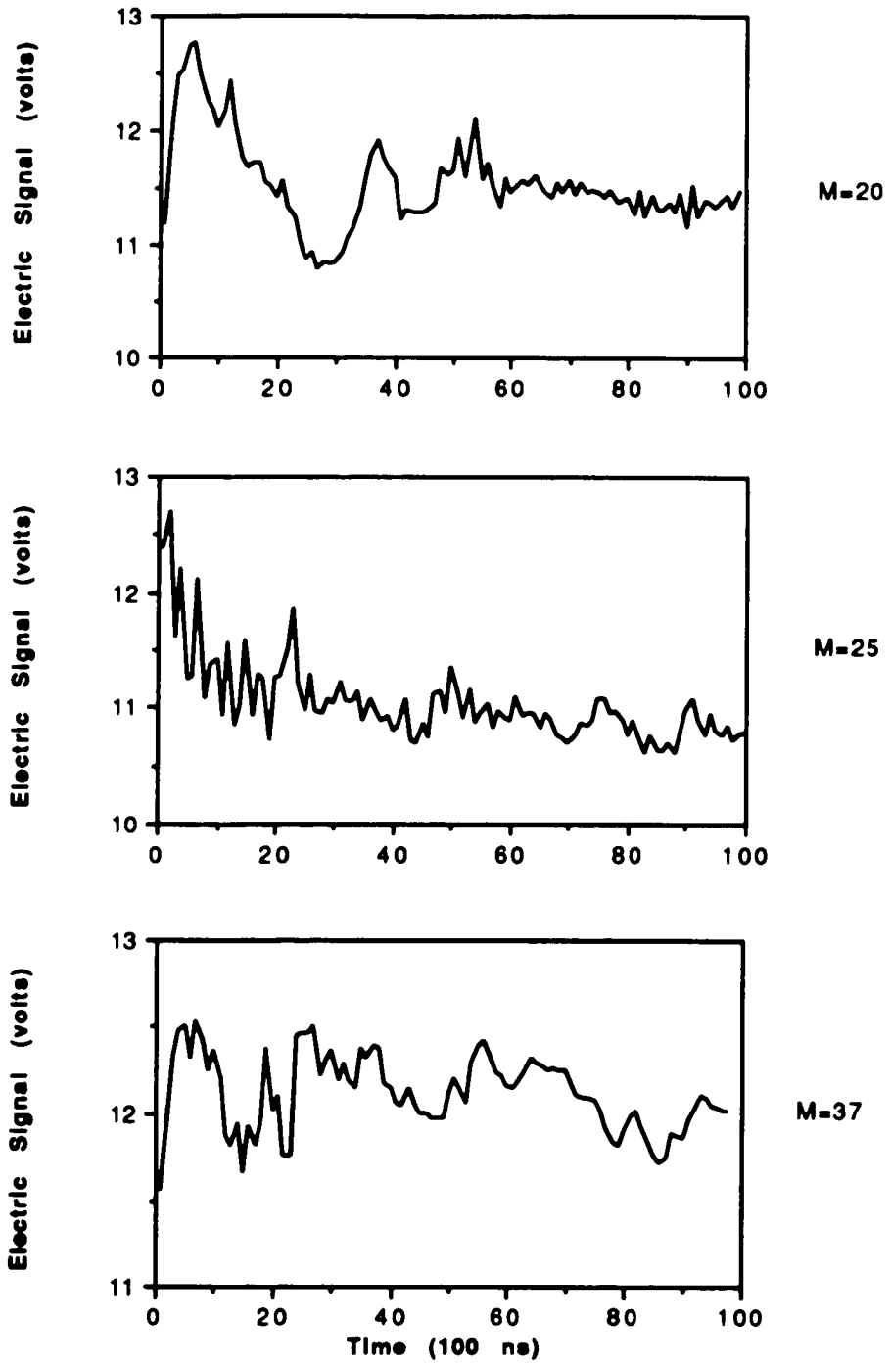

Figure 5.2 Electric probe signals behind shock fronts.

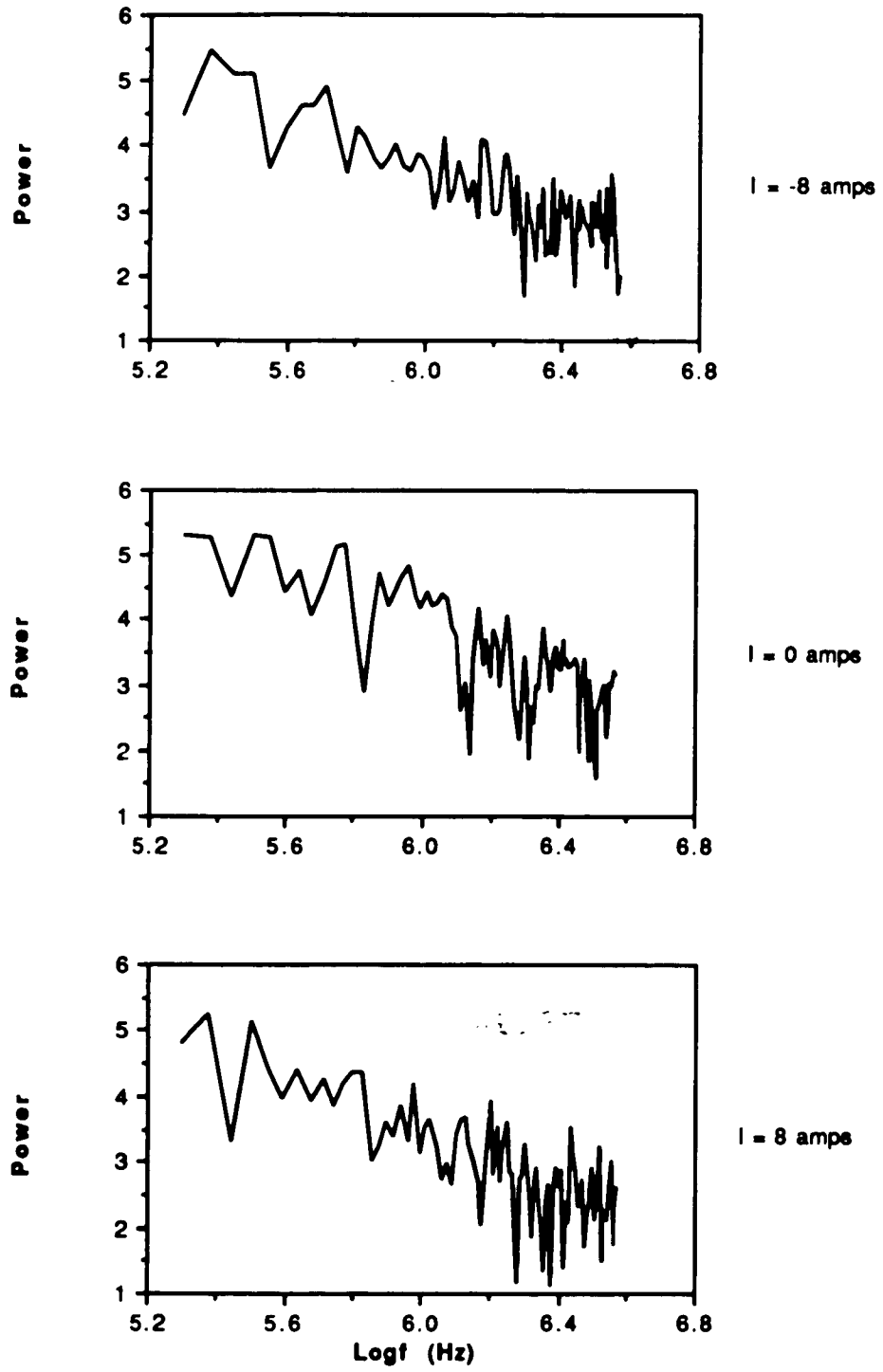

Figure 5.3 Power spectra from fluorescence measurements.

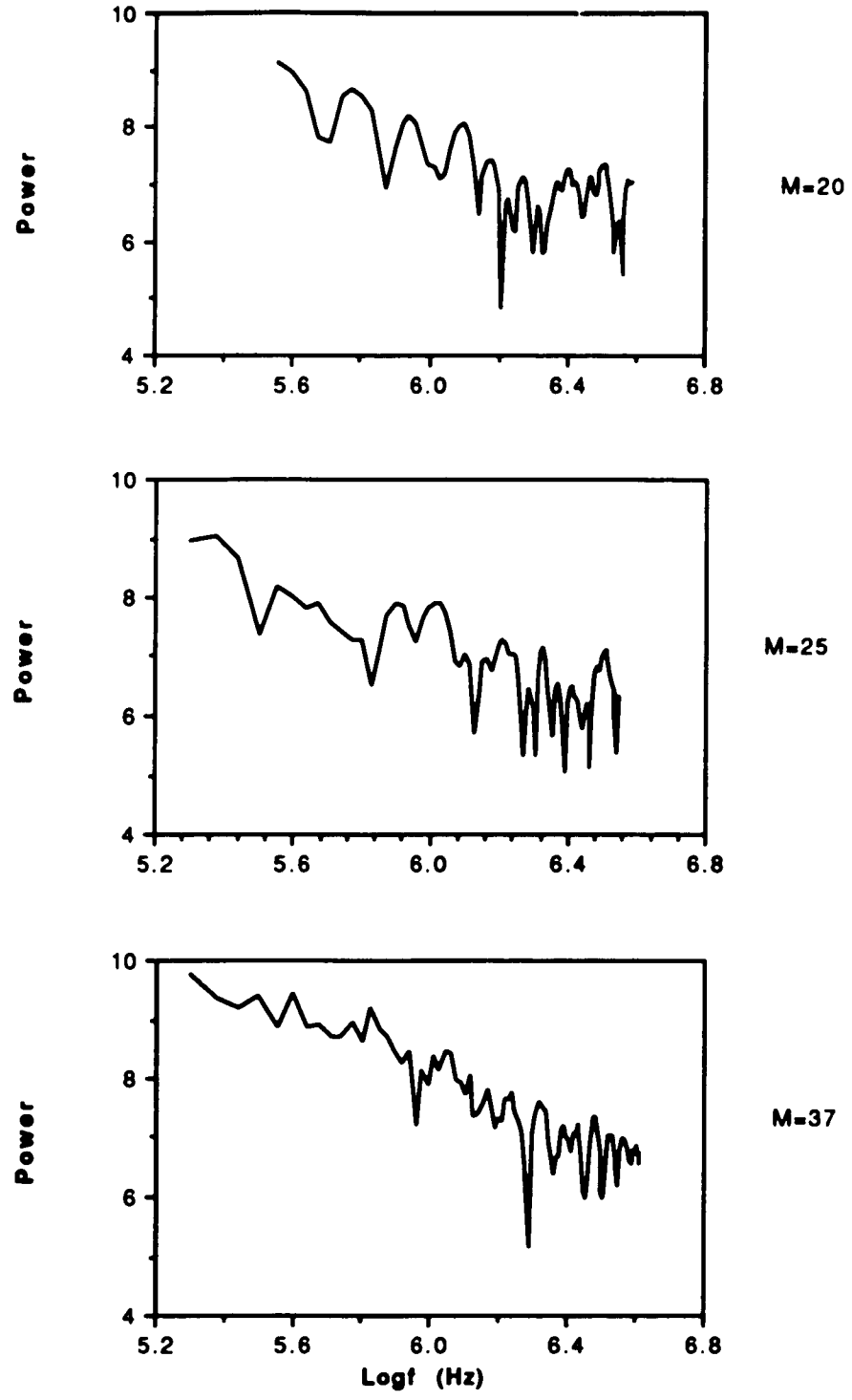

Figure 5.4 Power spectra from electric probe measurements.

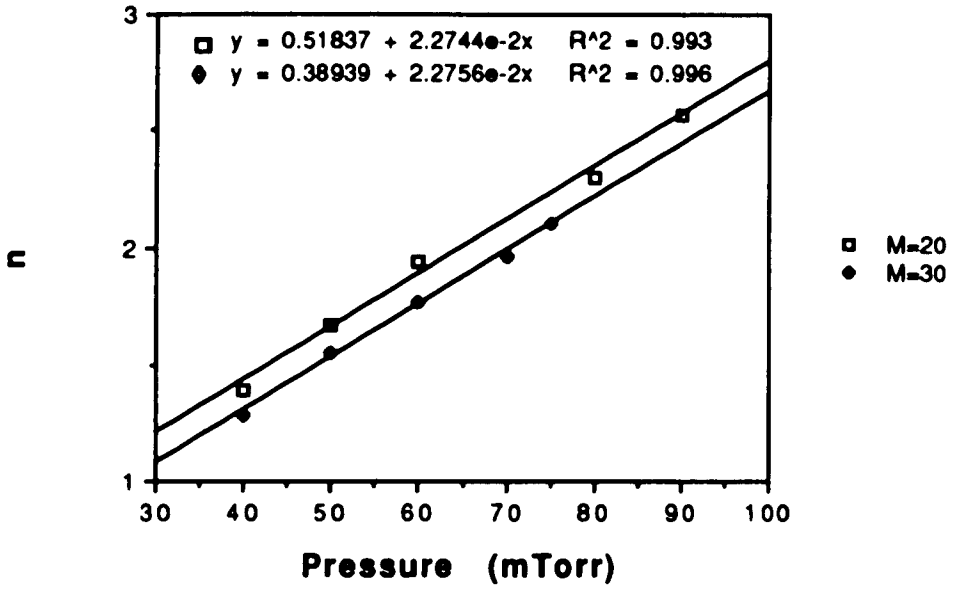

Figure 5.5 Spectral index versus pressure at fixed Mach number and magnetic field.

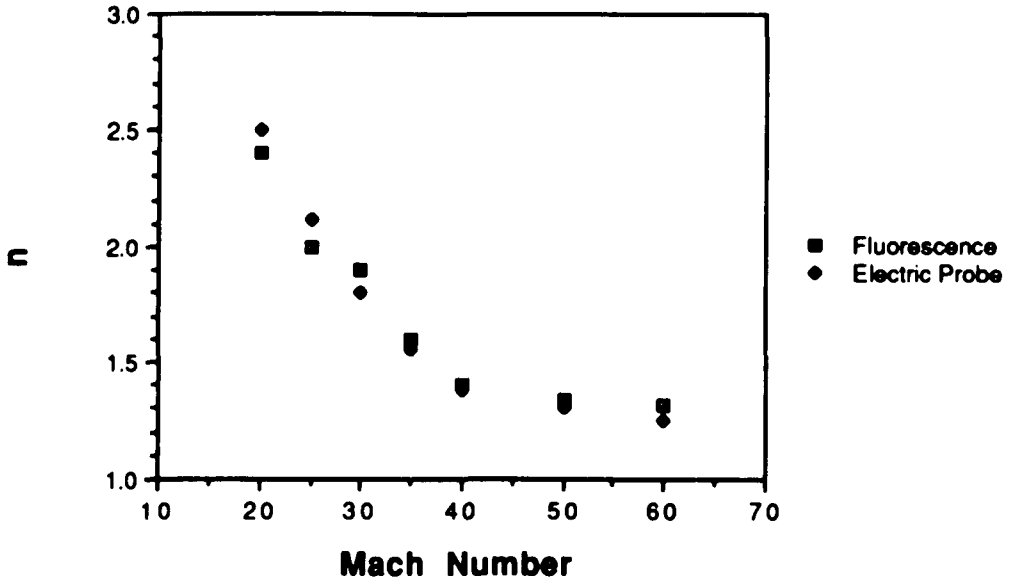

Figure 5.6 Spectral index versus Mach number at a constant magnetic field.

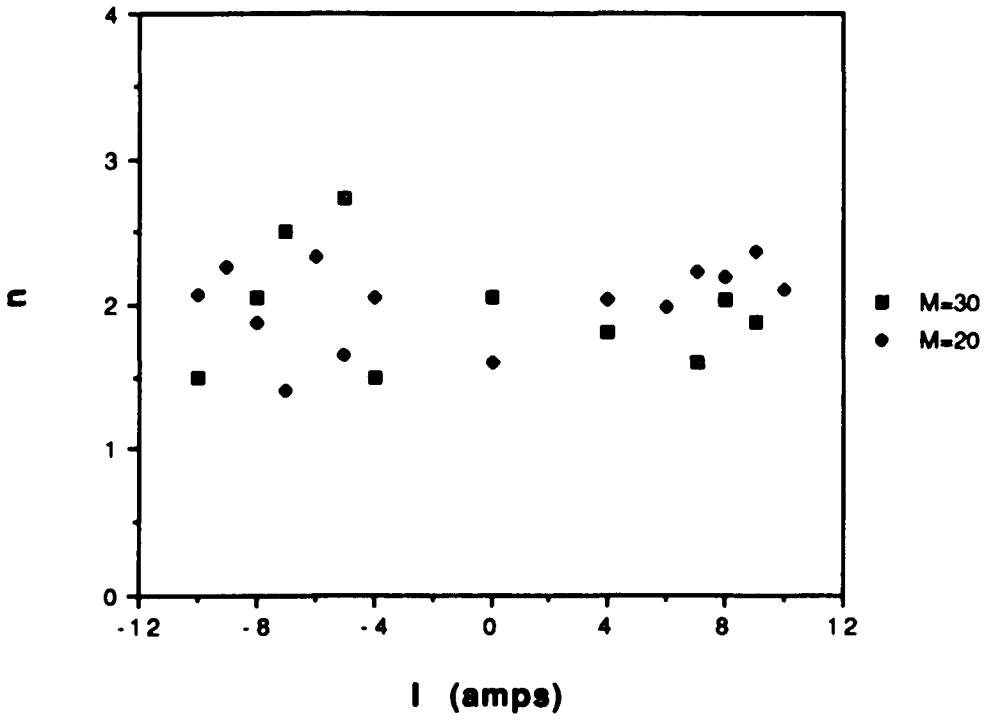

Figure 5.7 Spectral index versus magnetic field at a constant Mach number.

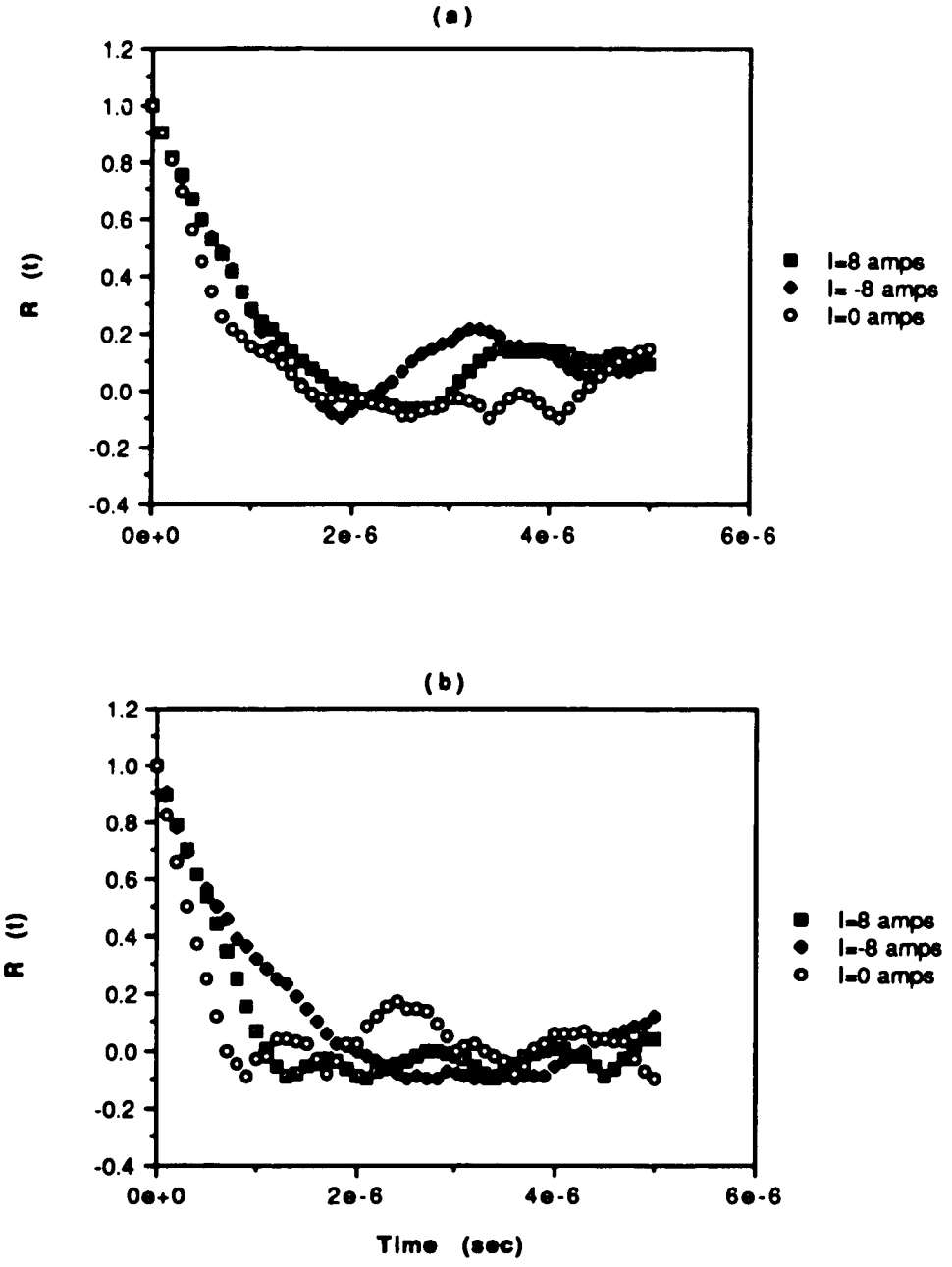

Figure 5.8 Autocorrelation profiles. (a) M=30; (b) M=20.

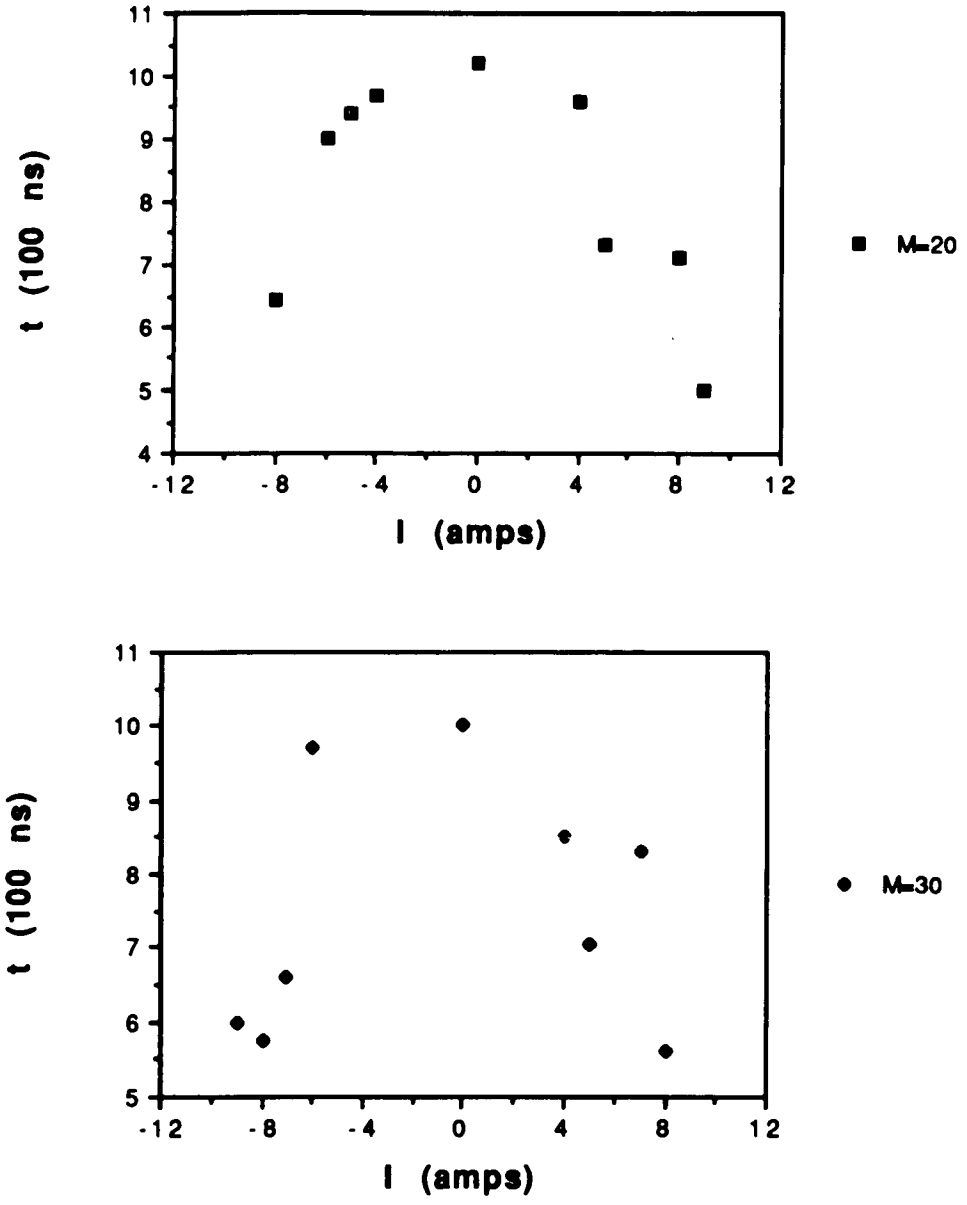

Figure 5.9 Small correlation times calculated from light measurements versus magnetic field at fixed Mach numbers.

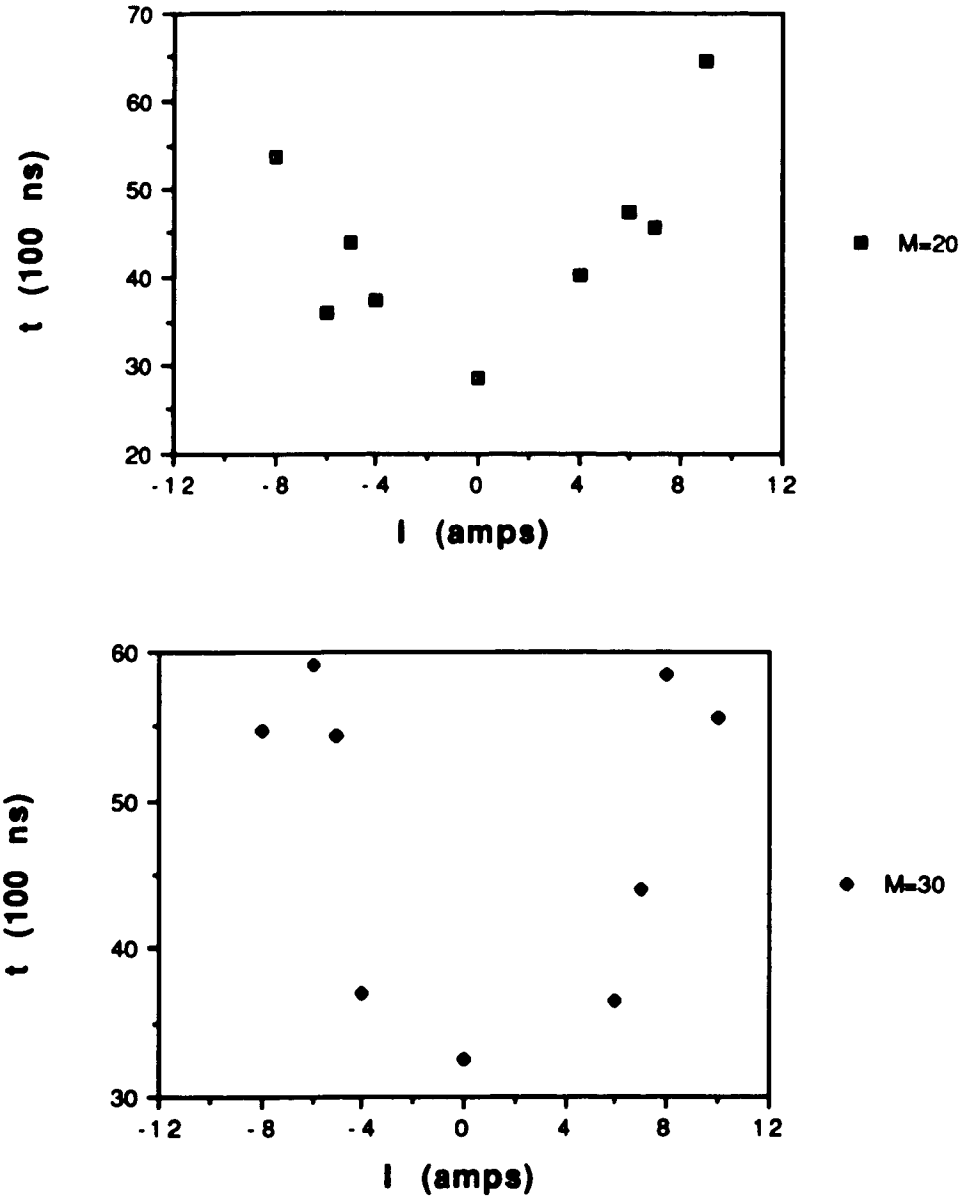

Figure 5.10 Characterizing correlation times from light measurements versus magnetic field current at fixed Mach numbers.

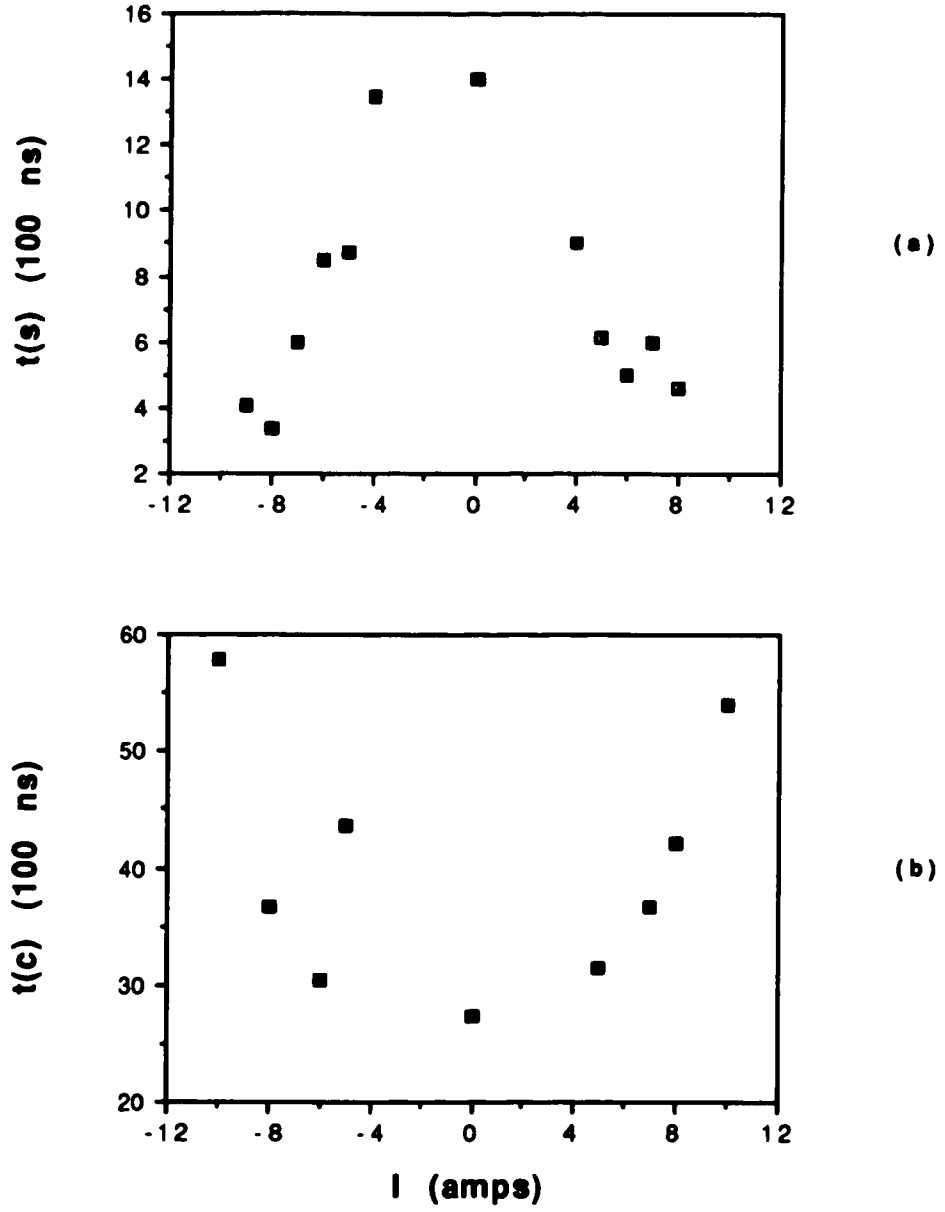

Figure 5.11 (a) Small correlation times from probe measurements versus magnetic field current at a constant Mach number; (b) Characterizing correlation times from probe measurements versus magnetic field current at a constant Mach number.

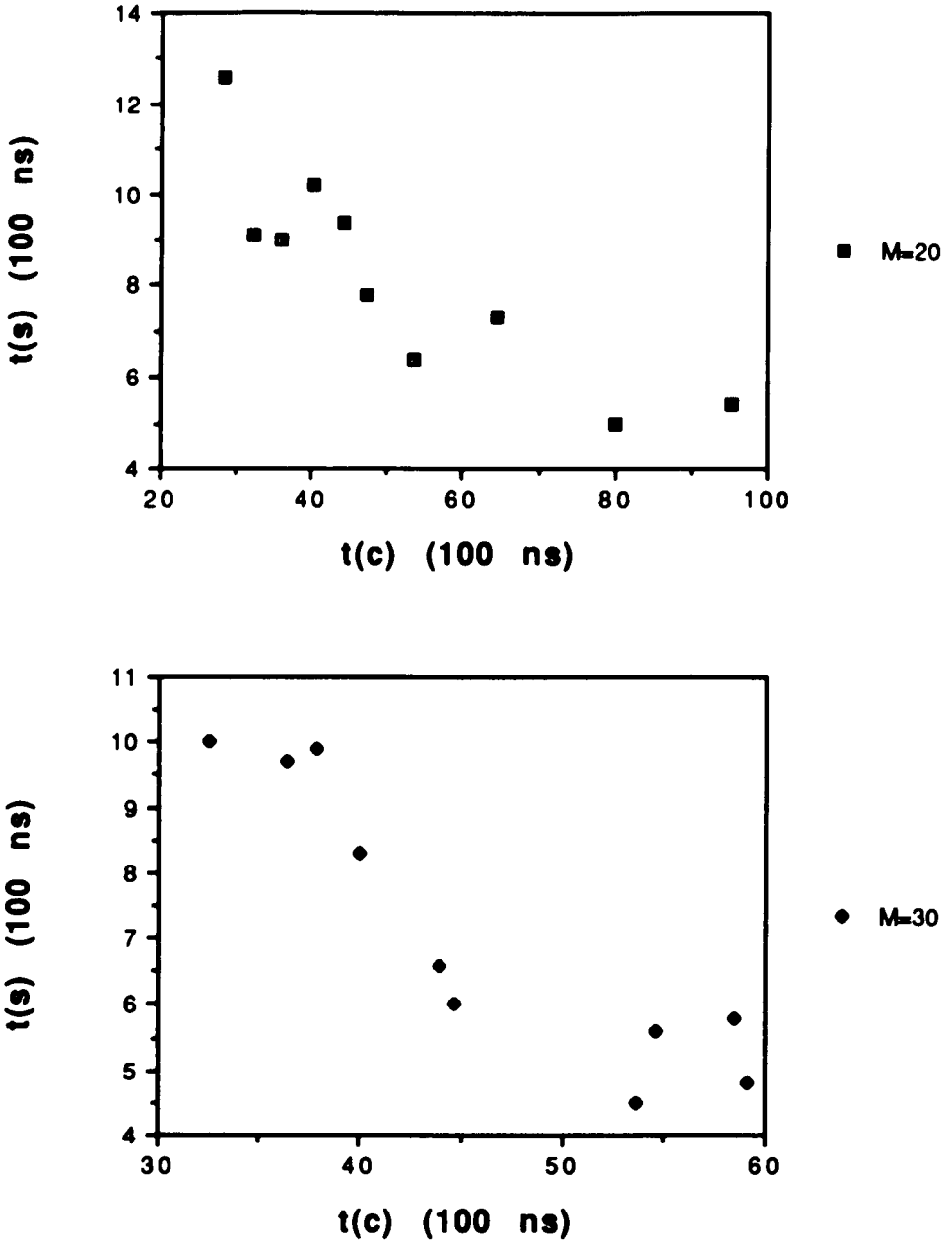

Figure 5.12 Evolution of small and characterizing correlation times under varying strengths of the magnetic field from light signals.

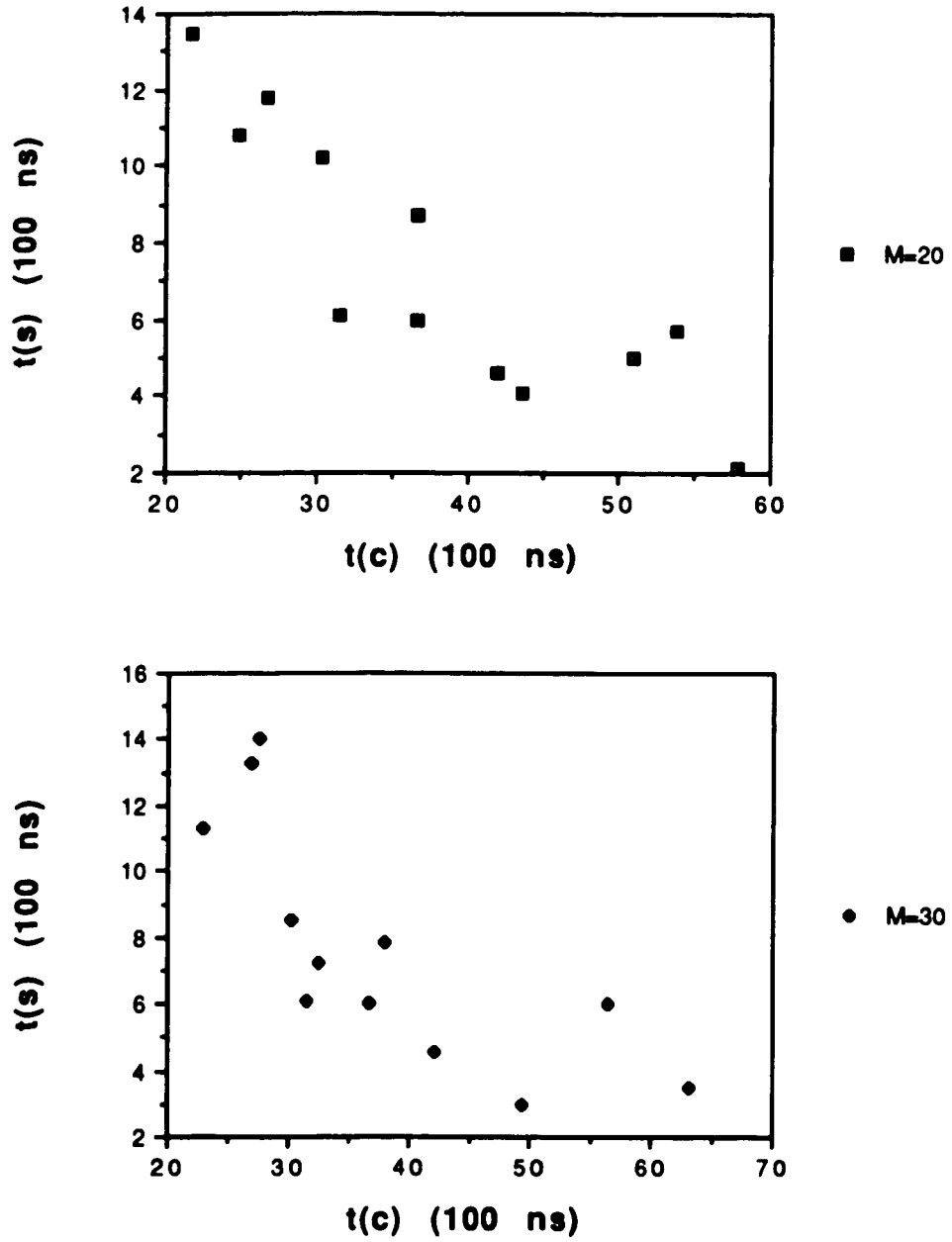

Figure 5.13 Evolution of small and characterizing correlation times under varying strengths of the magnetic field from probe signals.

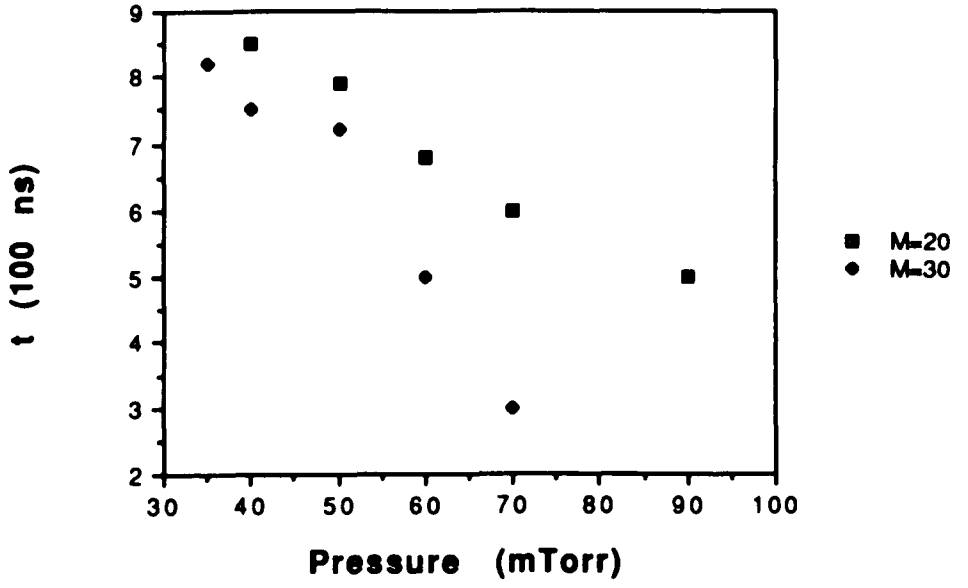

Figure 5.14 Small correlation time versus pressure at fixed Mach numbers and magnetic field.

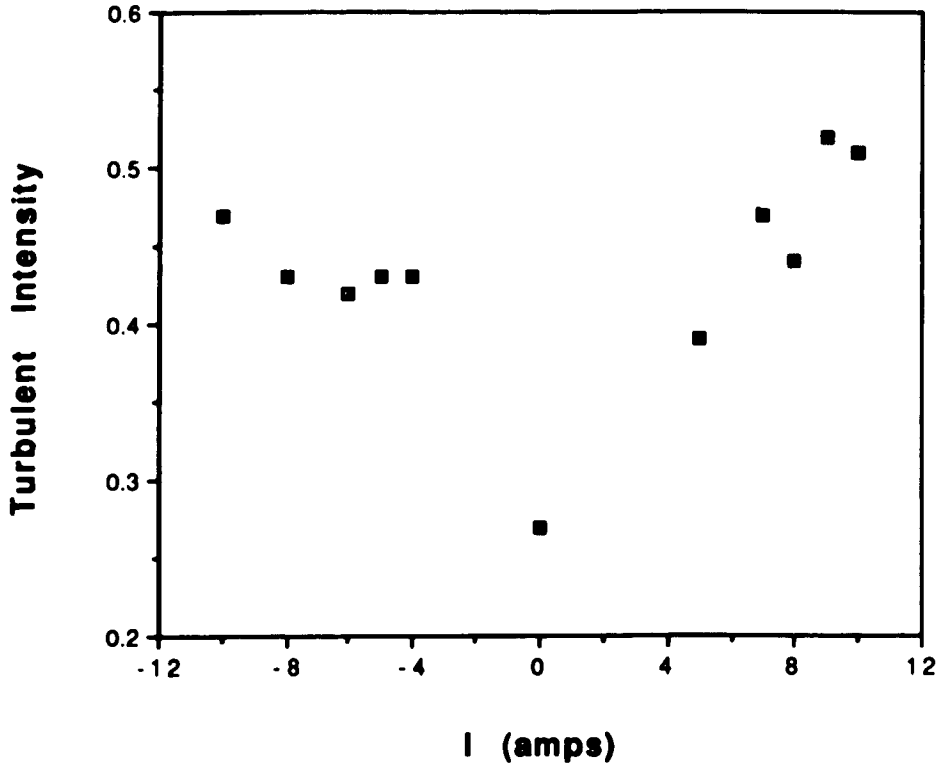

Figure 5.15 Turbulent intensity versus magnetic field at a fixed Mach number.

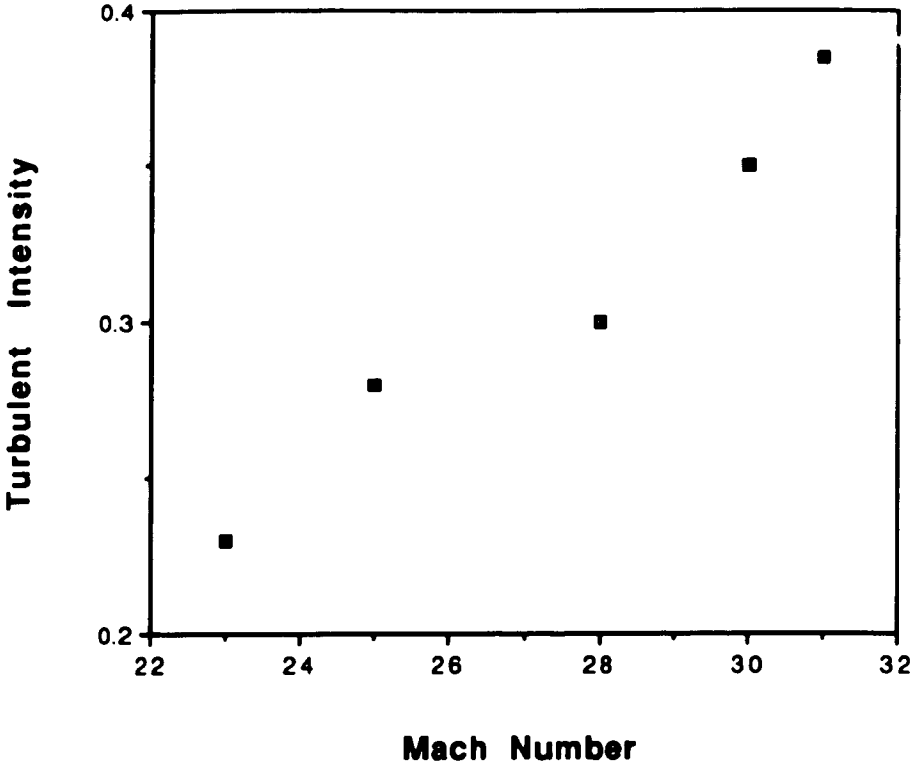

Figure 5.16 Turbulent intensity versus Mach number at a constant magnetic field.

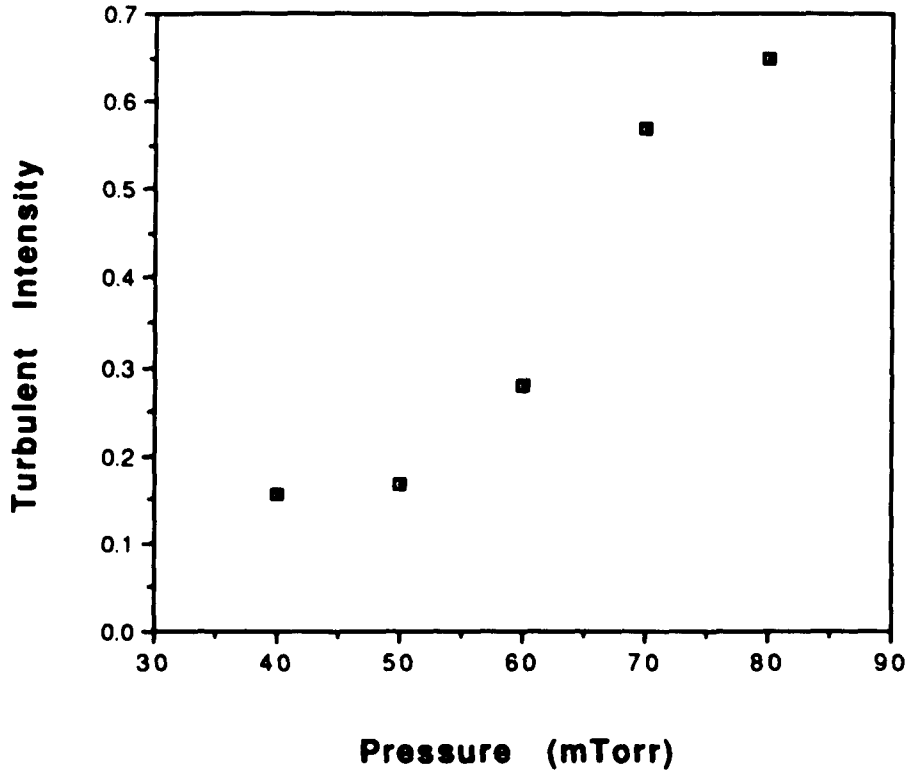

Figure 5.17 Turbulent intensity versus pressure in the case of unchanging Mach number and magnetic field.

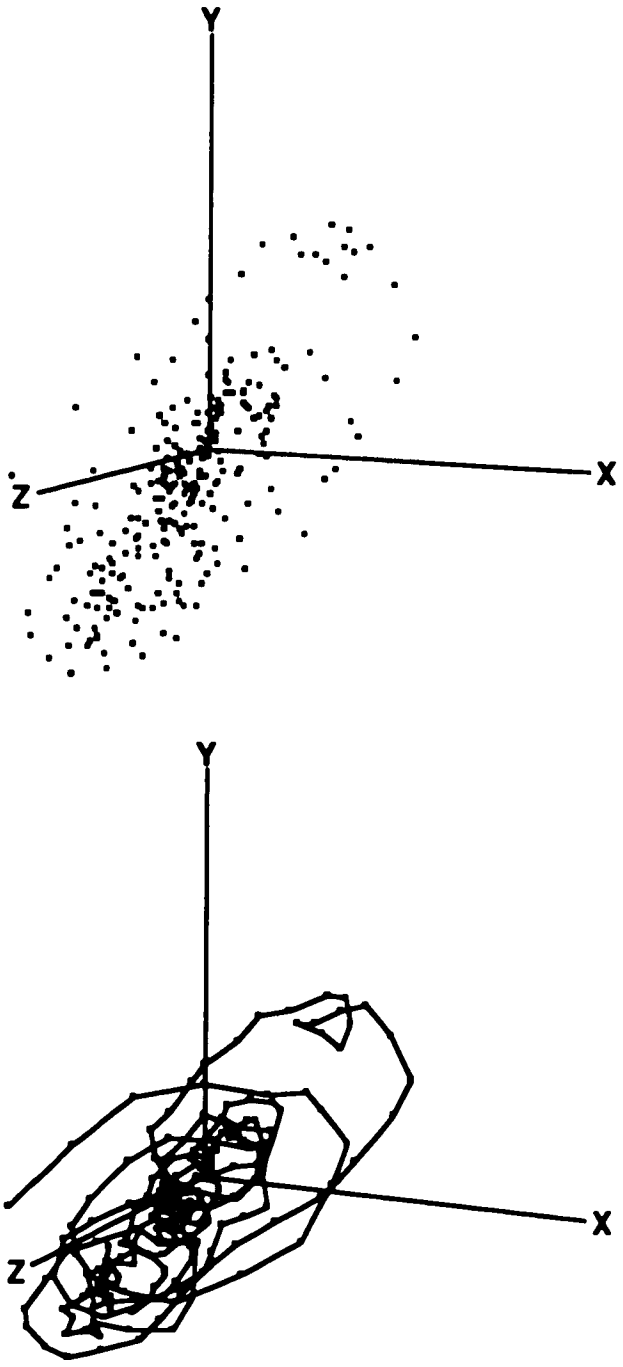

Figure 5.18 Phase space trajectory: I=8 amps.

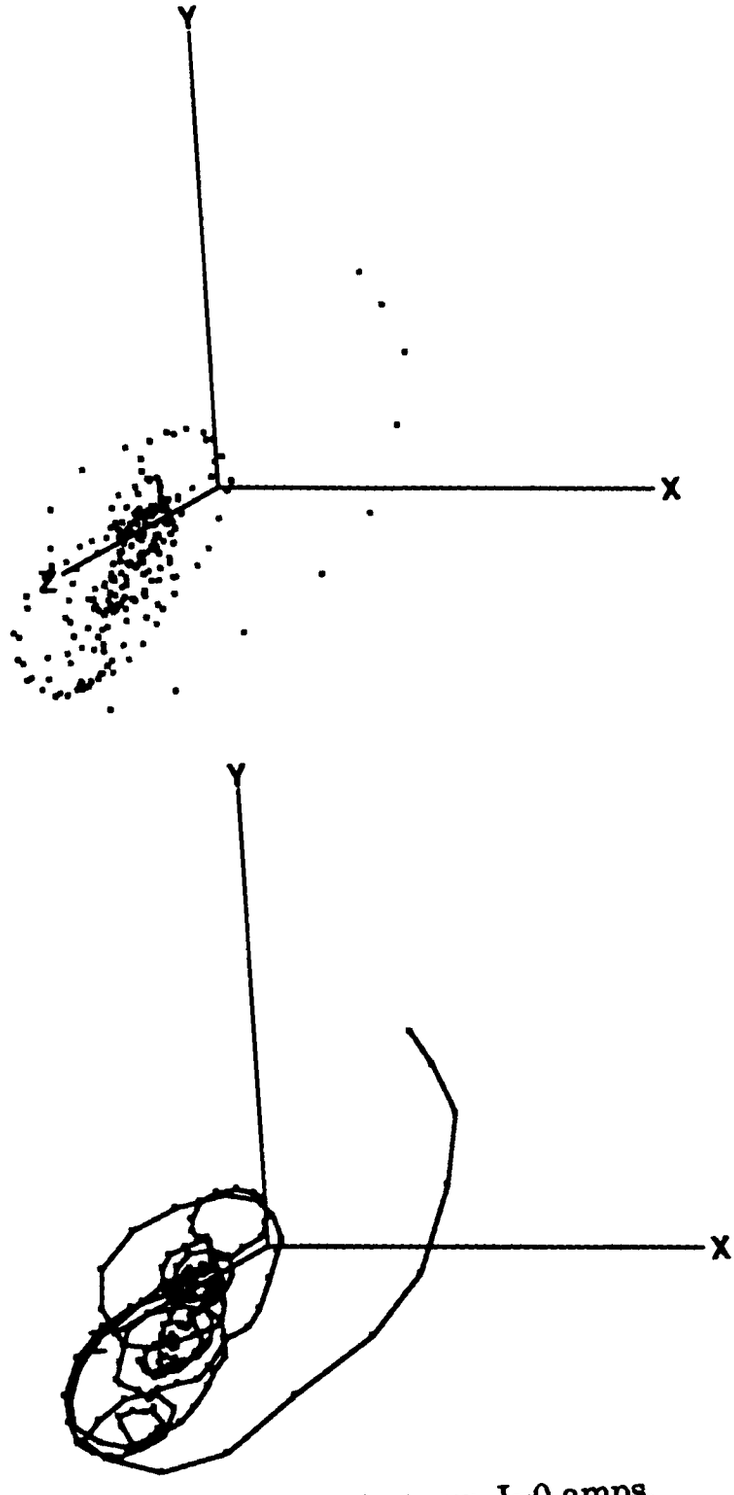

Figure 5.19 Phase space trajectory: I=0 amps.

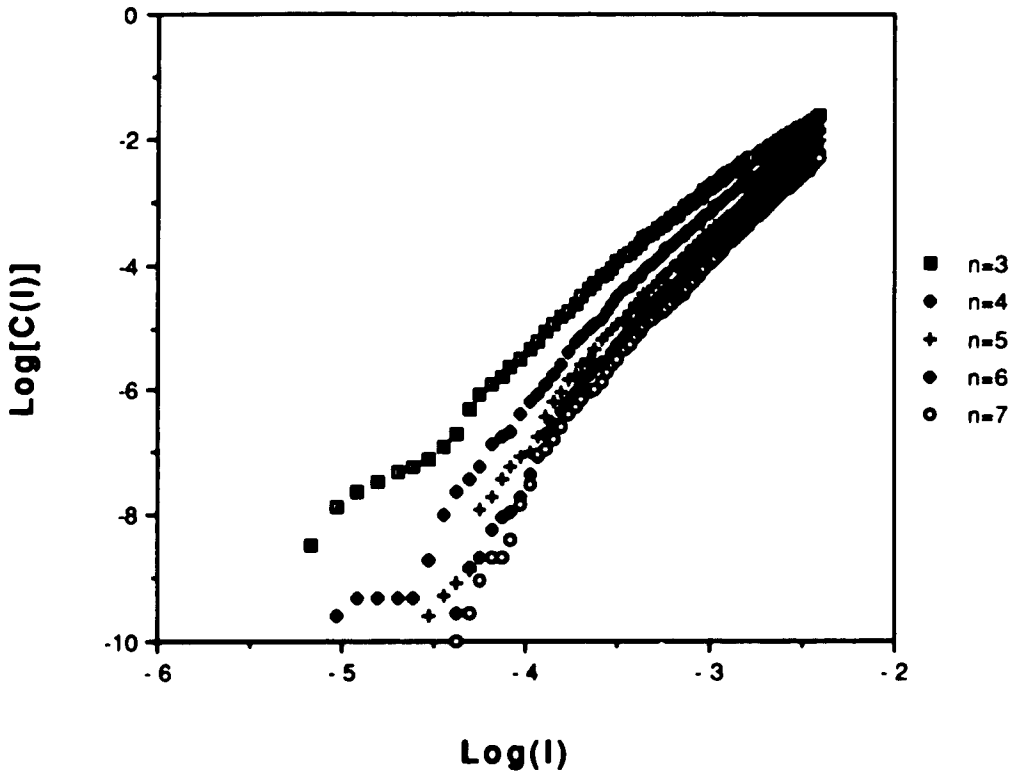

Figure 5.20 Sensitivities of the correlation function to the number of dimensions constructed for the phase space.

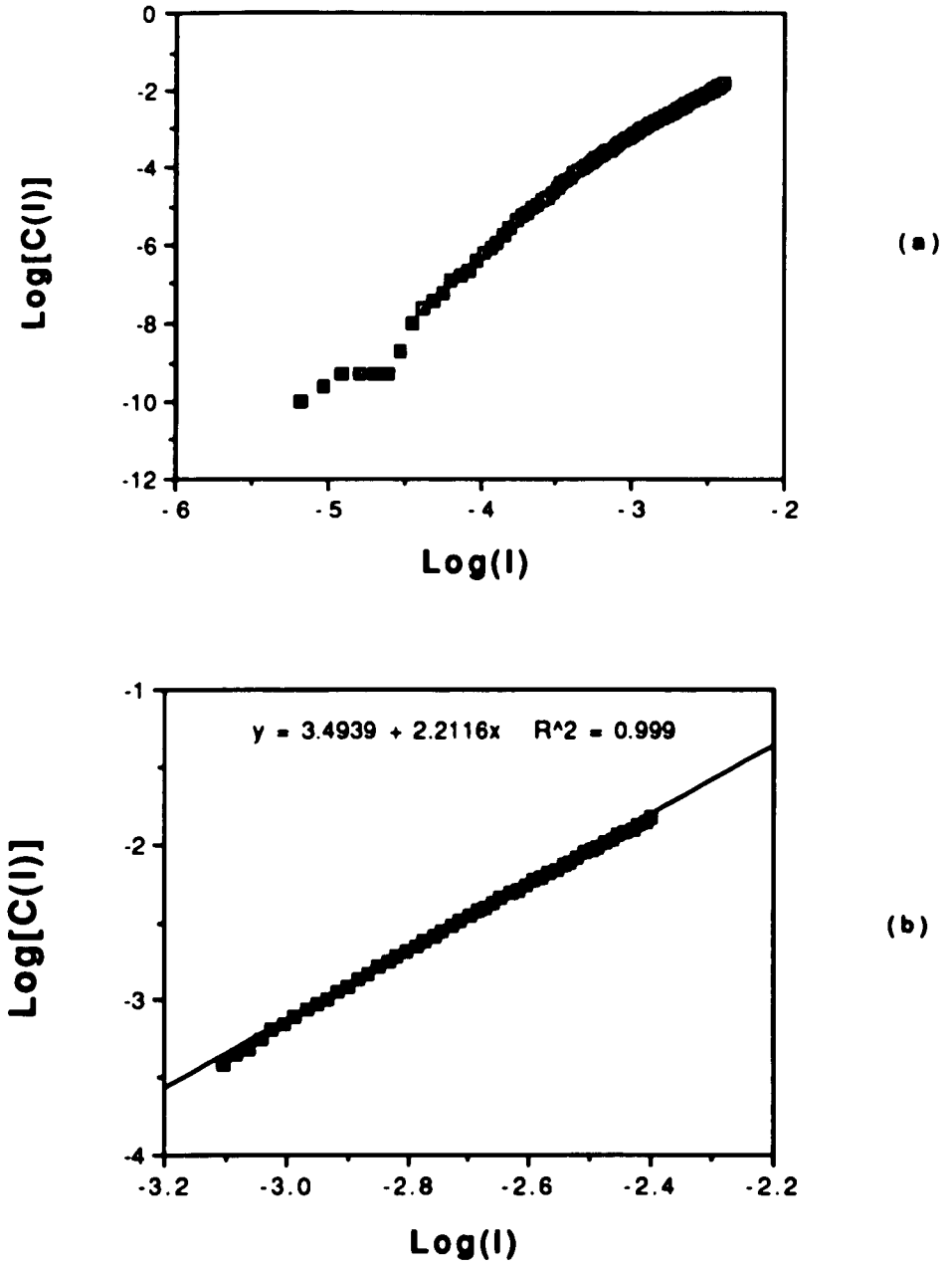

Figure 5.21 (a) Correlation function versus size l for dimension measurement; (b) Subset: Correlation function versus size l for dimension measurement.

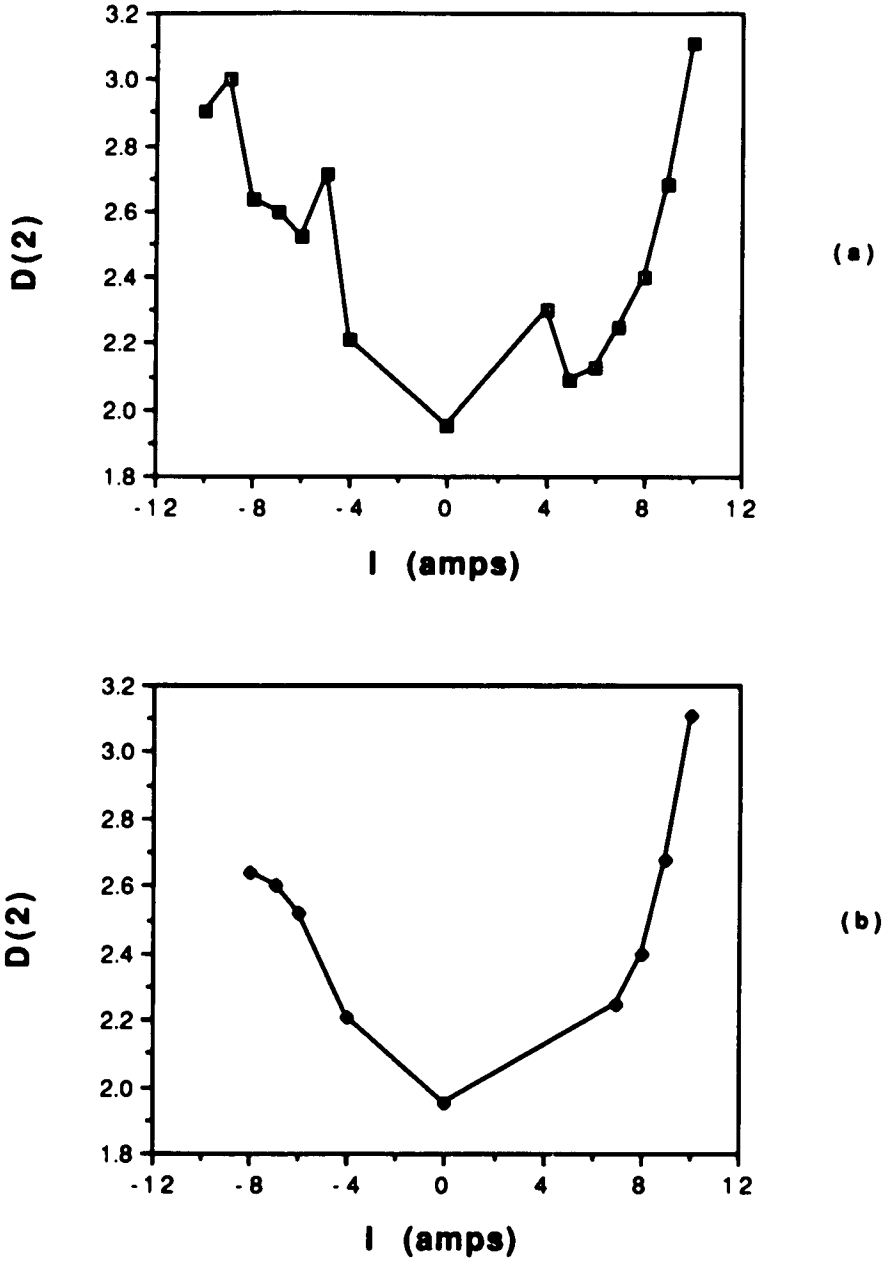

Figure 5.22 (a) Chaotic dimension versus magnetic field in the range of 21<M<33; (b) Chaotic dimension versus magnetic field in the range of 30<M<33.

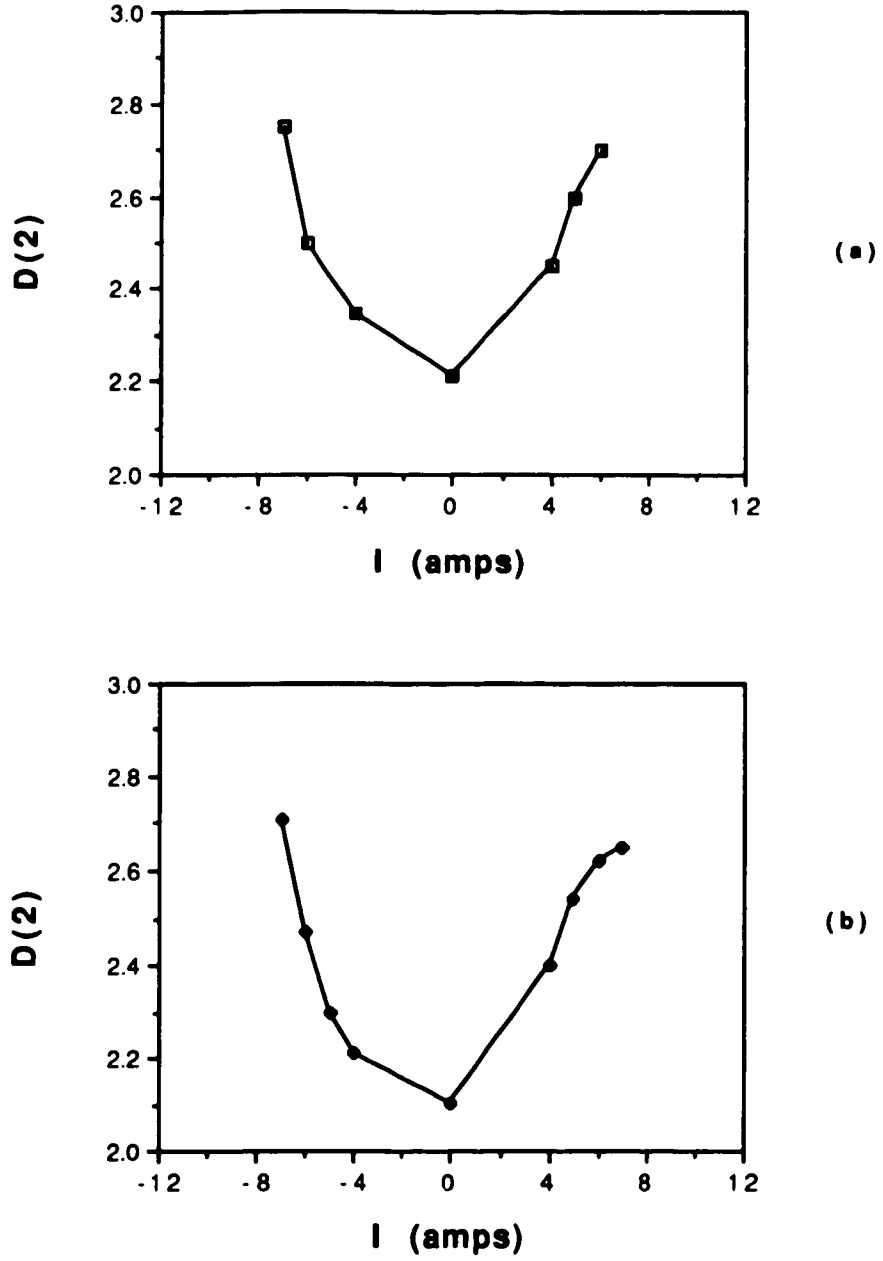

Figure 5.23 (a) Chaotic dimension versus magnetic field in the range of 19<M<21; (b) Chaotic dimension versus magnetic field in the range of 23<M<25.

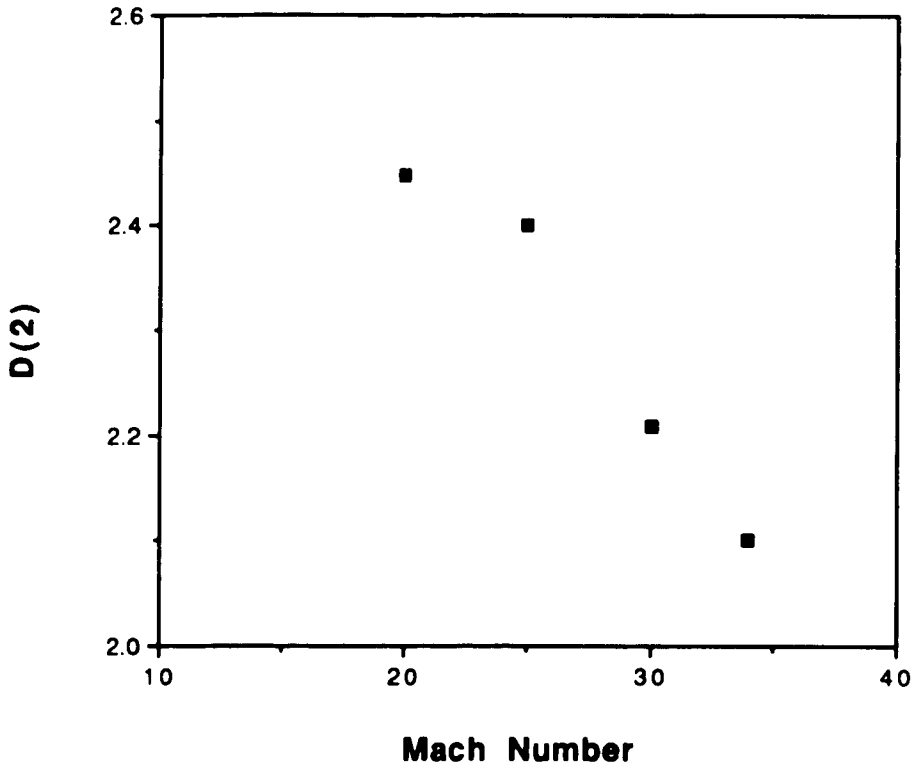

Figure 5.24 Chaotic dimension versus Mach number at a constant magnetic field.

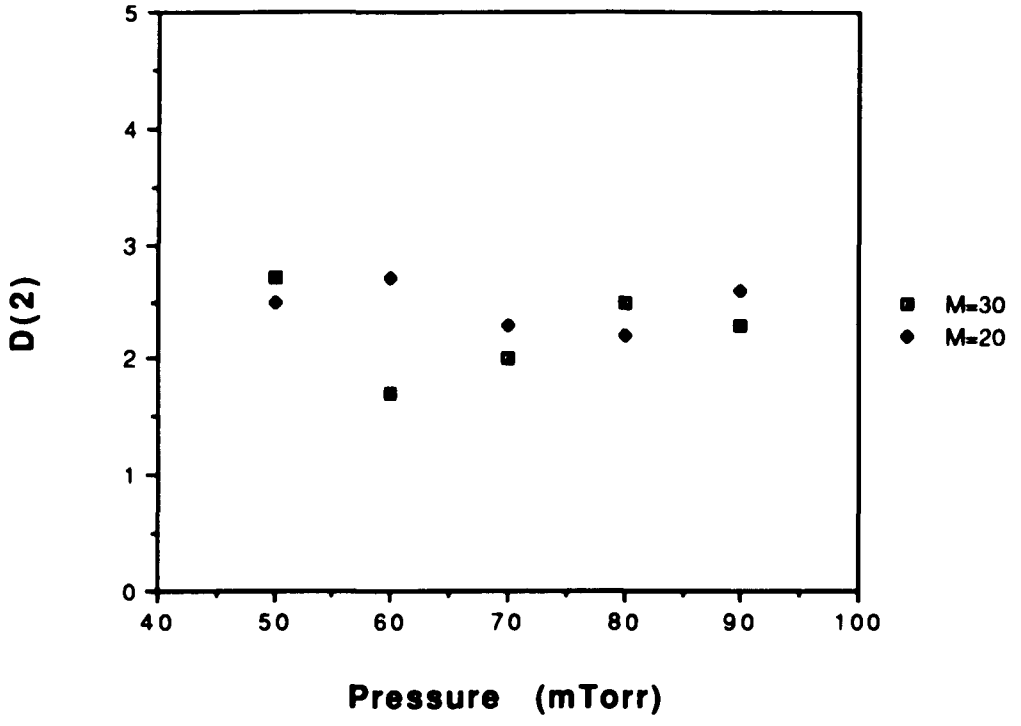

Figure 5.25 Chaotic dimension versus pressure at fixed Mach number and magnetic field.

Chapter VI Discussions and Conclusions

6.1 Comparison with Theory

As discussed in 4.1, turbulent plasma theories predict that in the turbulent state the power spectra should fall off as k^{-n}, k being wave number and n being the spectral index. Since wave number and frequency are linearly related, we are allowed to interpret the experimentally observed f^{-n} in terms of the theoretical k^{-n} spectrum. Experiments have found, generally, a rather large spread in n, $1 \leq n \leq 7$. Examination of the slope of each spectrum shows that over a frequency interval of 0.3~3 MHz the spectra fall off as f^{-n}, where n is between 1.3 and 2.8 for various firing conditions. This is in agreement with the theoretical prediction as well as with previous experimental results of other investigators. Our shock produced plasma is in a turbulent state.

A correlation length scale can be deduced from the characterizing correlation time and measured velocity; i.e. $l_c = v\tau_c$. For a typical case, $v=10^6$ cm/s, $\tau_c=5$ μs, the correlation length is 5 cm. This constitutes a direct measurement of the large scale length parameter for the turbulent system. Since the shock tube's diameter is 5 cm, the length parameter we found is reasonable.

6.2 Turbulent Velocity-Field-Coupling Model

In plasma systems, a charged particle is, at any instant, interacting electrostatically with many other charged particles. Boltzmann's equation gives the basic kinetic description of plasmas. In this equation, there is a collisional term due to interactions (see Equation (2.4)). In a turbulent plasma there exist not only the interactions between the charged particles but also the interactions between the turbulent motions, which are called turbulent interactions. Energy is transferred during the turbulent interactions. Therefore, in general, the collisional term in Boltzmann's equation should include both interaction effects. Furthermore, the rate of change of energy due to the turbulent interaction can be much larger than that due to the particle-particle interaction.[81]

The rate of change of energy due to the interaction of charged particles ($\sim 10^{-9}$ J/s) is much smaller the rate of change of energy due to the turbulent interaction ($\sim 10^{-7}$ J/s) in our case. Since the turbulent interaction is much more important than the particle interaction, we assume that the particle-particle interaction term in Boltzmann's equation can be neglected and only the turbulent interaction term is counted. Under this assumption, the Boltzmann's equation (2.4) for fluid species s can be written as

$$\partial_t \mathbf{V}_s + (\mathbf{V}_s \cdot \nabla)\mathbf{V}_s + \frac{1}{m_s n_s}\nabla P_s - \frac{q_s}{m_s}\mathbf{E} - \frac{q_s}{m_s c}(\mathbf{V}_s \times \mathbf{B}) = \mathbf{f}_{turb.} \quad (6.1)$$

where $\mathbf{f}_{turb.}$ is the term due to the presence of turbulence. In a turbulent plasma a magnetic field fluctuation, **B'**, is generated due to the turbulent motion.[56] This fluctuation quantity has three components. It will couple with the turbulent motion of the plasma flow. This interaction between the turbulent motion and the magnetic field will play an important role in magnetized turbulent plasma systems. Therefore we assume that the interaction term $\mathbf{f}_{turb.} \propto \mathbf{V'} \times \mathbf{B'}$ increases in magnitude with the magnetic field strength, as discussed in 2.4 and as shown in Equation (2.23).

As indicated in 2.4, based on the Boltzmann's equation, and combining it with the continuity equation and Maxwell's equations, we can study the wave propagating in plasmas. We now consider the case of quasineutrality, as discussed in 2.4. In our case the magnetic field is parallel or antiparallel to the direction of shock wave propagation. Therefore the mean velocity of plasma flow is in the same or opposite direction with respect to the mean magnetic field. Therefore, the $\mathbf{V} \times \mathbf{B}$ term vanishes. However, the turbulent interaction term should be included as we argued above. It can be seen from equation (2.22) that the local magnetic field fluctuation is an integral effect of the velocity fluctuation. This means that the magnetic field fluctuation varies much slower than the velocity fluctuation. Therefore, within a time interval, which can be chosen as the mean period of the velocity fluctuation, the magnetic field can be considered unchanged. Under this consideration, the magnetic

field fluctuation B' is assumed to be a constant. By adding the interaction term into the equations (2.17) and (2.19), we obtain

$$m_e n_0 \partial_t \mathbf{V}_e' + \gamma_e T_e \nabla n_{e1} + e n_0 \mathbf{E} = -\frac{e n_0}{c}(\mathbf{V}_e' \times \mathbf{B}') \tag{6.2}$$

$$\partial_t n_{e1} + n_0 \nabla \cdot \mathbf{V}_e' = 0 \tag{6.3}$$

$$m_i n_0 \partial_t \mathbf{V}_i' + \gamma_i T_i \nabla n_{i1} - e n_0 \mathbf{E} = \frac{e n_0}{c}(\mathbf{V}_i' \times \mathbf{B}') \tag{6.4}$$

$$\partial_t n_{i1} + n_0 \nabla \cdot \mathbf{V}_i' = 0 \tag{6.5}$$

For simplicity, assume $\mathbf{B}' = B' \mathbf{z}$, where $\mathbf{z}$ is a unit vector in z direction, and the wave vector $\mathbf{k}$ lies in the x-z plane. Looking for plane wave solutions, and adding (6.2) to (6.4), we obtain

$$-i\omega n_0 (m_e \mathbf{V}_e' + m_i \mathbf{V}_i') + i\mathbf{k} (\gamma_e T_e + \gamma_i T_i) n_{e1} = \frac{e n_0}{c}(\mathbf{V}_i' - \mathbf{V}_e') \times \mathbf{B}' \tag{6.6}$$

Taking the dot product of the wave number $\mathbf{k}$ with (6.6), and inserting $\mathbf{k} \cdot \mathbf{V}_{e,i}' = \omega n_{e1} / n_0$ from (6.3) and (6.5), yields

$$-i\omega n_0 (m_e + m_i) \omega n_{e1} / n_0 + ik^2 (\gamma_e T_e + \gamma_i T_i) n_{e1} = \frac{e n_0}{c} \mathbf{k} \cdot [(\mathbf{V}_i' - \mathbf{V}_e') \times \mathbf{B}'] \tag{6.7}$$

The last term is

$$\mathbf{k} \cdot [(\mathbf{V}_i' - \mathbf{V}_e') \times \mathbf{B}'] = k_x (V_{iy}' - V_{ey}') B' \tag{6.8}$$

In order to express V_{ey}', V_{iy}' in terms of n_{e1}, we use (6.2) and take its cross product with the wave number $\mathbf{k}$, obtaining

$$- i\omega n_0 m_e(\mathbf{k} \times \mathbf{V_e'}) = - \frac{e n_0}{c} \mathbf{k} \times (\mathbf{V_e'} \times \mathbf{B'}) \tag{6.9}$$

or

$$\mathbf{k} \times \mathbf{V_e'} = \frac{\Omega_e'}{- i\omega} \mathbf{k} \times (\mathbf{V_e'} \times \mathbf{z}) \tag{6.10}$$

where $\Omega_e' = \frac{- eB'}{m_e c}$. Equation (6.10) gives three equations

$$- V_{ey}' \, k_z = i \frac{\Omega_e'}{\omega} V_{ex}' \, k_z \tag{6.11}$$

$$- V_{ez}' \, k_x + V_{ex}' \, k_z = i \frac{\Omega_e'}{\omega} V_{ey}' \, k_z \tag{6.12}$$

$$V_{ey}' \, k_x = - i \frac{\Omega_e'}{\omega} V_{ex}' \, k_x \tag{6.13}$$

These can be solved for V_{ex}', V_{ez}' in terms of V_{ey}',

$$V_{ex}' = \frac{i\omega}{\Omega_e'} V_{ey}' \tag{6.14}$$

$$V_{ez}' = - V_{ey}' \frac{k_z}{k_x} i \frac{\Omega_e'}{\omega} (1 - \frac{\omega^2}{\Omega_e'^2}) \tag{6.15}$$

By the continuity equation,

$$V_{ex}' \, k_x + V_{ez}' \, k_z = \omega \, n_{e1} / n_0$$

or

$$\frac{\omega n_{e1}}{n_0} = [k_x (\frac{i\omega}{\Omega_e'}) + k_z (\frac{- i \Omega_e'}{\omega}) \frac{k_z}{k_x} (1 - \frac{\omega^2}{\Omega_e'^2})] V_{ey}' \tag{6.16}$$

Then we ignore the mass of electron ($m_e << m_i$) and using (6.8), invert (6.16) for V_{ey}', insert in (6.7), and obtain

$$- i\omega^2 n_{e1} m_i = - ik^2 (\gamma_e T_e + \gamma_i T_i) n_{e1} + \frac{en_0}{c} k_x B' \frac{\omega n_{e1}}{n_0} \; x$$

$$x \left[\frac{1}{k_x \left(\frac{i\omega}{\Omega_e'}\right) - \left(\frac{i\,\Omega_e'}{\omega}\right) \frac{k_z^2}{k_x} \left(1 - \frac{\omega^2}{\Omega_e'^2}\right)} - \right.$$

$$\left. - \frac{1}{k_x \left(\frac{i\omega}{\Omega_i'}\right) - \left(\frac{i\,\Omega_i'}{\omega}\right) \frac{k_z^2}{k_x} \left(1 - \frac{\omega^2}{\Omega_i'^2}\right)} \right] \qquad (6.17)$$

Finally, the dispersion relation for the modes generated by turbulent interaction is obtained

$$1 - \frac{k^2(\gamma_e T_e + \gamma_i T_i)}{m_i \omega^2} + \frac{\Omega_i'}{\omega} \left[\left(\frac{1}{\frac{\omega}{\Omega_e'} - \frac{\Omega_e'}{\omega} \frac{k_z^2}{k_x^2} \left(1 - \frac{\omega^2}{\Omega_e'^2}\right)} - \right. \right.$$

$$\left. \left. - \frac{1}{\frac{\omega}{\Omega_i'} - \frac{\Omega_i'}{\omega} \frac{k_z^2}{k_x^2} \left(1 - \frac{\omega^2}{\Omega_i'^2}\right)} \right] = 0 \right. \qquad (6.18)$$

The dispersion relation shows that, due to the presence of the term $\mathbf{f}_{turb.}$, a variety of new modes is generated. In the presence of magnetic fields, the turbulent motion of plasmas will couple with the external fields and generate more waves. These waves will interact each other and therefore result in more turbulence in the system as discussed in 2.4. The magnitude of the term $\mathbf{f}_{turb.}$ increases with the strength of the external magnetic field as shown in Equation (2.23).

The conclusions from this velocity-field fluctuation coupling model are strongly supported by our experiment results. Figure 5.3 shows that more modes are produced when magnetic fields are imposed on a turbulent plasma system. If more modes are generated, the plasma system will be more turbulent through the nonlinear mode-mode coupling and wave-particle interactions as indicated in 2.4. From our model we can see that the turbulent interaction which results in the generation of new modes is proportional to the strength of external magnetic field; therefore the stronger the external magnetic field, the more turbulent the system becomes. This is also strongly supported by our chaotic dimension results as shown in Figures 5.21 and 5.22. The plots show that the magnetic field increases the chaotic dimensionality in the turbulent plasma, both in the parallel and the antiparallel cases. In other words, the magnetic field adds more modes to the system and makes the system more complex. Furthermore, as the magnetic field becomes stronger, the value of chaotic dimension becomes larger. With this kind of reasoning, the turbulent velocity-field-coupling model explains the results of our experiment.

6.3 Conclusions

The influence of an external weak magnetic field on the turbulent plasmas behind an ionizing shock front has been determined in detail by using standard turbulent and chaotic analytical procedures on the data under different experimental conditions. The results are summarized as follows:

(1) Turbulent ion density fluctuation takes place behind the shock front and they persist for a time in the order of 10 μs.

(2) The power spectra show a general trend $P \sim f^{-n}$ with $1.3<n<2.8$ for different firing conditions. The spectral index n increases with the increasing initial filling pressure and decreases with the increasing Mach number but it is insensitive to the change of the magnetic field.

(3) An increasing magnetic field increases the characterizing correlation time τ_c and decreases the small correlation time τ_s. Here and below, the sensitivity to magnetic field strengths does not depend on the sign (direction) of the field. The values of small and characterizing correlation times are coupled when the changes arise from changes in the magnetic field strength; increasing τ_c means decreasing values for τ_s. It is also found that the small correlation time decreases with the operating pressure.

(4) The turbulent intensity tends to increase with the increasing magnetic field, Mach number, and the initial filling pressure.

(5) Any increase in the magnetic field increases the chaotic dimension and thereby increases the complexity of the plasma system. This increase in complexity from the magnetic field is consistent with qualitative expectations from our velocity-field-coupling model.

(6) Both fluorescence emissions and ion probe measurements of density fluctuations exhibit the same kind of turbulent properties. The parameters of turbulence in the two diagnostics are quite consistent. Both methods provide a reliable density diagnostic for the fluid-like turbulent parameters in a collisional plasma.

6.4 Suggestions for Further Work

It would be interesting to find the trend of chaotic dimensionality with increasing magnetic field past the highest current strength used in our experiment. There may be a turning point when the field increases to a certain value.

The Reynolds stresses $<\rho u_i u_j>$ are fluctuation-velocity correlation terms. Turbulence can be characterized by Reynolds stresses. They play a dominant role in the theory of mean momentum transfer by turbulent motion. It may be desirable to study effects of the magnetic field on the Reynolds stresses by obtaining simultaneous multiple-point density measurement using laser induced fluorescence.

REFERENCES

1. J. O. Hinze, Turbulence, McGraw-Hill, New York (1987).

2. R. A. Gross, A Shock Heated Wall-Confined Fusion Cycle, Nuclear Fusion, 13, 293 (1973).

3. F. L. Ribe, Fusion Reactor Systems and Associated Technological Problems, Review paper given at APS Plasma Physics Section, November 1973, Bull. APS, Ser. II, 18, 1288 (1973).

4. G. L. Baker and J. P. Gollub, Chaotic Dynamics, Cambridge University Press, New York, (1990).

5. P. Berge, Y. Pomeau and C. Vidal, Order Within Chaos, Wiley, New York (1986).

6. R. Z. Sagdeev, D. A. Usikov and G. M. Zaslavsky, Nonlinear Physics, Harwood Academic Publishers, New York (1988).

7. J. A. Johnson III, L. I and J. P. Santiago, Turbulent collisional ionizing shock waves in argon, J. Phys. D: Appl. Phys., 23, 662 (1990).

8. J. P. Barach and R. E. Vermillion, Flow Modes in Electric Shock Tubes, Phys. Fluids, 8, 1976 (1965).

9. M. A. Levine, Phys. Fluids, Turbulent Mixing at the Contact Surface in a Driven Shock Wave, 13, 1166 (1970).

10. J. P. Barach, Probe Measurements on a Shock Precursor, Phys. Fluids, 22, 837 (1979).

11. I. I. Glass and W. S. Liu, Effects of Hydrogen Impurities on Shock Structure and Stability in Ionizing Monatomic Gases, Part 1. Argon, J. Fluid Mech., 84, 55 (1978).

12. A. F. P. Houwing, T. J. McIntyre, P. A. Taloni and R. J. Sandeman, On the Population of the Metastable States

behind Unstable Shock Waves in Ionizing Argon, J. Fluid Mech., 170, 319 (1986).

13. S. Qian, Y. C. Lee and H. H. Chen, A Study of Nonlinear Dynamical Models of Plasma Turbulence, Phys. Fluids, B1, 87 (1988).

14. C. K. Chu and R. A. Gross, Shock Waves in Plasma Physics, article in Advances in Plasma Physics, vol. 2, A. Simon and W. B. Thompson, eds., J. Wiley, New York (1969).

15. R. A. Gross, The Physics of Strong Shock Waves in Gases, article in Proceedings of the International School of Physics Enrico Fermi, Academic Press, New York (1971).

16. P. L. Similon and R. N. Sudan, Plasma Turbulence, Annu. Rev. Fluid Mech., 22, 317 (1990).

17. S. H. Schneider, Numerical Study of Strong Plasma Shock Waves Produced in an Electromagnetic Shock Tube, Phys. Fluid, 15, 805 (1972).

18. D. H. McNeill, Electron Heating in Collisional Shocks, Phys. Fluids, 18, 44-50 (1975).

19. E. N. Lorenz, Deterministic Non-Periodic Flow, J. Atmos. Sci. 20, 130 (1963).

20. D. Ruelle and F. Takens, On the Nature of Turbulence, Comm. Math. Phys., 82, 137 (1971).

21. H. Mori, Fractal Dimensions of Chaotic Flows of Autonomous Dissipative Systems, Prog. Theor. Phys., 63, 1044 (1980).

22. H. Mori and H. Fujisaka, Statistical Dynamics of Chaotic Flows, Prog. Theor. Phys., 63, 1931 (1980).

23. D. A. Tidman and N. A. Krall, Shock Waves in Collisionless Plasma, Wiley, New York (1971).

24. S. A. Colgate and C. W. Hartman, Collisionless Electrostatic Shocks, Phys. Fluids, 10, 1288 (1967).

25. R. W. Means, F. V. Coroniti, A. Y. Wong and R. B. White, Turbulence in Electrostatic Ion-acoustic Shock, Phys. Fluids, 16, 2304 (1973).

26. Y. Kuramoto, Chemical Wave and Chemical Turbulence, article in Synergetics - a Workshop, edited by H. Haken, 164, Springer-Verlag, New York (1977).

27. Y. Kuramoto, Diffusion-Induced Chaos in Reaction System, Prog. Theor. Phys. Suppl., 64, 346 (1978).

28. Y. Kuramoto, Instability and Turbulence of Wavefronts, Prog. Theor. Phys., 63, 1885 (1980).

29. D. R. Nicholson, Introduction to Plasma Theory, John Wiley & Sons, New York (1983).

30. A. G. Gaydon and I. R. Hurle, The Shock Tube in High-Temperature Chemical Physics, Reinhold Publishing Corporation, New York (1963).

31. H. D. Weymann, Electron Diffusion ahead of Shock Waves in Argon, Phys. Fluids, 3, 545 (1960).

32. J. R. Grieg and G. Palumbo, Precursor Vacuum Ultraviolet Radiation in a T-type Shock Tube, Phys. Fluids, 12, 1211 (1969).

33. M. Y. Jaffrin, Shock Structure in Partially Ionized Gas, Phys. Fluids, 8, 606 (1965).

34. T. J. M. Boyd and J. J. Sanderson, Plasma Dynamics, Barnes & Noble, New York (1969).

35. C. K. Chu and R. A. Gross, Shock Waves in Plasma Physics, article in Advances in Plasma Physics, Vol. 2, A. Simon and W. B. Thompson, eds., J. Wiley, New York (1969).

36. R. T. Taussig, Plasma Heating by Reflected Ionizing Shock Waves, Phys. Fluids, 13, 2270 (1970).

37. H. A. Rose and P. L. Sulem, Fully Developed Turbulence and Statistical Mechanics., J. Phys. 39, 441 (1978).

38. R. H. Kraichnan and D. Montgomery, Two-dimensional Turbulence, Rep. Prog. Phys., 43, 547 (1980).

39. R. M. Kulsrud and R. N. Sudan, On Kraichnan's "direct interaction approximation" and Kolmogoroff's theory in two-dimensional plasma turbulence, Commun. Plasma Phys. Control. Fusion, 7, 47 (1982).

40. R. N. Sudan and D. Pfirsch, On the Relation between "Mixing Length" and "Direct Interaction Approximation" Theories of Turbulence, Phys. Fluids, 28, 1702 (1985).

41. R. N. Sudan, Strong Plasma Turbulence, In From Particles to Plasmas, Lectures Honoring Marshall N. Rosenbluth, ed. J. W. VanDam, 273-94, Addison-Wesley, New York (1987).

42. G. Nicolis and I. Prigogine, Self-Organization in Nonequilibrium Systems, Wiley, New York (1977).

43. H. Yamazaki, Y. Ono and K. Hirakawa, Experimental Study on Chemical Turbulence, J. Phys. Soc. Japan, 44, 335 (1978).

44. R. N. Franklin, Ionization Wave, Plasma Phenomena in Gas Discharges, Chap. 8, 159, Clarendo Press, Oxford (1975).

45. S. Suganomato, I. Ishikawa, H. Yamagishi and M. Matsumato, Excitation of Nonlinear Wave by Repeated Pulsed Electron Beam in Low Pressure SF_6 Gas, Phys. Lett., 78, 71 (1980).

46. K. Ohe, K. Asano and S. Takeda, Propagation of Wave Packets of Ionization Waves, J. Phys. Soc. Japan, 49, 350 (1980).

47. L. Pekarek and V. Krejci, A Nonlinear Oscillator as a Possible Source of Self-Modulation and Ran-domization of an Ionization Wave, Phys. Lett., 81A, 228 (1981).

48. Y. M. Aliev, V. P. Silin and C. Watson, Sov. Phys. JETP, 28, 626 (1966).

49. N. Tzoar, Parametric Excitations in Plasma in a Magnetic Field, Phys. Rev., 178, 356 (1969).

50. J. McBride, Parametric Excitation of Purely Growing Modes in Magnetoplasmas, Phys. Fluids, 13, 2725 (1970).

51. A. Y. Wong and D. R. Baker, Measurements of Diffusion in Velocity Space from Ion-Ion Collisions, Phys. Rev. 188, 326 (1969).

52. N. Nishikawa, H. Hojo, K. Mima and H. Ikeji, Coupled Nonlinear Electron-Plasma and Ion-Acoustic Waves, Phys. Rev. Lett., 33, 148 (1974).

53. V. D. Djordjevic and L. G. Redekopp, On Two-Dimensional Packets of Capillary-Gravity Waves, J. Fluid Mech., 79, 703 (1977).

54. C. G. Koop and L. G. Redekopp, The Interaction of Long and Short Gravity Waves: Theory and Experiment, J. Fluid Mech., 111, 367 (1981).

55. T. Yoshinaga, M. Wakamiya and T. Kakutani, Recurrence and Chaotic Behavior Resulting from Nonlinear Interaction between Long and Short Waves, Phys. Fluids A 3, 83 (1991).

56. M. Steenbeck, F. Krause and K.-H. Radler, A calculation of the Mean Electromotive Force in an Electrically Conducting Fluid in Turbulent Motion, Under the Influence of Coriolis Forces, NCAR, TN/IA-60, 29 (1971).

57. M. Steenbeck and F. Krause, The Generation of Stellar and Planetary Magnetic Fields by Turbulent Dynamo Action, NCAR, TN/IA-60, 49 (1971).

58. E. Halmoy, Production and Investigation of Very Strong Ionizing Shock Waves, Phys. Fluids, 14, 2134 (1971).

59. P. E. Dimotakis, R. C. Miake-Lye and D. A. Papantoniou, Structure and Dynamics of Roud Turbulent Jets, Phys. Fluids, 26, 3185 (1983).

60. R. R. Prasad and K. R. Sreenivasan, Scalar boundaries in digital images of turbulent flows, Exp. Fluids, 7, 259 (1989).

61. R. R. Prasad and K. R. Sreenivasan, Quantitative three-dimensional imaging and the structure of passive scalar fields in fully turbulent flows, J. Fluid Mech., 216, 1 (1990).

62. R. A. Stern and J. A. Johnson, III, Plasma Ion Diagnostics Using Resonant Fluorescence, Phys. Rev. Lett., 34, 1548 (1975).

63. F. F. Chen, Electric Probes, in Plasma Diagnostic Techniques, edited by R. H. Huddlestone and S. L. Leonard, 191-95, Academic Press, New York (1965).

64. R. P. Smy, The Use of Langmuir Probes, Adv. in Phys., 25, 517 (1976).

65. M. A. Heald and C. B. Wharton, Plasma Diagnostics with Microwaves, John Wiley & Sons Inc., New York, (1965).

66. Lin I, Ph.D. thesis, Rutgers University (1981).

67. E. B. Hooper Jr., Correlation Techniques in Experimental Plasma Physics, Plasma Phys., 13 , 1 (1971).

68. D. E. Smith and E. J. Powers, Experimental determination of the spectral index of a turbulent plasma from digitally computed power spectra, Phys. Fluids, 16, 1373 (1973).

69. J. R. Roth, Experimental Study of Spectral Index, Mode Coupling, and Energy Cascading in a Turbulent, Hot-Ion Plasma, Phys. Fluids, 14, 2193 (1971).

70. J. H. Noon, H. A. Schmidt and E. H. Holt, Connection between Self-Excited Low Frequency Oscillations and Anomalous Plasma Diffusion, Plasma Phys., 12, 477 (1970).

71. N. F. Barber, Experimental Correlograms of Fourier Transforms, Pergamon Press, Oxford (1961).

72. F. H. Lange, Correlation Techniques, Van Nostrand, New York (1967).

73. J. C. Roux, A. Rossi, S. Bachelart and C. Vidal, Experimental Observations of Complex Behavior During a Chemical Reaction, Physica, 2D, 395 (1981).

74. E. Ott, Strange Attractors and Chaotic Motions of Dynamical Systems, Rev. Mod. Phys. 53, 655 (1981).

75. F. Takens, Lecture Notes in Math., 898, Springer, Heidelberg-New York (1981).

76. H. Froehling, J. P. Crutchfield, D. Farmer, N. H. Packard, and R. Shaw, On Determining the Dimension of Chaotic Flows, Physica, 3D, 605 (1981).

77. B. Mandelbrot, The Franctal Geometry of Nature, W. H. Freeman, San Francisco, (1982).

78. P. Grassberger and I. Procaccia, Characterization of Strange Attractors, Phys. Rev. Lett., 50, No.5, 346 (1983).

79. H. S. Greenside, A. Wolf, J. Swift, and T. Pignataro, Impracticality of a Box-Counting Algorithm for Calculating the Dimensionality of Strange Attractors, Phys. Rev. A 25, 3453 (1982).

80. R. R. Prasad and K. R. Sreenivasan, The Measurement and Interpretation of Fractal Dimensions of the Scalar Interface in Turbulent Flows, Phys. Fluids A 2 , 729 (1990).

81. X. Li, Z. Zhang and Y. Zhang, A Heating Model for the Transition Zone and Inner Corona, Solar Phys. 91, 289 (1984).